OCEANIC AND TERRESTRIAL SOURCES OF CONTINENTAL PRECIPITATION

Luis Gimeno,[1] Andreas Stohl,[2] Ricardo M. Trigo,[3,4] Francina Dominguez,[5] Kei Yoshimura,[6] Lisan Yu,[7] Anita Drumond,[1] Ana María Durán-Quesada,[1,8] and Raquel Nieto[1]

Received 18 January 2012; revised 31 August 2012; accepted 5 September 2012; published 8 November 2012.

[1] The most important sources of atmospheric moisture at the global scale are herein identified, both oceanic and terrestrial, and a characterization is made of how continental regions are influenced by water from different moisture source regions. The methods used to establish source-sink relationships of atmospheric water vapor are reviewed, and the advantages and caveats associated with each technique are discussed. The methods described include analytical and box models, numerical water vapor tracers, and physical water vapor tracers (isotopes). In particular, consideration is given to the wide range of recently developed Lagrangian techniques suitable both for evaluating the origin of water that falls during extreme precipitation events and for establishing climatologies of moisture source-sink relationships. As far as oceanic sources are concerned, the important role of the subtropical northern Atlantic Ocean provides moisture for precipitation to the largest continental area, extending from Mexico to parts of Eurasia, and even to the South American continent during the Northern Hemisphere winter. In contrast, the influence of the southern Indian Ocean and North Pacific Ocean sources extends only over smaller continental areas. The South Pacific and the Indian Ocean represent the principal source of moisture for both Australia and Indonesia. Some landmasses only receive moisture from the evaporation that occurs in the same hemisphere (e.g., northern Europe and eastern North America), while others receive moisture from both hemispheres with large seasonal variations (e.g., northern South America). The monsoonal regimes in India, tropical Africa, and North America are provided with moisture from a large number of regions, highlighting the complexities of the global patterns of precipitation. Some very important contributions are also seen from relatively small areas of ocean, such as the Mediterranean Basin (important for Europe and North Africa) and the Red Sea, which provides water for a large area between the Gulf of Guinea and Indochina (summer) and between the African Great Lakes and Asia (winter). The geographical regions of Eurasia, North and South America, and Africa, and also the internationally important basins of the Mississippi, Amazon, Congo, and Yangtze Rivers, are also considered, as is the importance of terrestrial sources in monsoonal regimes. The role of atmospheric rivers, and particularly their relationship with extreme events, is discussed. Droughts can be caused by the reduced supply of water vapor from oceanic moisture source regions. Some of the implications of climate change for the hydrological cycle are also reviewed, including changes in water vapor concentrations, precipitation, soil moisture, and aridity. It is important to achieve a combined diagnosis of moisture sources using all available information, including stable water isotope measurements. A summary is given of the major research questions that remain unanswered, including (1) the lack of a full understanding of how moisture sources influence precipitation isotopes; (2) the stationarity of moisture sources over long periods; (3) the way in which possible changes in intensity (where evaporation exceeds precipitation to a greater of lesser degree), and the locations of the sources, (could) affect the distribution of continental precipitation in a changing climate; and (4) the role played by the main modes of climate variability, such as the North Atlantic Oscillation or the El Niño–Southern Oscillation, in the variability of the moisture source regions, as well as a full evaluation of the moisture transported by low-level jets and atmospheric rivers.

[1]Ephyslab, Departamento de Física Aplicada, Facultad de Ciencias de Ourense, Universidad de Vigo, Ourense, Spain.
[2]NILU - Norwegian Institute for Air Research, Kjeller, Norway.
[3]CGUL, IDL, University of Lisbon, Lisbon, Portugal.
[4]Departamento de Engenharias, Universidade Lusófona, Lisbon, Portugal.
[5]Department of Atmospheric Sciences, University of Arizona, Tucson, Arizona, USA.
[6]Atmosphere and Ocean Research Institute, University of Tokyo, Tokyo, Japan.
[7]Department of Physical Oceanography, Woods Hole Oceanographic Institution, Woods Hole, Massachusetts, USA.
[8]Now at Department of Atmospheric, Oceanic and Planetary Physics (School of Physics) and the Center for Geophysical Research, University of Costa Rica, San Jose, Costa Rica.

Corresponding author: L. Gimeno, Ephyslab, Departamento de Física Aplicada, Facultad de Ciencias de Ourense, Universidad de Vigo, Campus As Lagoas s/n, ES-32004 Ourense, Spain. (l.gimeno@uvigo.es)

8755-1209/12/2012RG000389
Paper number 2012RG000389

Citation: Gimeno, L., A. Stohl, R. M. Trigo, F. Dominguez, K. Yoshimura, L. Yu, A. Drumond, A. M. Durán-Quesada, and R. Nieto (2012), Oceanic and terrestrial sources of continental precipitation, *Rev. Geophys.*, *50*, RG4003, doi:10.1029/2012RG000389.

1. INTRODUCTION

[2] Given the importance of global climate change, an understanding of the nature and intensity of the hydrological cycle and of its development over time is one of the most pressing challenges currently faced by mankind. Although the atmosphere contains only a small proportion of the total global water, it nevertheless plays a key role in connecting the major reservoirs of the oceans, lakes, soils, inland and sea ice, and rivers via the transport of moisture, evapotranspiration, and precipitation. Water vapor accounts for only about 0.25% of the total mass of the atmosphere [*Seidel*, 2002], but its importance in regulating global climate and weather patterns is beyond dispute [*Held and Soden*, 2000]. The hydrological cycle may be summarized as the evaporation of moisture at one location and precipitation elsewhere, balanced by the atmospheric, oceanic, and hydrological transport of water. In oceanic regions, the rate of evaporation generally exceeds the rate of precipitation, and oceans therefore represent a net source of moisture that is then transported by the atmosphere to the continents; landmasses act as net sinks of atmospheric moisture where precipitation exceeds evapotranspiration. Surface water then feeds rivers, groundwater, and other bodies that discharge into the ocean, thereby completing the cycle. In global terms, the hydrological cycle is responsible for an annual rate of evaporation of about half a million cubic kilometers of water, around 86% of which is from the oceans, with the remainder having its origin in the continents [*Quante and Matthias*, 2006]. Most of the water that evaporates from the oceans (90%) is precipitated back into them. Only 10% falls as precipitation over the continents (Figure 1). Of this precipitation, approximately two thirds is recycled over the continents, and only one third runs off directly into the oceans [e.g., *Trenberth et al.*, 2007a]. Because human society is becoming increasingly reliant on the security of its freshwater resources, and has adapted to the present-day hydrological cycle and in particular to the current precipitation regime, it is essential to understand the processes of evaporation from the oceans (via the study of oceanography [*Yu*, 2007]), the transport of atmospheric moisture (meteorology [*Trenberth et al.*, 2003]), and the effects of these two processes in particular on the hydrological cycle (hydrology [*Bales*, 2003]), all of which are affected by global climate change [*Intergovernmental Panel on Climate Change* (*IPCC*), 2007].

[3] Recent years have seen an increasing number of studies using novel remote sensing techniques, which has allowed ever more sophisticated and robust estimates of oceanic evaporation to be made (e.g., the Objectively Analyzed air-sea Flux project (OAFlux) [*Yu et al.*, 2008]). New data assimilation methods have improved meteorological reanalyses, which now provide a much better closure of the hydrological cycle [*Trenberth et al.*, 2011]. There has also been a dramatic increase in the number of water vapor isotopes observations [*Risi et al.*, 2012], which are fundamental to the validation of analytical and numerical models [e.g., *Yoshimura et al.*, 2004]. Global circulation models with advanced cloud microphysics and a realistic representation of orography have also incorporated new parametrizations that better represent processes involving soil moisture and have afforded significant improvements to the ability of general circulation models (GCMs) to represent the atmospheric water cycle [*Andersson et al.*, 2005]. Furthermore, the trajectory-based ("Lagrangian") methods used to identify sources of moisture available for precipitation have been widely used to assess both global [e.g., *Stohl and James*, 2005; *Dirmeyer and Brubaker*, 2007; *Gimeno et al.*, 2010a] and regional sources [e.g., *Nieto et al.*, 2006; *Sodemann et al.*, 2008].

[4] In the following sections, recent work related to all the foregoing different aspects of the hydrological cycle is summarized, but with a focus on the atmospheric part of the hydrological cycle. The review concentrates on works published in the last three decades, but there is more historical information that is not being discussed here. In Section 2, the general distribution of evaporation, water vapor, and precipitation is described, as are the general patterns of water vapor transport. In Section 3, the source-sink relationships are examined, first in a discussion of the different methods, their assumptions, and their advantages and disadvantages, and second by summarizing the main evaporative source regions and transport paths of moisture for global and regional precipitation. In Section 4, the transport of moisture during extreme episodes such as drought and flood events is discussed. In Section 5, some of the implications of climate change for the hydrological cycle are reviewed, and it is proposed that if it is indeed critical to understand the processes that govern moisture transport in the troposphere, it is even more so in a changing climate [*Christensen and Christensen*, 2003; *Schär et al.*, 2004]. To understand the transport is to understand the relationship among the changes in evaporation, in atmospheric moisture content, and in precipitation, which provides the only means of explaining why the patterns predicted by different climate models differ so substantially. In the final section (Section 6), some topics are highlighted that require further research in the coming years.

2. GLOBAL DISTRIBUTION OF WATER VAPOR

2.1. Evaporation and Precipitation

[5] Evaporation is the process by which water molecules change phase from liquid to gas. Turbulent eddies transport moisture away from the evaporating surface. For practical applications, we simplify these turbulent fluxes using bulk

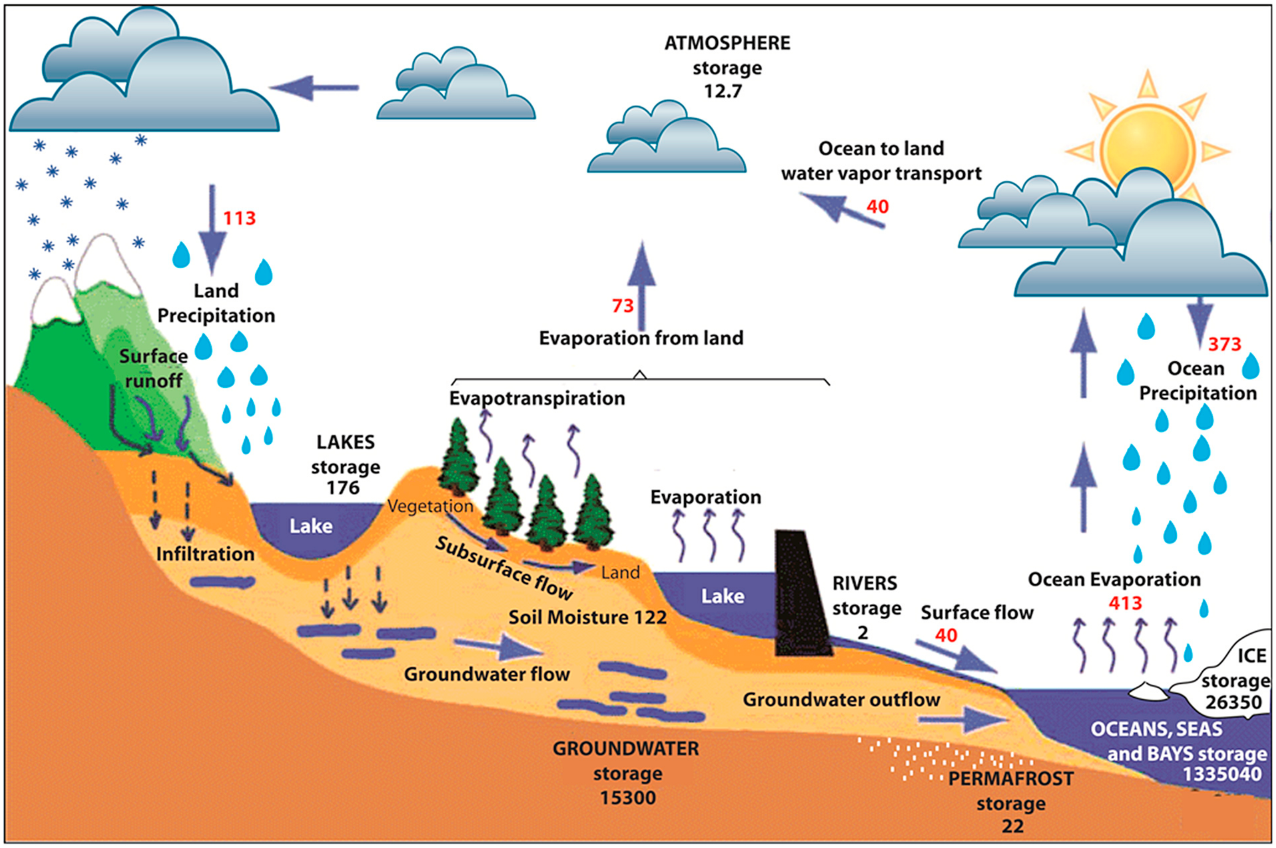

Figure 1. The hydrological cycle. Estimates of the observed main water reservoirs (black numbers, in 10^3 km^3) and the flow of moisture through the system (red numbers, in 10^3 km^3 yr^{-1}). Adjusted from *Trenberth et al.* [2007a] for the period 2002–2008 as in *Trenberth et al.* [2011].

transfer coefficients to relate the fluxes to the mean properties of the flow. Consequently, evaporation E can be expressed as

$$E = c_e U dq = c_e U(q_s - q_a), \quad (1)$$

where U is the near-surface wind speed, c_e is a turbulent exchange coefficient, q_s is the saturation specific humidity at the evaporating surface, and q_a is the near-surface atmospheric specific humidity. This basic equation is then modified to reflect the nature of the evaporating surface. Over the oceans, the following parametrization [*Fairall et al.*, 2003] is often used:

$$E = c_e U dq = c_e U(q_s(\mathrm{SST}) - q_a(T_a, \mathrm{RH})), \quad (2)$$

where q_s is the saturation specific humidity for a given sea surface temperature (SST) and q_a is the near-surface atmospheric specific humidity.

[6] The global distribution over ocean of E is commonly constructed from equation (2) using air-sea variables that can be obtained from satellite observations [e.g., *Chou et al.*, 2003; *Kubota and Tomita*, 2007; *Andersson et al.*, 2011] and/or from reanalysis data. A key limitation of satellite data is the challenge of retrieving near-surface air humidity and temperature [e.g., *Curry et al.*, 2004; *Yu*, 2009], which requires certain assumptions to be made. To reduce this problem, satellite observations were combined with reanalysis outputs [e.g., *Large and Yeager*, 2009]. One such product was developed by the OAFlux project [*Yu and Weller*, 2007; *Yu et al.*, 2008]. Figures 2a and 2b show the temporally averaged ocean evaporation for January and July. Oceanic evaporation obtained from other data sets is qualitatively similar in terms of its main characteristics, although significant quantitative differences exist [e.g., *Andersson et al.*, 2011].

[7] Over land, equation (1) is usually presented in a slightly different form, using bulk aerodynamic resistance (r_a) rather than the turbulent exchange coefficient (c_e), where $r_a = (c_e\ U)^{-1}$, using vapor pressures rather than specific humidity, and assuming $q \approx 0.622e/p$:

$$E = \frac{0.622\rho(e_s(T_0) - e(T))}{p_s r_a}, \quad (3)$$

where the constant 0.622 is the ratio of the molecular weight of water vapor to the effective molecular weight of dry air, $e_s(T_0)$ is the saturation vapor pressure for a given surface temperature T_0, e is the vapor pressure above the surface, T is the near-surface air temperature, and p_s is the atmospheric pressure at the surface. Meteorological observations over land generally only provide the temperature 2m above the surface, and for this reason the Penman-Monteith equation may be derived from equation (3) and the expression for

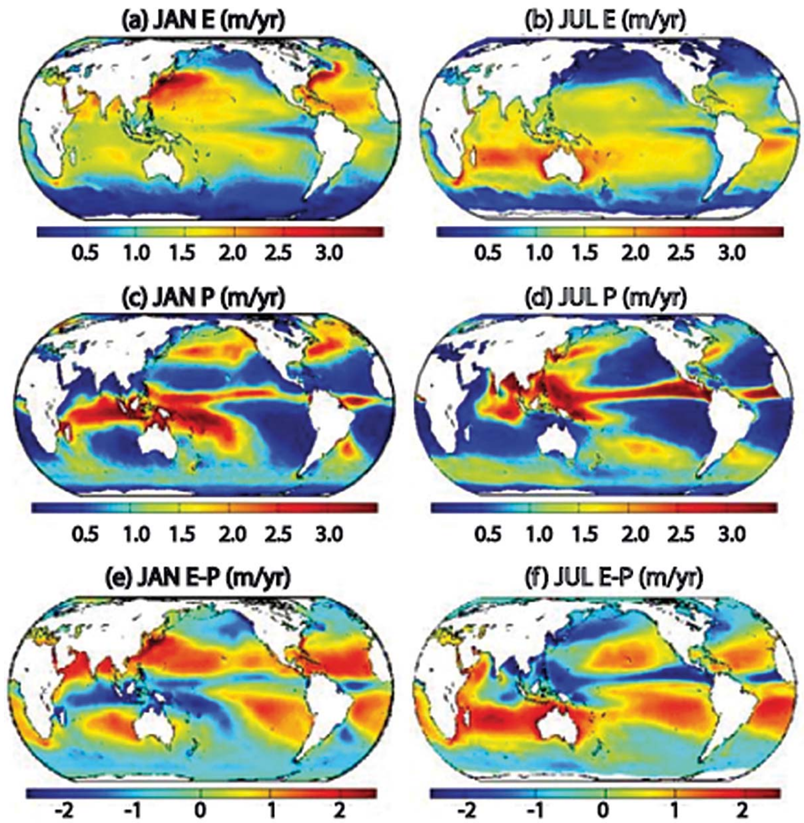

Figure 2. Ocean time-mean rates of (a, b) *E*, (c, d) *P*, and (e, f) *E-P* for January and July. *E* is from OAFlux [*Yu and Weller*, 2007] for 1988–2008, *P* is from GPCP [*Adler et al.*, 2003] for 1988–2008, and *E-P* is the combination of these.

sensible heat flux (see *Shuttleworth* [2012] for a derivation) in order to give an expression for evaporation that only requires observations of humidity, temperature and wind speed at a single level:

$$L_v E = \frac{\Delta(R_n) + \frac{\rho c_p}{r_a}(e_s(T) - e(T))}{\Delta + \gamma\left(1 + \frac{r_s}{r_a}\right)}, \tag{4}$$

where L_v is the latent heat of vaporization, Δ is the slope of the saturation vapor pressure versus temperature curve at temperature T, R_n is the net incoming radiation, ρ is the density of air, c_p is the specific heat of air, $\gamma = c_p p/(0.622\, L_v)$, and r_s is the canopy-averaged leaf stomatal resistance obtained using the big-leaf approximation [see *Shuttleworth*, 2012]. The Penman-Monteith equation (4) is perhaps the best known expression for evaporation over land.

[8] Over land, the global network of eddy covariance (EC) towers (towers that measure surface fluxes based on turbulence theory) FLUXNET provides continuous data on water and energy fluxes for a wide range of ecosystems and climates [*Baldocchi et al.*, 2001]. At a larger scale, recent merged flux tower and satellite data [*Reichstein et al.*, 2007; *Mu et al.*, 2007] and merged satellite and gridded climate data [*Fisher et al.*, 2008] provide global estimates of terrestrial evapotranspiration.

[9] A complete review of the basic theories, observational methods, satellite algorithms, and land surface models for evaporation over land may be found in *Wang and Dickinson* [2012]. The principal methods of measuring evapotranspiration are summarized in Table 1 (eddy covariance, Bowen ratio (BR), weighable lysimeters, scintillometer, surface water balance, and atmosphere water balance methods), as reviewed by the authors.

[10] Figure 3 shows both the ensemble average and the uncertainty of the mean annual and seasonal values of global evapotranspiration for the period 1984–2007, as derived using two surface radiation budget products and three process-based models [from *Vinukollu et al.*, 2011]. The ensemble mean shows the spatial distribution of evapotranspiration, with low values in arid regions, highest values in the humid tropics, and intermediate values in midlatitude forests and agricultural regions. The seasonal cycle shows the greening of the midlatitudes during their respective hemispheric spring and summer. There is some interseasonal variability in the uncertainties, which are greatest in humid tropical and subtropical monsoon regions.

[11] Once evaporated, water vapor molecules typically spend about 10 days in the atmosphere before condensing and falling to the Earth as precipitation [*Numaguti*, 1999]. The 10 day period considered is a median of a broad probability density function of residence times of water vapor in the atmosphere. Most of the water vapor evaporated from the

TABLE 1. A Summary of Observation and Estimation Methods for Evapotranspiration[a]

Method	Temporal Scale	Spatial Scale	Advantages	Disadvantages
Eddy Covariance	Half hour to yearly.	Hundreds of m depending on measurement height above canopy layer and wind speed.	Direct measurement of turbulence fluxes and independent observation.	Regional and global estimation can be made.
Bowen Ratio	Half hour to yearly.	Hundreds of m depending on measurement height above canopy layer and wind speed.	Energy is balanced.	Diffusivity for water and heat are assumed to be equal. Energy balance is assumed (energy components are point measurements and fluxes have a large footprint).
Lysimeter	Half hour to yearly.	Point measurement.	Direct observation.	Environment is disturbed.
Scintillometer	Half hour to yearly.	Tens of m to tens of km.	Captures turbulence fluxes over large scale with known footprints.	Depends on MOST universal functions.
Surface Water Balance	Monthly to yearly.	Hundreds to thousands of km.	Direct estimate, regional and global estimation can be made.	Accuracy can only be guaranteed at low temporal (multiyear average) and spatial resolution.
Atmospheric Water Balance	Monthly to yearly.	Hundreds to thousands of km.	Regional and global estimation can be made.	Low accuracy.

[a]From *Wang and Dickinson* [2012].

oceans falls back into the oceans as precipitation, while about 10% is transported over land and influences terrestrial hydrological processes [*Oki*, 2005]. The climatological mean distribution of global precipitation rate, *P*, is shown in Figures 2c and 2d for January and July using the precipitation data set from the Global Precipitation Climatology Project (GPCP [*Huffman et al.*, 1997; *Adler et al.*, 2003]). Other commonly used precipitation data sets include the Tropical Rainfall Measuring Mission (TRMM) Multisatellite Precipitation Analysis (TMPA [*Huffman et al.*, 2007]), the Climate Prediction Center (CPC) Merged Analysis of Precipitation (CMAP [*Xie and Arkin*, 1997]), the precipitation estimates from the CPC MORPHing technique (CMORPH [*Joyce et al.*, 2004]), the Unified Microwave Ocean Retrieval Algorithm (UMORA [*Hilburn and Wentz*, 2008]), and Precipitation Estimation from Remotely Sensed Information using Artificial Neural Networks (PERSIANN [*Hsu et al.*, 1997]).

[12] A combination of satellite-derived *E* and *P* data sets yields estimates of global ocean freshwater flux. However, as pointed out by *Schlosser and Houser* [2007], these estimates are quite uncertain because each time series is calibrated differently, data sources are usually inhomogeneous, and more critically, there are no comprehensive in situ validation data.

[13] Nevertheless, in their study of the ocean freshwater budget (*E-P*) using ocean salinity observations *Schanze et al.* [2010] showed that among a variety of possibilities, the *E-P* pair from OAFlux *E* and GPCP *P* [*Yu et al.*, 2008; *Adler et al.*, 2003] was the only pair capable of balancing the ocean freshwater budget within the measurement uncertainties (Figures 2e and 2f). The combined use of these two data sets may be seen in a variety of applications, including the validation of climate model simulations [e.g., *Allan*, 2009; *Liepert and Previdi*, 2009], explanation of observed changes in ocean salinity [*Lagerloef et al.*, 2010; *Bingham et al.*, 2010; *Ren and Riser*, 2009; *Yu*, 2011], estimation of the freshwater budget balance in regional and global oceans [*Sanchez-Gomez et al.*, 2011; *Schanze et al.*, 2010], and inference of the mean and variability of the continental freshwater discharge to the global oceans [*Seo et al.*, 2009; *Syed et al.*, 2010]. The balance of *E* and *P* indicates the major sources and sinks of water vapor over the globe. The major net sources ($E > P$) are located over the subtropical belts of high evaporation, and the major net sinks ($E < P$) are found in the Intertropical Convergence Zone (ITCZ), the South Pacific Convergence Zone (SPCZ), and the midlatitude storm tracks where the convection of moisture results in high precipitation.

2.2. Water Vapor Flux and Divergence

[14] To gain improved understanding of the transport of atmospheric moisture, great efforts have been made to advance space and in situ observational platforms to better quantify the distribution and variation of water vapor in the atmosphere. For instance, *Ross and Elliott* [1996] provided quality-controlled long-term radiosonde observations in the United States, and these observations were later extended to the whole of the Northern Hemisphere [*Ross and Elliott*, 2001]. Satellite observations have also been available for some time thanks to Meteosat-3 and -4 [*Pierrehumbert and Roca*, 1998], Special Sensor Microwave/Imager (SSM/I) [*Wentz and Schabel*, 2000; *Santer et al.*, 2007; *Wentz et al.*, 2007], High-Resolution Infrared Radiation Sounder (HIRS) [*Bates et al.*, 2001], the Global Ozone Monitoring Experiment (GOME) [*Wagner et al.*, 2005], Atmospheric Infrared Sounder (AIRS) [*Dressler et al.*, 2008], Global Positioning

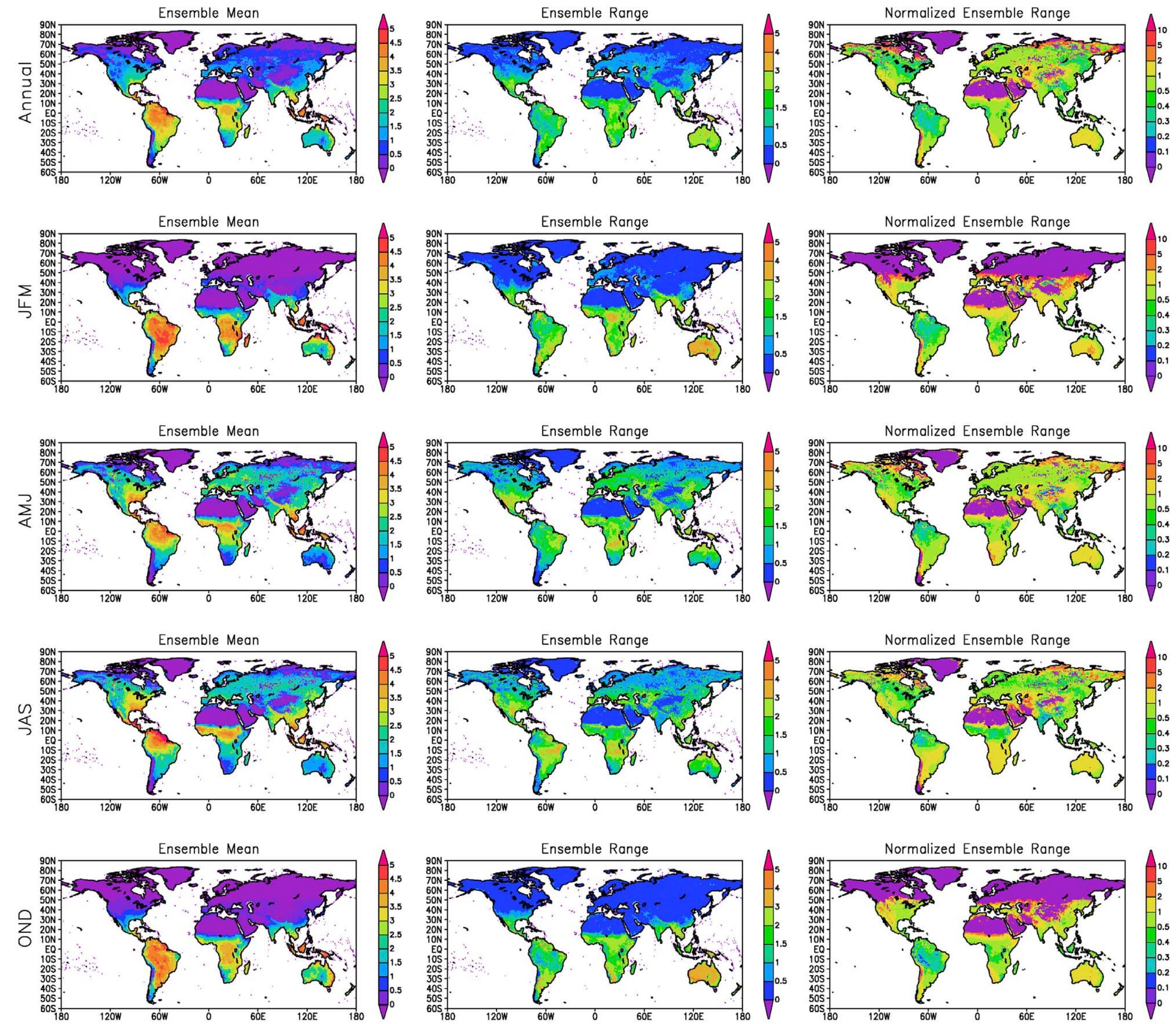

Figure 3. Map of (left column) the ensemble average, (middle column) ensemble range, and (right column) normalized ensemble range in global evapotranspiration for (top row) annual mean and (bottom four rows) seasonal means. The ensemble used outputs from two surface radiation budgets and three process-based evapotranspiration models. The normalized ensemble range is calculated as the range divided by the ensemble mean. From *Vinukollu et al.* [2011].

System (GPS) [*Wolfe and Gutman*, 2000], and other techniques.

[15] The global distribution of water vapor is shown in Figures 4a and 4b for January and July using the total column water vapor (TCWV) obtained from SSM/I observations. As shown in *Trenberth et al.* [2011], the overall patterns and temporal variation of water vapor over the oceans generally follow those of SST, because according to the Clausius-Clapeyron (C-C) equation, the saturation water vapor pressure is a nonlinear function of temperature. According to C-C equation a change in temperature of 1° typically causes a 7% change in water vapor content [*Held and Soden*, 2000; *Wentz et al.*, 2007]. Because of its sensitivity to temperature, the water vapor content is high in the lower atmosphere, and decreases with height. Moreover, water vapor occurs at high concentrations in the tropics and is less prevalent at higher latitudes. If the total water vapor content in the atmosphere were to condense and precipitate, the depth of precipitation would be about 50 mm at equatorial latitudes, but only about 5 mm at the poles [*Quante and Matthias*, 2006]. The highest TCWV occurs over the tropical Pacific warm pool, and its location and seasonal variation are shown in Figures 4a and 4b.

[16] The global distribution of evaporation (Figures 2a and 2b) differs from that of atmospheric water vapor (Figures 4a and 4b), and also from that of precipitation (Figures 2c and 2d). This is because for precipitation to occur, three factors are important, namely (1) the availability of atmospheric moisture, (2) a cooling mechanism, and (3) the presence of cloud condensation nuclei (CCN). All of these are necessary for the condensation process to occur and for droplets to form and grow sufficiently large to fall out of the

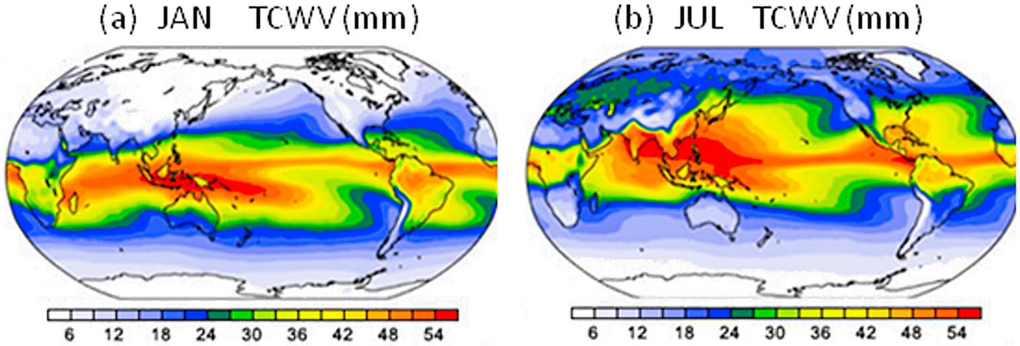

Figure 4. Mean total column water vapor (TCWV) for (a) January and (b) July. Adapted from *Trenberth et al.* [2011].

atmosphere. Typically, cooling is caused by the uplift of an air mass, either due to convection, large-scale ascent, or flow over a topographic obstacle, but radiational cooling is also possible (e.g., through the formation of fog). Usually, condensation in the free atmosphere is not possible without the presence of aerosols. It is the microphysics that controls the formation of cloud droplets or ice crystals through collision or coalescence, as well as their growth and precipitation [*Houze*, 1993]. The global distribution of precipitation is more similar to the distribution of TCWV, particularly in the tropics, in areas of low-level convergence and high SST. In the tropics, there is also far more structure to the patterns of rainfall, due to the effects of major circulation regimes such as the monsoons and the Hadley cell.

[17] The transport of water vapor in the atmosphere is typically represented by the vertically integrated total horizontal flux of water vapor, which can be expressed as

$$\Theta = \frac{1}{g}\int_0^{p_s} q\mathbf{V}dp, \tag{5}$$

where g is the acceleration due to gravity, p is the pressure, p_s is the pressure at the surface, q is the specific humidity, and $\mathbf{V}$ is the horizontal wind vector at a given level, composed of both mean and eddy components. Using the conservation of mass, the hydrological balance in the atmosphere can be formulated as follows:

$$\frac{\partial W}{\partial t} + \nabla \cdot \Theta = E - P, \tag{6}$$

Equation (6) states that the temporal rate of change of precipitable water, $W = \frac{1}{g}\int_0^{p_s} qdp$, and the divergence of the water vapor transport integrated over the depth of the atmosphere ($\nabla \cdot \Theta$) must balance the fresh water flux *E-P* at the surface.

[18] Early studies [e.g., *Benton and Estoque*, 1954; *Starr and Peixoto*, 1958; *Rasmusson*, 1967] have demonstrated that, provided that the water vapor flux Θ can be measured with sufficient accuracy, equation (6) is useful for evaluating the combined change in surface and subsurface water storage. Following these earlier publications, continuing efforts have been made to estimate Θ using available observational data, such as those obtained from rawinsondes [e.g., *Rasmusson*, 1967; *Peixoto et al.*, 1981] and satellites [*Liu and Tang*, 2005; *Xie et al.*, 2008], and also from atmospheric reanalyses [e.g., *Trenberth and Guillemot*, 1995; *Mo and Higgins*, 1996]. Satellite observations with near-global coverage and fine temporal and spatial resolution have shown great promise in improving the estimation of Θ. Figures 5a and 5b show the satellite-derived mean vector field of Θ superimposed on the mean flux divergence ($\nabla \cdot \Theta$) for January and July. The Θ fields are constructed from the combined use of multiple satellite observations, including near-surface wind vectors from QuikScatterometer (QuikSCAT), cloud drift wind vectors from the Multi-angle Imaging Spectroradiometer (MISR) and geostationary satellites, and precipitable water from SSM/I [*Xie et al.*, 2008]. The transport of moisture integrated over the depth

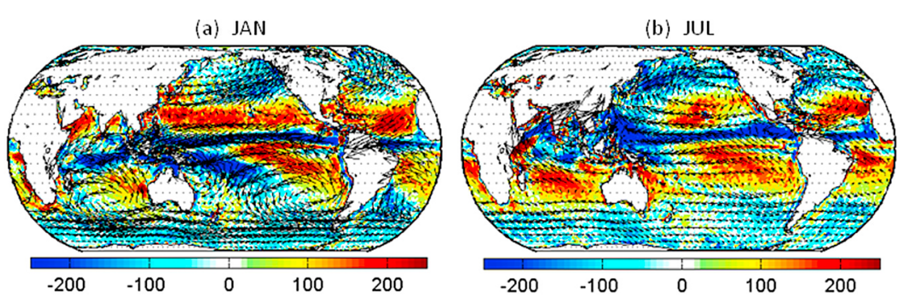

Figure 5. Vector field of the vertically integrated total horizontal flux of water vapor Θ (unit: kg/m/s) superimposed on the flux divergence ($\nabla \cdot \Theta$; unit: cm/yr) for (a) January and (b) July. Data are from *Xie et al.* [2008] for 1999–2008.

of the atmosphere estimated over oceans using satellite data was validated using independent daily rawinsonde observations (a total of 28,408 rawinsonde observations), monthly mean reanalysis data, and regional water balance [*Xie et al.*, 2008]. The means (standard deviations) of the differences between the two values of Θ obtained from rawinsonde and satellite data were -2.75 kg/m/s (69.83) for $\Delta\Theta x$, and -8.58 kg/m/s (60.16) for $\Delta\Theta y$. The correlation coefficients between Θ from rawinsonde and Θ from satellite were 0.948 for $\Delta\Theta x$, and 0.867 for $\Delta\Theta y$. By comparing time series at individual rawinsonde stations it is seen that the satellite data capture not only the seasonal changes but also the synoptic variations of the observations. Values of Θ from the National Centers for Environmental Prediction (NCEP) reanalysis data furthermore showed significant correlation (with a correlation coefficient greater than 0.9 in most areas) with Θ from satellite data over global oceans.

[19] There is a good agreement between the geographical distributions of $\nabla \cdot \Theta$ in Figures 5a and 5b and *E-P* in Figures 2e and 2f, demonstrating that, averaged over time, the rate of change of water storage is small, and *E-P* is largely balanced by $\nabla \cdot \Theta$. Throughout the year, the transport of water vapor in the tropics is characterized by a broad band of easterly transport in the Atlantic Ocean and the central and eastern Pacific and by a seasonal reversal of direction in the Indian Ocean and its vicinity, in association with monsoons [*Peixoto and Oort*, 1992]. Outside the tropics, water vapor is transported poleward.

2.3. Long-Range Transport of Water Vapor

[20] As shown in Figure 5, the strong easterly fluxes of moisture in the tropics are due to the highest global values of precipitable water. Almost equally strong fluxes occur around the major subtropical anticyclones in the summer hemisphere, and year-round strong westerly and northwesterly fluxes are found in the midlatitude stormtrack. However, while the tropical and subtropical fluxes are quasi-permanent in nature, with relatively little daily variation, the averaging in Figure 5 masks strong daily variability at the midlatitudes.

[21] At any time, there are typically three to five major conduits in each hemisphere, each of which transports large amounts of water vapor in narrow streams from the tropics to the higher latitudes. *Newell et al.* [1992] termed these conduits "atmospheric rivers" (ARs), because they transport water at volumetric flow rates similar to those of the world's largest rivers. These structures account for most of the long-distance transport of water vapor and contain 95% of the meridional flux of water vapor at latitude 35° [*Zhu and Newell*, 1998; *Ralph et al.*, 2004]. In contrast to terrestrial rivers, however, these conceptual ARs change course every day with shifting synoptic patterns, and it is only their net effect (moisture transport from the (sub)tropics east-northeastward to the high midlatitudes) that can be seen in Figure 5. The term "atmospheric river" is not universally accepted, and others have suggested different names such as "moisture conveyor belt" [*Bao et al.*, 2006] or "tropical moisture export flow" [*Knippertz and Wernli*, 2010]. In their objective climatology, *Knippertz and Wernli* [2010] showed that such exports of tropical moisture are most frequent in four particular regions of the Northern Hemisphere, namely (1) the "Pineapple Express," which connects tropical moisture sources near Hawai'i with precipitation near the North American West Coast and has a marked peak in activity in boreal winter; (2) over the western Pacific in summer; (3) over the Great Plains of North America, starting over the Gulf of Mexico and the Caribbean Sea and peaking in summer and spring; and (4) over the western North Atlantic, with a maximum in winter and fall. Some of these ARs (like the example shown in Figure 6) cause extreme precipitation and floodings over those regions (e.g., the 1993 and 2008 floods over the central United States [*Dirmeyer and Kinter*, 2009], flooding in western Washington [*Neiman et al.*, 2011], in California [*Ralph and Dettinger*, 2011], in the UK [*Lavers et al.*, 2011], and in Norway [*Stohl et al.*, 2008]).

2.4. Limitations of Available Data Sets and Uncertainties in the Estimation of the Components of the Water Budget

[22] Over continental regions, a high density of precipitation data is available, including for most of Europe, the United States, Australia and some parts of Asia. For large parts of Africa, continental South America, and some regions in Asia and northern North America, however, data are more scarce [*New et al.*, 2001]. Prior to the advent of satellites, over the oceans all data were collected using shipborne in situ measurements. The ability of radiosondes to measure water vapor accurately has improved over time [*Dai et al.*, 2011], although gaps in coverage and missing data remain problems to be overcome.

[23] *Schanze et al.* [2010] reviewed the temporal evolution of the availability of data (Table 2) in order to improve understanding of historical limitations to data sets. Although high-resolution SST data became available as early as 1978, and continuously available from 1982 onward, the accuracy of observations from the advanced very high resolution radiometer (AVHRR) was significantly improved by a database that matched these observations to buoy data; this process of cross-checking began in 1985 [*Smith et al.*, 1996]. The Defense Meteorological Satellite Program's (DMSP) first SSM/I instrument became operational in July 1987 [e.g., *Robinson*, 2004, and references therein]. This sensor brought about several improvements to the reliability of the variables used in the data sets of both evaporation and precipitation. For evaporation, for example, SSM/I was the first satellite to provide estimates of sea surface roughness, and consequently of wind speed [*Goodberlet et al.*, 1990], as well as specific surface humidity and precipitation from estimates of TCWV [*Chou et al.*, 2003].

[24] For tropical regions, it is possible to use infrared measurements from geostationary satellites to provide estimates of precipitation because a strong correlation exists between the height and temperature of the top of tropical clouds and precipitation [e.g., *Adler et al.*, 2003, and references therein]. However, such observations are spatially limited to the area over which the satellite is positioned, and

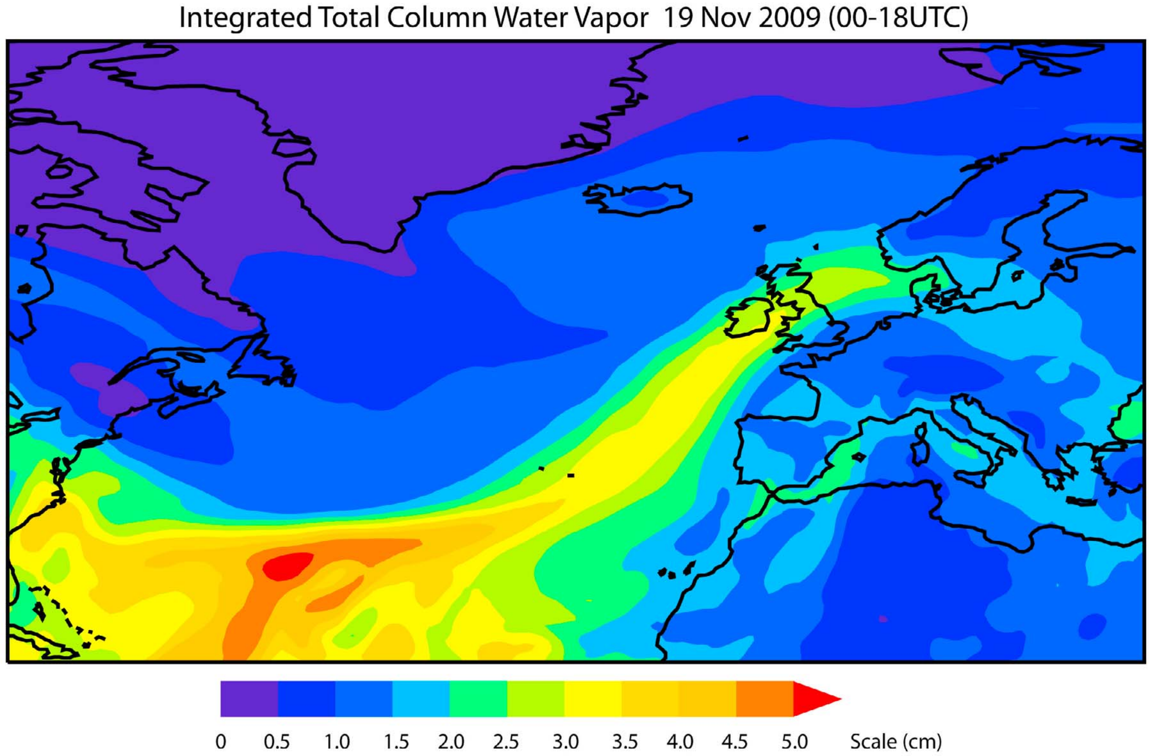

Figure 6. Daily integrated total column of water vapor showing the AR that affected the UK on 19 November 2009. Data: ERA-Interim.

uncertainties increase toward higher latitudes [*Schanze et al.*, 2010].

[25] Hence, various "merged" satellite and gauge analyses have been made in an attempt to maximize the benefits of using both satellite and gauge measurements of precipitation [e.g., *Adler et al.*, 2003; *Xie and Arkin*, 1997]. Uncertainties associated with measurements of precipitation collected by gauge with careful maintenance should be less than about 10% for liquid precipitation but can be much larger for satellite retrievals and for solid forms of precipitation.

[26] The incompleteness of records reduces the accuracy of estimates of freshwater discharge from the land to oceans [*Di Baldassarre and Montanari*, 2009; *Legates et al.*, 2005]. Furthermore, nonriverine flows that connect to coastal surface waters, such as from submarine groundwater discharge or seawater inflow, have not been adequately observed [*Michael et al.*, 2005]. Consequently, few global analyses of riverine outflow have been made to quantify the freshwater discharge from the land to the oceans [*Dai and Trenberth*, 2002; *Wang and Dickinson*, 2012].

[27] The Gravity and Climate Experiment (GRACE) satellite [*Tapley et al.*, 2004a, 2004b] was launched in 2002 and allows estimates to be made of the change in terrestrial water storage on a regional and global scale. The spatial low-resolution (∼200 km) gravimetric data are adequate for studies of large basins, but it does not provide reliable estimates for medium-scale river basins [*Werth and Güntner*, 2010]. GRACE also has problems with near-coastal rivers and watersheds because of coastal "leakage."

[28] The basic theories used by the scientific community to estimate evapotranspiration are the Monin-Obukhov similarity theory, the Bowen ratio method, and the Penman-Monteith equation. The advantages and disadvantages of the six major methods of measuring evapotranspiration (EC, BR, weighable lysimeters, scintillometer, surface water balance,

TABLE 2. Date of First Continuous Availability of Different Data Sources[a]

Data	Variable	Source	Available
E	All	In situ and NWP	1948
	T_{sea}	AVHRR	1985[c]
		AMSR-E[b]	2002
	U_{air}	SSM/I	1987
		QuikSCAT	1999
	T_{air}	In situ/NWP only	1948
	Q_{air}	SSM/I	1987
		AIRS[b]	1999
P	P_{total}	In situ and NWP	1948
		OPI	1979
		GPI	1986
		SSM/I	1987
		TOVS	1987
		TRMM-TMI[b]	1997

[a]In situ measurements prior to 1948 are not considered. Only commonly used satellite missions that have enhanced the data quality significantly are listed. New sources are only listed if they provide a potential significant advantage in the future.

[b]These data sources are not commonly used in order to preserve data homogeneity.

[c]Even though AVHRR was first launched in 1978 and was fully operational from 1981 onward, sufficient buoy data to constrain the data only became available after 1985. From *Schanze et al.* [2010].

and atmospheric water balance) were summarized in Table 1 [*Wang and Dickinson*, 2012]. While surface- and satellite-based measurement systems can provide accurate estimates of the diurnal, daily, and annual variability of evapotranspiration, their reliability for longer timescales is poor. The surface water budget method can provide a reasonable estimate of global mean evapotranspiration, but its regional distribution is still rather uncertain. Current land surface models provide widely differing values for the ratio of transpiration by vegetation to total evapotranspiration. This source of uncertainty therefore limits the ability of models to provide the sensitivities of evapotranspiration to precipitation deficits and changes in land cover. Recent evaluations of global evapotranspiration using different methodologies indicate great uncertainty across the data sets, of the order of 50% of the global annual mean value [*Vinukollu et al.*, 2011].

[29] Advances in computer technology have allowed the use of computational fluid dynamics and numerical weather prediction for large data assimilation reanalysis projects, such as the NCEP Global Reanalysis Project 1 [*Kistler et al.*, 2001], hereafter NCEP-1, available from 1948 to the present, the NCEP Global Reanalysis Project 2 [*Kanamitsu et al.*, 2002], hereafter NCEP-2, which uses only satellite data for the whole of the period of analysis (1979–present), the Modern Era Retrospective-Analysis for Research and Applications [*Bosilovich et al.*, 2006], hereafter MERRA (1979–present), the European Centre for Medium-Range Weather Forecasts (ECMWF) Re-Analysis 40 [*Uppala et al.*, 2005], hereafter ERA-40, which is available for 1957–2002, and the ERA-Interim data set [*Dee et al.*, 2011].

[30] However, the homogeneity of any reanalysis model is strongly dependent on the homogeneity of the input data [e.g., *Schanze et al.*, 2010; *Trenberth et al.*, 2011], which can be demonstrated by the climatological discontinuities due to the introduction of satellite data in the NCEP-1 reanalysis [*Sturaro*, 2003], as well as in ERA-40 [*Sterl*, 2004]. *Schanze et al.* [2010] evaluated the current quantification of the oceanic freshwater cycle using new observations from satellite data and reanalysis models for evaporation and precipitation over the oceans. They found discontinuities in the year 1987 for all data sets, which they attributed to the launch of the SSM/I microwave imaging satellite. There are considerable variations in the precipitation obtained from reanalyses that incorporate moisture from satellite observations; such variations are a reflection of the changes in the observational system used [*Trenberth et al.*, 2011]. These changes also affect the quality of the satellite-derived evapotranspiration data set [*Vinukollu et al.*, 2011], as well as the estimation of evaporation via reanalysis models, because this is estimated using bulk flux formulas. The surface variables required for a bulk flux formulation must be estimated from finite values of moisture and temperature for a given layer, which can change over time as satellite instruments change [*Schlosser and Houser*, 2007]. In the high-latitude extratropics, where remote sensing is much less reliable, studies have shown that the oceanic satellite estimates of precipitation are less accurate when compared with reanalysis data [e.g., *Sapiano et al.*, 2008]. The greatest uncertainties relative to the mean annual evapotranspiration are in transition zones between dry and humid regions and monsoon regions [*Vinukollu et al.*, 2011].

[31] A key source of uncertainty in the reanalysis data is the possible violation of the freshwater cycle, because the underlying prediction models are generally forward integrating [*Wunsch and Heimbach*, 2007]. The moisture budget is generally not closed in the reanalyses owing to the analysis increment that arises from errors in the state variable fields and observational uncertainties and also a very small term that represents a negative filling to ensure that values of q and w are positive definite [*Trenberth et al.*, 2011]. Although the reanalyses produce quite good results for precipitation over land, over the ocean E, P, and E-P based on model output are not stable [*Trenberth et al.*, 2011]. The poorer representation of coastlines and orography may be a source of uncertainty in low-resolution reanalyses. When coastal ranges are too smooth, the onshore advection of moisture can be excessive [*Trenberth et al.*, 2011].

[32] Most reanalysis models, with the exception of MERRA, predict water cycling (P and E) that is too intense over the ocean, although ocean-to-land transports are very close to their observed values [*Trenberth et al.*, 2011]. The results from all the available reanalyses for the main atmospheric components of the hydrological cycle are given in Figure 7 for 2002–2008 [from *Trenberth et al.*, 2011]. All P ocean estimates are high relative to the estimate of GPCP. Apart from MERRA, E ocean estimates from reanalyses are also high when compared with the reference values used herein.

[33] Recent reanalyses make use of either a four-dimensional system of data assimilation [e.g., *Simmons et al.*, 2010] or an incremental analysis update technique [*Bloom et al.*, 1996], both of which allow the analyzed fields to evolve smoothly in time, rather than in sudden jumps at times of analyses, which reduces the spin-up problem in simulations of the hydrological cycle [*Trenberth et al.*, 2011].

[34] As part of the World Climate Research Program's (WCRP) Global Energy and Water-Cycle Experiment (GEWEX) Continental-scale International Project (GCIP), a preliminary water and energy budget synthesis (WEBS) was developed by *Roads et al.* [2003] for the period 1996–1999 from the "best available" observations and models. According to these authors, observations cannot adequately characterize budgets because too many of the fundamental processes are missing. Models that properly represent the many complex atmospheric and near-surface interactions are also required.

3. SOURCES AND SINKS OF ATMOSPHERIC MOISTURE

3.1. Methods Used to Establish Source-Receptor Relationships

[35] Three principal methods are available for identifying the source and sink regions of atmospheric moisture, namely analytical or box models, numerical water vapor tracers, and physical water vapor tracers (isotopes).

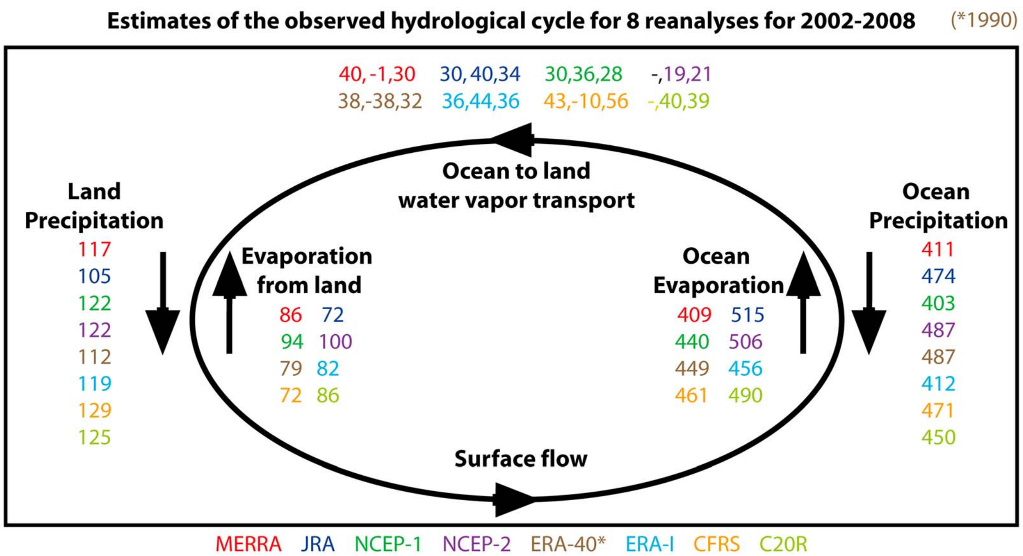

Figure 7. Estimated values of the observed hydrological cycle using eight reanalyses for 2002–2008, with the exception for ERA-40, which starts from 1990 (color coded as given at the bottom of the figure). For the ocean-to-land water vapor transport, the three estimates given for each are (1) the actual transport estimated from the moisture budget (based on analyzed winds and moisture), (2) *E-P* from the ocean, and (3) *P-E* from the land, which should be identical. Units: 1000 km^3 yr^{-1}. Adapted from *Trenberth et al.* [2011].

3.1.1. Analytical or Box Models

[36] The underlying motivation for the development of analytical models to show the source and sink regions of atmospheric moisture has historically been an understanding of how changes in the surface hydrology of a region, due to anthropogenic influences or natural variability, are likely to modify the climate through changes in the water cycle [*Eltahir and Bras*, 1996; *Brubaker et al.*, 1993].

[37] The earliest quantitative theory and analytical models of source-sink regions focused on the contribution of evapotranspiration to local precipitation, or precipitation recycling. All analytical models can be derived from the equation of the vertically integrated balance of water vapor (following the review of *Burde and Zangvil* [2001a]):

$$\frac{\partial(w)}{\partial t} + \frac{\partial(wu)}{\partial x} + \frac{\partial(wv)}{\partial y} = E - P, \qquad (7)$$

where w is the amount of water vapor contained in a column of air of unit base area, u is the vertically integrated zonal water vapor flux divided by w (this is equivalent to a water vapor-weighted zonal wind), v is the water vapor weighted meridional wind, E is evaporation, and P is precipitation. The equation can be used separately for moisture entering the region from the outside (advection) and for moisture originating within it (recycling). *Budyko and Drozdov* [1953] and later (in English) *Budyko* [1974] developed a model by assuming the following: (1) a negligible change in storage of atmospheric water, (2) a one-dimensional (1-D) estimation of recycling, and (3) a well-mixed atmosphere. Considering the basic equation of the conservation of mass, assumptions (1) and (2) imply that the first and third terms in equation (7) may be neglected. This is then a simple 1-D estimate of the recycling that takes place within a region (see *Burde and Zangvil* [2001a] for a derivation of the model). After Budyko's initial conceptualization, a number of authors have developed models to expand and improve the quantification of precipitation recycling. The initial 1-D approach was later extended to two dimensions [*Brubaker et al.*, 1993; *Eltahir and Bras*, 1996; *Burde and Zangvil*, 2001a, 2001b; *Savenije*, 1995]; however, all these models continued to work on monthly or longer timescales, and hence the first term in equation (7) could be neglected. *Dominguez et al.* [2006] later developed the "Dynamic Recycling Model (DRM)" in which the assumption of negligible moisture storage was relaxed, and the model could then be used at timescales shorter than a month. In the DRM, equation (7) is solved in a Lagrangian framework, and the local recycling ratio R (the amount of precipitation for a particular cell that originates as evapotranspiration within the selected region) is

$$R = 1 - \exp\left[-\int_0^{\tau} \frac{E}{W} d\tau'\right], \qquad (8)$$

where E is evapotranspiration and W is precipitable water, calculated at different times τ, following the trajectory of the parcel. When applied to monthly timescales, the DRM estimates very similar spatial and temporal variability of recycling to the *Brubaker et al.* [1993] and *Eltahir and Bras* [1996] models, but the estimates are slightly higher. In addition, the DRM can be used to calculate particular source and sink regions of precipitation [*Dominguez et al.*, 2008], making it more versatile than the traditional bulk models. At about the same time, *Burde et al.* [2006] relaxed the assumption of a well-mixed atmosphere by accounting for the "fast" recycling that takes place when the precipitation that originates from evapotranspiration does not mix with advected moisture. This model can be used in regions where the ratios of recycled to total precipitation, and precipitable water, are known.

[38] The foregoing analytical models have generally been applied to specific regions at the subcontinental scale. The estimates of recycling are a function of the size of the area under consideration, where the recycling increases with the area considered. However, there is a strong logarithmic relationship between recycling ratio and area for different regions of the world [*Brubaker et al.*, 2001; *Dominguez et al.*, 2006; *Dirmeyer and Brubaker*, 2007], which allowed *Dirmeyer and Brubaker* [2007] to scale recycling to a common area and produce a meaningful global gridded analysis of the recycling ratio.

[39] An alternative approach is via the evaluation of the percentage of precipitation falling in a region that originates as continental evapotranspiration or "continental precipitation recycling ratio" (as opposed to "local" evapotranspiration). To do this, *van der Ent et al.* [2010] formulated a variation of the traditional analytical models using a numerical solution of the same underlying equation of atmospheric moisture balance (equation (7)). This formulation allows the estimation of the percentage precipitation of terrestrial origin at the global scale. Using this numerical approach, *Keys et al.* [2012] were able to delineate "precipitation sheds," or evaporation source areas that contribute moisture to precipitation downwind. Unlike terrestrial watersheds, precipitation sheds are variable in space and time. The concept of a precipitation shed is useful for understanding how precipitation in regions depends on upwind surface hydrological conditions.

3.1.2. Numerical Water Vapor Tracers

[40] The second method of studying source-sink regions makes use of numerical water vapor "tagged" tracers (WVT), which is also known as a water vapor "tagging" approach. We can divide these methods into Eulerian and Lagrangian. In the Lagrangian frame of reference the observer follows an individual fluid parcel as it moves through space and time. On the other hand, the Eulerian frame of reference focuses on specific locations in the space through which the fluid flows as time passes. Initially developed by *Joussaume et al.* [1984] and *Koster et al.* [1986], Eulerian tagging techniques not only yield information on recycled precipitation but also account for the specific origin and destination of advected moisture. Numerical tracers are implemented in GCMs and experience the same processes as atmospheric water. Because they are embedded in climate models, numerical WVT models incorporate state-of-the-art understanding of how moisture moves and is transformed as it passes through the atmosphere. *Bosilovich and Schubert* [2002] described the use of numerical WVTs specifically to address the question of recycling. In their study, as in the studies of *Koster et al.* [1986] and *Joussaume et al.* [1984], passive constituents in the GCMs are predicted forward in time, in parallel with the prognostic water vapor variable of the model. The prognostic equation for any given water vapor tracer follows:

$$\frac{\partial q_T}{\partial t} = -\Delta_3 \cdot (q_T V) + \left.\frac{\partial q_T}{\partial t}\right|_{\text{turb}} + (E_{\text{surf}})_T + f_c \left.\frac{\partial q_T}{\partial t}\right|_{\text{cond}} + f_R \left.\frac{\partial q_T}{\partial t}\right|_{\text{revap}} + f_{\text{RAS}} \left.\frac{\partial q_T}{\partial t}\right|_{\text{RAS}}, \tag{9}$$

which indicates that the changes in the water vapor tracer are affected by advection by winds, turbulence including convection (turb), evaporation in the source region of the tracer, condensation (cond), rain evaporation (revap) and redistribution by convection (RAS), and the f terms are proportionality relationships. One potential limitation of the numerical WVT approach is that the results depend on how realistically the numerical model can simulate all the relevant processes.

[41] During recent years, the use of Lagrangian methods has become popular for diagnosing the transport of moisture and, in particular, for determining the origin of moisture that precipitates in particular regions. At first, simple back trajectories from areas of precipitation were used to infer the origins of air masses [e.g., *D'Abreton and Tyson*, 1995]. Precipitation rates were calculated from the decrease of specific humidity along trajectories [*Wernli*, 1997] and then used to diagnose the origin of the moisture for heavy precipitation events [*Massacand et al.*, 1998]. *Dirmeyer and Brubaker* [1999] and *Brubaker et al.* [2001] combined large sets of back trajectories using gridded information on evaporation and precipitation rates (generally from reanalysis data), accounting for uptake and loss of moisture as the trajectories pass over these sources and sinks. In this method, described in *Dirmeyer and Brubaker* [1999], back trajectories are computed from each grid square at which precipitation has occurred. Parcels are launched backward in time at a rate proportional to the precipitation, from a vertical location that is determined probabilistically depending on the moisture at that level. As a parcel (k) is tracked backward in time, the fraction of precipitable water (W) of the parcel assumed to have been contributed by surface evaporation (E) at point (x, y) at each time step (t) is

$$R_{i,k}(x, y, t) = \frac{E(x, y, t)}{W_i} \tag{10}$$

where $R_{i,k}(x, y)$ represents the evaporative contribution of surface grid (x, y) to the precipitable water that contributed to rainfall in grid box (i) from parcel (k). The total mass contribution of evaporation from grid square (x, y) to precipitation on an area A with a total of n grid squares is then calculated using all k parcels launched from A.

$$E_A(x, y) = \sum_{i=1}^{n} \sum_{k=1}^{k} \sum_{t=0}^{t_f} R_{i,k}(x, y, t), \tag{11}$$

where t_f is the ending time of the longest back trajectory calculation.

[42] This method allows a detailed budget of moisture along the trajectories and provides estimates of precipitation

recycling. However, unlike the Eulerian tracer methods, the transport of and changes in water vapor do not depend on the detailed physical equations of the underlying reanalysis model.

[43] Subsequently, *Stohl and James* [2004, 2005] developed an analog method that accounts for the net loss and/or gain of moisture along trajectories using

$$(e-p)_k = m\frac{dq}{dt}, \tag{12}$$

where $(e\text{-}p)_k$ are the rates of increase and decrease of moisture along the trajectory of each particle and (q) is the specific humidity taken from the meteorological (e.g., reanalysis) data, which are also used as input to the Lagrangian model. By filling the atmosphere with a large number of computational air particles, the surface freshwater flux in an area A can be determined using

$$E-P = \frac{\sum_{k=1}^{K}(e-p)_k}{A}, \tag{13}$$

where a budget is calculated for all K particles that reside above A. Thus, the surface freshwater flux $E\text{-}P$ can be accounted for, using information on the trajectories of the particles. Net loss or gain of moisture can be identified both along individual particle trajectories as well as on a regular grid, using only particle information. With this methodology, the evaporative source and sink regions for a given area can be identified and linked using the trajectory information.

[44] The method of *Stohl and James* [2004, 2005] differs from that of *Dirmeyer and Brubaker* [1999] in a number of respects: (1) the trajectory information is obtained from a particle dispersion model [*Stohl et al.*, 1998] and includes sub-grid turbulence [*Stohl et al.*, 2005], and (2) the only input to the moisture diagnostics is the change in specific humidity with time, while *Dirmeyer and Brubaker* [1999] use evaporation and precipitable water.

[45] One disadvantage of the *Stohl and James* [2004, 2005] method is that evaporation and precipitation are not clearly separable. Furthermore, the quantity ($E\text{-}P$) is obtained using the time derivative of humidity along the particle trajectories. In consequence, if the reanalysis data used to drive the model do not properly close the water budget (in fact, the analysis increment is often the dominant term in the budget), then the method may suffer from considerable inaccuracies. In fact this last inconvenience is shared with *Dirmeyer and Brubaker* [1999] method since this is based on calculated evaporation, which is probably the most uncertain term and it also does not close the water budget. Lagrangian methods have been used to study the origin of water that falls during extreme precipitation events [e.g., *Stohl et al.*, 2008; *Gustafsson et al.*, 2010]. However, these methods are also sufficiently computationally efficient to establish the climatologies of moisture source-receptor relationships [e.g., *Stohl and James*, 2005; *Gimeno et al.*, 2010a].

3.1.3. Physical Water Vapor Tracers

[46] Although analytical and numerical models are powerful tools for studying atmospheric recycling, they must be validated using physical measurements. The heavy stable isotopes of hydrogen and oxygen, D (deuterium) and ^{18}O in precipitation and/or water vapor, are ideal measurable parameters because they are an integrated product of both the history of an air mass and the specific prevailing meteorological conditions (temperature as well as humidity and wind speed) at the time of condensation [*Gat and Carmi*, 1970]. The isotopic compositions are usually denoted δD and δ^{18}O and expressed in parts per thousand (‰) relative to the standard mean ocean water (SMOW) composition. Because of differences in mass, mixtures of $H_2^{16}O$/$HD^{16}O$ and $H_2^{16}O$/$H_2^{18}O$ have different chemical and physical properties. Therefore, when the water changes phase, the heavy isotopes ($HD^{16}O$ and $H_2^{18}O$) become preferentially enriched in the liquid rather than the gas phase and in the solid rather than the liquid phase. This is called isotopic fractionation. Phase changes always occur during the circulation of atmospheric water, and geographical and temporal differences in isotopic ratios therefore emerge in vapor and precipitation. It is noteworthy that no fractionation occurs between the water taken up by and transpired from plants because of the fact that isotopic fractionation actually occurs against leaf water.

[47] By adding the isotopic processes in the analytical and numerical models and by comparing modeled and measured isotopic composition in precipitation and/or water vapor, one can directly validate the model's transport processes. These types of validation are common, both in studies of atmospheric vapor cycling during large-scale transport (e.g., *Yoshimura et al.* [2004], where large-scale moisture flux in major reanalysis products is validated) and for in-cloud processes [e.g., *Blossey et al.*, 2010], where isotopic processes associated with all microphysical interactions were incorporated in a cloud-resolving model. Furthermore, recycling due to transpiration in Amazonia was suggested by *Salati et al.* [1979] using evidence of a decrease of isotopic depletion with distance from the coast. This was revisited by *Henderson-Sellers et al.* [2002] in their investigation of the deforestation and warming in Amazonia.

[48] Notice, however, that two additional isotopic tracers are not sufficient to constrain all influencing processes. Furthermore, the isotopic fractionations during evaporation from surface water [*Craig and Gordon*, 1965; *Merlivat and Jouzel*, 1979] and from falling droplets in a cloud [*Stewart*, 1975], as well as the reevaporation from land and plant surfaces are often not described accurately by available parameterizations.

[49] Isotopic data related to precipitation have been collected since the 1960s. With the worldwide effort led by the International Atomic Energy Agency/World Meteorological Organization (IAEA/WMO), *Dansgaard* [1964] suggested a temperature effect, a latitudinal effect, an altitude effect, and an amount effect on isotopic composition. These effects have been repeatedly confirmed by others following different observational studies. *Friedman et al.* [1992] measured the isotopic composition of precipitation samples at numerous sites in southeastern California over a 7 year period, and based on seasonally integrated samples, they suggested that atmospheric circulation is likely to be the leading cause of

isotopic variability. Other studies have also shown that the isotopic composition of rain in individual storms is closely tied to a storm's trajectory [*Benson and Klieforth*, 1989; *Friedman et al.*, 2002; *Ingraham and Taylor*, 1991]. Isotopic variability among storms also results from local meteorological conditions [*Coplen et al.*, 2008], and much of this variability has to do with dynamical processes during a storm's evolution in addition to the isotopic variability of the vapor source, because of changes in wind speed/direction [*Fudeyasu et al.*, 2008; *Yoshimura et al.*, 2008].

[50] Stable water isotopes are also a useful tool for partitioning fluxes of evaporation and transpiration at the ecosystem scale and their use has been steadily increasing [*Moreira et al.*, 1997; *Yakir and Sternberg*, 2000; *Yepez et al.*, 2003; *Williams et al.*, 2004; *Yakir and Wang*, 1996; *Wang and Yakir*, 2000; *Ferretti et al.*, 2003; *Yepez et al.*, 2007]. Evaporation and transpiration fluxes have distinctive isotopic compositions. Evaporated water is significantly lighter than transpired water because when the latter leaves the stomata, it remains isotopically closer to that taken up by the plant because unfractionated water is continuously being replenished through the stem; in fact when transpiration is at isotopic steady state (ISS) there is no isotopic fractionation and the isotopic composition of transpired vapor can be the same as that of the stem water [*Farquhar and Cernusak*, 2005]. On the other hand, evaporation from the soil and wet surfaces is heavily fractionated as lighter isotopes are preferentially transferred to the vapor phase [*Craig and Gordon*, 1965].

[51] Until recently, observations of the isotopic composition of water vapor were severely lacking because traditional isotopic measurement techniques are somewhat complex (e.g., the cryogenic method). Recent advances in remote sensing of vapor isotopes from satellites, particularly HDO (heavy water where one proton is replaced by deuterium), have dramatically increased the availability of observed data. After *Zakharov et al.* [2004] first retrieved latitudinal climatology for column vapor HDO using IMG (the Interferometric Monitor for Greenhouse gases sensor) on ADEOS (Advanced Earth Observing Satellite), *Worden et al.* [2006] then retrieved data on low-level atmospheric vapor HDO. Over tropical regions at fine temporal and spatial resolutions using TES (Tropospheric Emission Spectrometer) on the satellite Aura, *Payne et al.* [2007] retrieved monthly data on the global distribution of upper troposphere and stratosphere vapor HDO using MIPAS (the Michelson Interferometer for Passive Atmospheric Sounding) on Envisat (environmental satellite), and *Frankenberg et al.* [2009] measured the atmospheric column vapor deuterium ratio using SCIAMACHY (Scanning Imaging Absorption Spectrometer for Atmospheric Chartography), also on Envisat. Although some limitations remain in terms of spatial and temporal coverage, resolution, precision, and accuracy, the resulting maps have improved the general understanding of the distribution of isotopes and the physical processes that trigger the isotopic distributions. It is also worth mentioning that remote sensing has been widely used with several ground-based Fourier transform spectroscopy instruments, which are essentially the same as those on satellites [e.g., *Schneider et al.*, 2010]. Recently, precise optical analyzers for in situ HDO measurements have become available [e.g., *Lee et al.*, 2006; *Welp et al.*, 2008]. The combination of these new measurements from satellites and ground truth observations will provide a wealth of information for future studies.

[52] The isotope-incorporated atmospheric general circulation models (AGCMs) initiated by *Joussaume et al.* [1984] have recently gained in popularity [e.g., *Yoshimura et al.*, 2008; *Risi et al.*, 2010a]. The work of the stable water isotope modeling intercomparison group (SWING) is now into its second phase, and there are more than ten isotope-incorporated AGCMs and a few regional climate models (RCMs) used for this purpose [*Noone and Sturm*, 2010]. By combining the recent vapor isotope observations described above with AGCM results, *Risi et al.* [2010b] pointed out the potential of isotopic information to find areas of misrepresentation of the model in terms of dehydrating processes in the Sahel region associated with the subsidence of the Hadley cell. Similarly, *Yoshimura et al.* [2011] showed the large-scale agreement between the AGCM and the satellite-based vapor isotopic distributions. They concluded that the parameterization for reevaporation from a falling droplet in a convective cloud affected the isotopic composition in the mid-troposphere over the Maritime Continent (Figure 8).

3.1.4. Intercomparison of the Source-Receptor Methods

[53] The establishment of the source-receptor relationship may often be best achieved in an integrated manner, using the results gathered from several of the different methods described herein. The use of Eulerian fields provides the large-scale characteristics of circulation involved in the transport and together with numerical WVT is constrained by the input data, which in turn depend on the numerical models. Lagrangian models may be used to assess the geographical origin of moisture that reaches a region. Physical WVTs (isotopes) are very useful for model validation. Table 3 summarizes the main advantages and disadvantages of each methodology. To illustrate the main points, two continental regions were chosen in order to compare results obtained using the different methods, namely Spain and the Orinoco River basin. The first region is located in the extratropics, with the extratropical storm track being the principal mechanism of precipitation [*Trigo et al.*, 1999]; and the second is located in the tropics, where the displacement of the ITCZ is the dominant factor in the precipitation regime [*Poveda et al.*, 2006]. Information on the sources of moisture derived from the different methods (box models, Eulerian fields, numerical WVT and isotopes) for these two regions is shown in Figures 9 and 10. This allows us to contrast the detail provided by each type of method and to show the complementary nature of the information. It is also of some interest to note the differences between a region where a vast number of specific studies and observational networks is available (Spain) and a region where observations and detailed analyses have historically been few (Orinoco River basin).

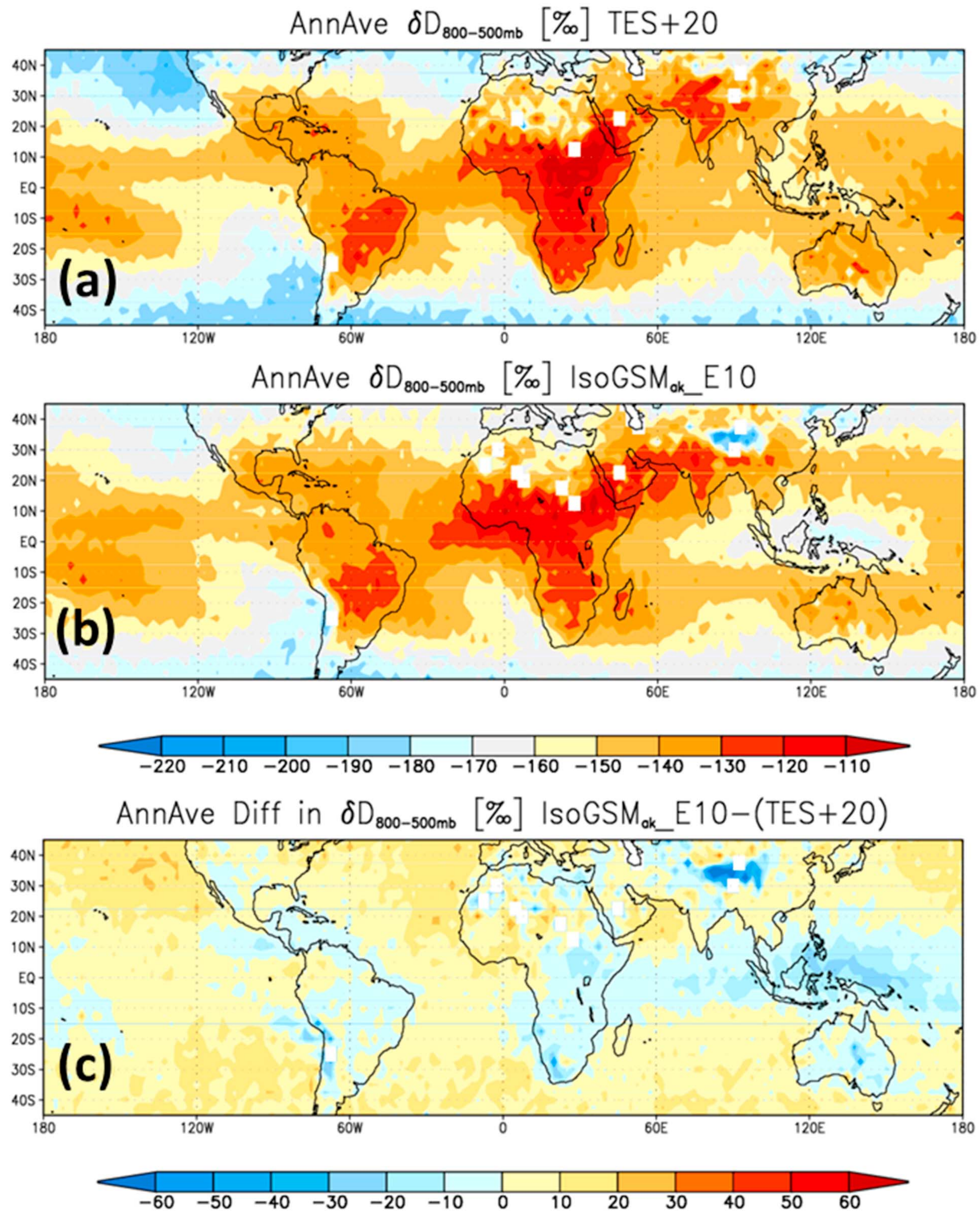

Figure 8. (a) Mean climatology of δD in midtropospheric water vapor (800 to 500 hPa pressure) for TES; (b) sensitivity simulation (E10) with an isotope-incorporated AGCM (IsoGSM), in which isotopic fractionation with reevaporation from falling droplets in convective clouds is more suppressed; (c) difference between the satellite measurements and model simulation. The global-scale biases in TES are arbitrarily corrected by +20‰ (indicated by "TES + 20"). Adapted from *Yoshimura et al.* [2011].

TABLE 3. Summary of the Main Strengths and Weaknesses of Analytical Box Models and Physical and Numerical (Eulerian and Lagrangian) Water Vapor Tracer Method

Type		Strength	Weakness	References (Nonexhaustive)
Analytical Box Models		Simple as few parameters are required and they consider grid based spatial variability.	Neglects in-boundary processes; some are based on the well mixed assumption (the local source of water is well mixed with all other sources of water in the whole vertical column); most are only valid for monthly or longer timescales.	*Budyko* [1974]; *Brubaker et al.* [1993]; *Eltahir and Bras* [1994]; *Burde and Zangvil* [2001a, 2001b]; *Dominguez et al.* [2006].
Physical Water Vapor Tracers		Simplicity; global coverage; include vertical processes; reanalysis input data (high spatiotemporal resolution); enable the combination of GCMs and Lagrangian Rayleigh models.	Sensitivity of the isotopic signal; calculation time; availability of data for validation; does not account for convection and rainwater evaporation/equilibration.	*Gat and Carmi* [1970]; *Salati et al.* [1979]; *Rozanski et al.* [1982]; *Coplen et al.* [2008].
Numerical Water Vapor Tracers	Eulerian	Detailed atmospheric processes; realistic moisture circulation.	Dependent on the model bias; global forcing is required; poor representation of short-timescale hydrological cycle parameters; does not include the remote sources of water for a region.	*Benton and Estoque* [1954]; *Starr and Peixoto* [1958]; *Peixoto and Oort* [1982]; *Joussaume et al.* [1984]; *Koster et al.* [1986]; *Bosilovich and Schubert* [2002].
	Lagrangian	High spatial resolution moisture sources diagnostics; quantitative interpretation of moisture origin allowed; not limited by a specific RCM domain and spin-up; establishment of source-receptor relationship can be easily assessed because budgets can be traced along suitably defined trajectory ensembles; net freshwater flux can be tracked from a region both forward and back ward in time; realistic tracks of air parcels; computationally efficient compared to performing multiyear GCM simulations or reanalyses; more information provided than a purely Eulerian description of velocity fields; parallel use of information from Eulerian tagging methods allowed.	Sensitivity of moisture flux computations to increases in data noise for shorter time periods or smaller regions; simple method does not provide a diagnostic of surface fluxes of moisture; surface fluxes under (over) estimation if dry (cold) air masses tracking as the budget is not closed; evaporation rates are based on calculations rather than observations in some methods; evaporation and precipitation are not clearly separable (in some methods); movement and extraction of water does not depend on the physical tendencies included in the reanalysis data.	*D'Abreton and Tyson* [1995]; *Wernli* [1997]; *Massacand et al.* [1998]; *Dirmeyer and Brubaker* [1999]; *Brubaker et al.* [2001]; *Dirmeyer and Brubaker* [2006]; *Stohl and James* [2004, 2005].

[54] The analysis was carried out for the 5 year period from 2000 to 2004. Using ERA-Interim vertically integrated water vapor fluxes and vertically integrated moisture flux divergence with a horizontal resolution of 0.5 degrees, a simple box model method was applied within the borders of Spain to identify the origins of moisture from the moisture flux through the borders. Figure 9a shows that the main result is moisture inflow from the lateral boundaries, from the Mediterranean Sea to the east and from the North Atlantic to the west. The box model allows the identification of the moisture inflow and outflow, and its approximation is good, but it lacks information on the physical processes between the boundaries and may not be suitable for analyzing relatively small regions. Figure 9b shows the Eulerian fluxes, using ERA-Interim data from 2000 to 2004 on a 0.5° horizontal grid, in which the large-scale characteristics of the transport of moisture may be seen. Moisture from the surrounding water bodies and northern Africa is advected into continental Spain, as shown by the vectors of moisture flux. Regions of strong evaporation are shown in yellowish shades, while moisture sinks are shown in bluish colors, as the regions where precipitation is found to occur. This type of method is the most widely used in the literature for several regions of the globe because of the simplicity and availability of the analysis data sets. Specific information on the moisture related to precipitation over a determined region is not immediately available from these fields.

[55] "Long-term" $\delta^{18}O$ values from Global Network of Isotopes in Precipitation (GNIP) stations over Spain are shown in Figure 9c; the gradients of $\delta^{18}O$ between western coastal and inner Iberian Peninsula are in good agreement with the westerly circulation regime shown in Figure 9b, which supports the result from the Eulerian fluxes that the North Atlantic is a major source of moisture for precipitation

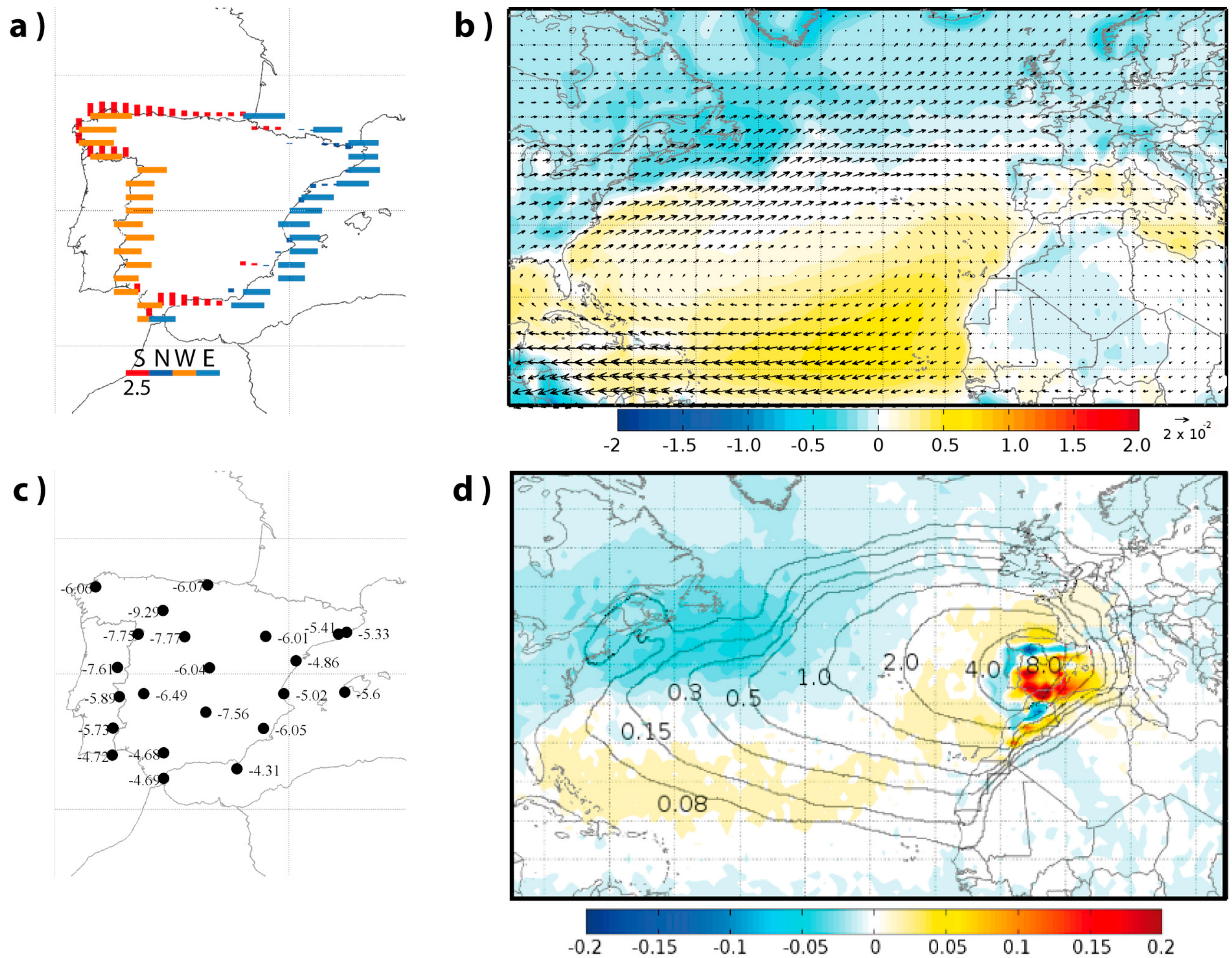

Figure 9. Comparison among the results obtained using different methods for the climatological mean pattern for 2000–2004 for Spain: (a) simple box model showing the moisture flux across the segments of zonal and meridional regional boundaries; (b) typical Eulerian field method using vertically integrated water vapor flux (shaded) and moisture flux vectors (black arrows); (c) long-term weighted delta^{18}O in precipitation in the GNIP stations; (d) identification of the sources of moisture using ten-day integrated net freshwater flux from FLEXPART backward trajectories (shaded contours) and from quasi-isentropic back trajectory analysis of atmospheric water vapor (solid lines) from *Dirmeyer and Brubaker* [2006]; see the atlas at http://www.iges.org/wcr. Data, Figures 9a and 9b: ERA-Interim 0.5° resolution.

over Spain. The gradient also shows the influence of the Mediterranean, again in agreement with the results from the box model and the Eulerian fluxes. Finally, Figure 9d shows the results for two trajectory methods: the contour lines show results obtained using quasi-isentropic back trajectories [*Dirmeyer and Brubaker*, 2007; see the atlas at http://www.iges.org/wcr], and the shaded colors show the results obtained using the Lagrangian FLEXPART model method of *Stohl and James* [2004], which accounts for the integrated net freshwater flux over 10 day periods. Both methodologies identify the patterns of the origins of moist air, but the quasi-isentropic approach cannot provide information on the “history” of the moisture variations along the trajectory, whereas the Lagrangian FLEXPART model method is able to show those areas where the particles along the trajectory gain moisture (evaporative sources of moisture, reddish colors in Figure 9d) or where they lose moisture (sinks, bluish colors). The difference, for the moisture sources of the Iberian Peninsula, is evident in an important part of the storm track area (latitudes higher than 30° in the Mid-Atlantic), which is considered to be a moisture source in the quasi-isentropic approach but not in the Lagrangian FLEXPART model. In the latter method, losses of moisture in these regions are much higher than uptakes; it is not a “true”source region for the Iberian Peninsula.

[56] The comparison for the Orinoco River basin is shown in Figure 10. Using a simple box model (Figure 10a), the importance of moisture inflow from the tropical Atlantic is highlighted, as is other inflow further inland. For the Orinoco River basin, the role of the tropical Atlantic as a principal source of moisture is well supported for the known circulation in the region. However, due to the proximity of the

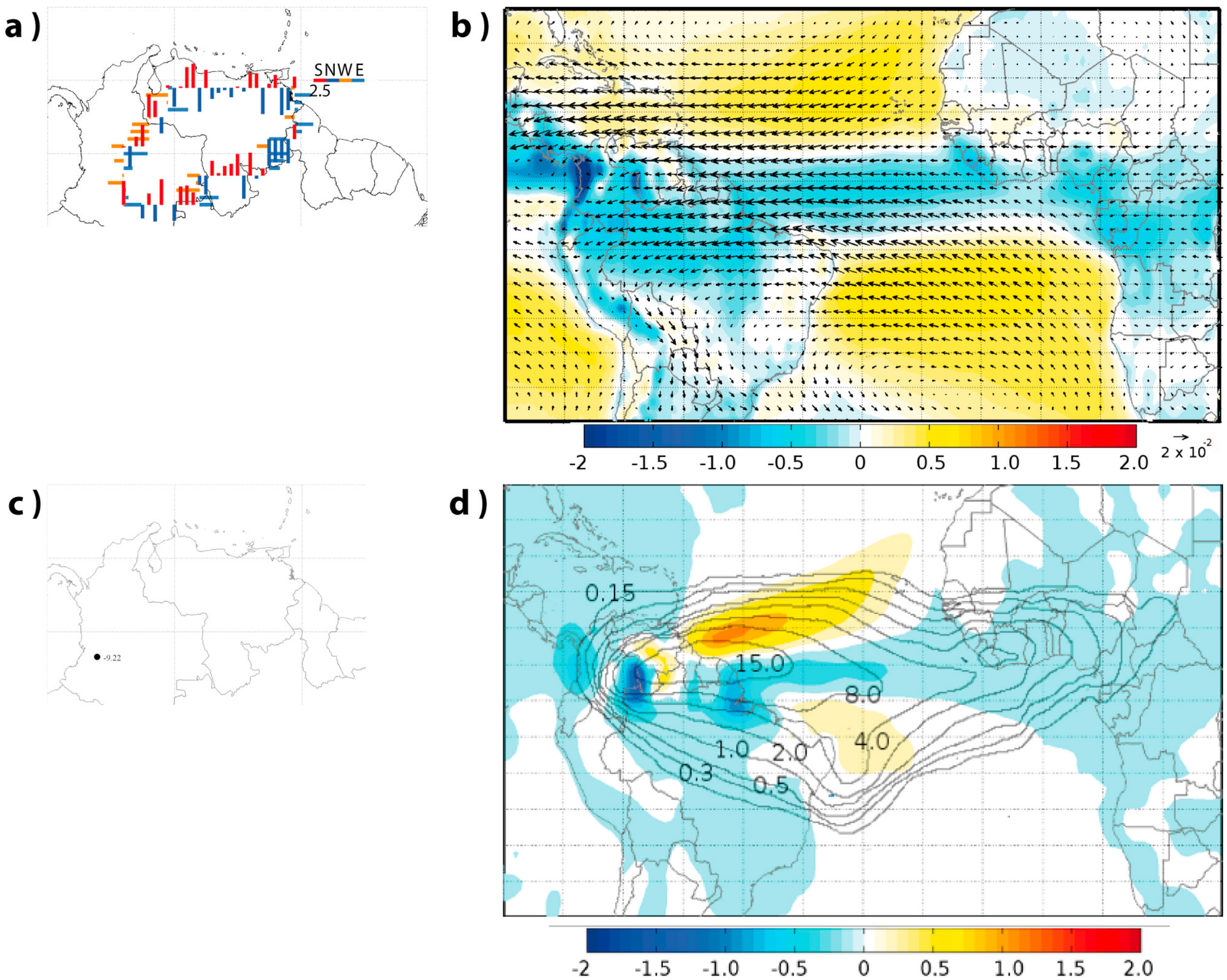

Figure 10. As Figure 9 but for the Orinoco River basin.

Amazon region, further detail is required in order to consider processes associated with recycling or even transport to the Amazon, which may exert an influence on the moisture patterns over the Orinoco River basin. From the Eulerian fluxes shown in Figure 10b, the fluxes into the Orinoco basin from the tropical Atlantic, as well as the importance of the inland fluxes, which connect the Orinoco and the Amazon basins can be noted. Isotopic data for the Orinoco basin is available for a single station (Figure 10c). The comparison between the quasi-isentropic trajectories and the Lagrangian FLEXPART model shows the marked differences between the two methods (Figure 10d). The identification of the origin of moisture in the first approach considers a broad picture of the source because the presence of the ITCZ is lacking. In the second case the presence of the ITCZ is shown in some detail, which is particularly important when studying climate in the tropics. The main difference between results from the method based on quasi-isentropic trajectories [*Dirmeyer and Brubaker*, 2007] and the method based on the Lagrangian FLEXPART model [*Stohl and James*, 2004] is due to the own objective of each method: the former diagnoses *E*, whereas the latter diagnoses *E-P*.

[57] Table 4 summarizes the results obtained with the various source-receptor diagnostics for two regions that have been studied in some detail, namely the Mississippi River basin and the Sahel region, again suggesting that the different methods provide complementary information.

3.2. Global Source and Sink Regions of Moisture

[58] The results of the last 20 years of work related to sources and sinks of precipitation using the methods described above provide us with an understanding of the ways in which global evapotranspiration contributes to precipitation. We will first summarize the results for precipitation of oceanic origin and then those for precipitation of terrestrial origin.

3.2.1. Oceanic Sources

[59] The principal oceanic sources of atmospheric moisture are summarized in Figure 11 (right). These areas were defined by *Gimeno et al.* [2011] using the threshold of 750 mm yr^{-1} for the climatological annual vertically integrated moisture flux divergence in the ERA40 reanalysis data set for the period 1958–2001 shown in Figure 11 (left) (only two sources of moisture were defined using the physical

TABLE 4. Summary of the Key Results Obtained From Selected Papers for the Mississippi River Basin and the Sahel Region Using Isotopes and Eulerian and Lagrangian Methodologies to Study the Source-Receptor Relationships

Method	Key Result	Reference
	Mississippi	
Isotopes	High evaporation in the lower Mississippi; locally derived groundwater is a source for nearby streams; latitudinal gradients in the Mississippi River valley are steeper during cold months.	*Kendall and Coplen* [2001]; *Vachon et al.* [2010].
Eulerian	Flood events have a strong link with local surface evaporation as recycling decreases while evaporation from the IAS is increased; the inflow of moisture from the south is dominated by the LLJ.	*Trenberth and Guillemot* [1996]; *Helfand and Schubert* [1995].
Lagrangian	Precipitation and recycling are correlated with evaporation at an interannual scale; evaporation is related to the moist and shallow PBL that provides moisture for convection; recycling is partly correlated with warm SSTs in the tropical Pacific Ocean; recycling and evaporation from the ocean are the dominant sources of moisture during spring whereas recycling is the dominant source during summer.	*Dirmeyer and Brubaker* [1999]; *Bosilovich and Chern* [2006]; *Brubaker et al.* [2001]; *Stohl and James* [2005]; *Gimeno et al.* [2010a].
	Sahel	
Isotopes	Recycling is the major source of moisture for precipitation; precipitation decreases at the onset of the monsoon as the ITCZ shifts northward from the Guinean coast to the Sahel.	*Bowen and Revenaugh* [2003]; *Bowen* [2009]; *Risi et al.* [2010a, 2008].
Eulerian	The Gulf of Guinea and its northern belt are a source of water vapor transported northward; moisture convergence and divergence patterns over northern Africa influence rainfall over sub-Sahara more than evaporation or moisture advection over/from over the adjacent oceans; recycling is a main source of precipitation over the Sahel in the "rainy" season; south of the Sahel, correlation between precipitation and evaporation is negative and large scale; evaporation over the Sahel peaks 1–3 days after precipitation, maximum contribution from small-scale processes occurs during the first day; over the western Africa two-thirds of rainfall at the seasonal scale being advected from the tropical Atlantic and central Africa, the remainder is recycling; moisture advected into WAM region originates in the Mediterranean Sea and central Africa; westerly moisture flux variability related to variations in the jet trigger variations in the content of low-level moisture, modulating atmospheric stability.	*Cadet and Nnoli* [1987]; *Druyan and Koster* [1989]; *Bielli and Roca* [2010]; *Gong and Eltahir* [1996]; *Fontaine et al.* [2003]; *Pu and Cook* [2011].
Lagrangian	Recycling was identified as the major source of moisture; important contributions from a band along the North Atlantic from the Sahel latitudes to the Iberian Peninsula coast; the Mediterranean Sea and the Red Sea are other important sources (note that these sources in some Lagrangian methods are likely erroneously large); there is a strong moisture uptake over the tropical South Atlantic following the fifth day of transport, including the Guinea Gulf, during summer; the Indian Ocean does not seem to be an important source, although it could have a minor influence during summer.	*Nieto et al.* [2006]; *Dirmeyer and Brubaker* [2006, 2007].

boundaries of oceanic basins, namely the Mediterranean and the Red Sea). Though the data and periods used in Figures 5 and 11 are different (multiple satellite observations for 1999–2008 [*Xie et al.*, 2008] and ERA40, for 1958–2001), the regions with higher vertically integrated moisture fluxes (reddish colors) occur over the same oceanic areas. The continental receptor regions of the evaporated moisture were obtained via forward tracking from the source areas using the Lagrangian method of *Stohl and James* [2004] (Figure 11, right, for the period 1980–2000). The productivity of the major oceanic sources of moisture is not evenly distributed, and some specific oceanic sources are responsible for more continental precipitation than others [*Gimeno et al.*, 2010a].

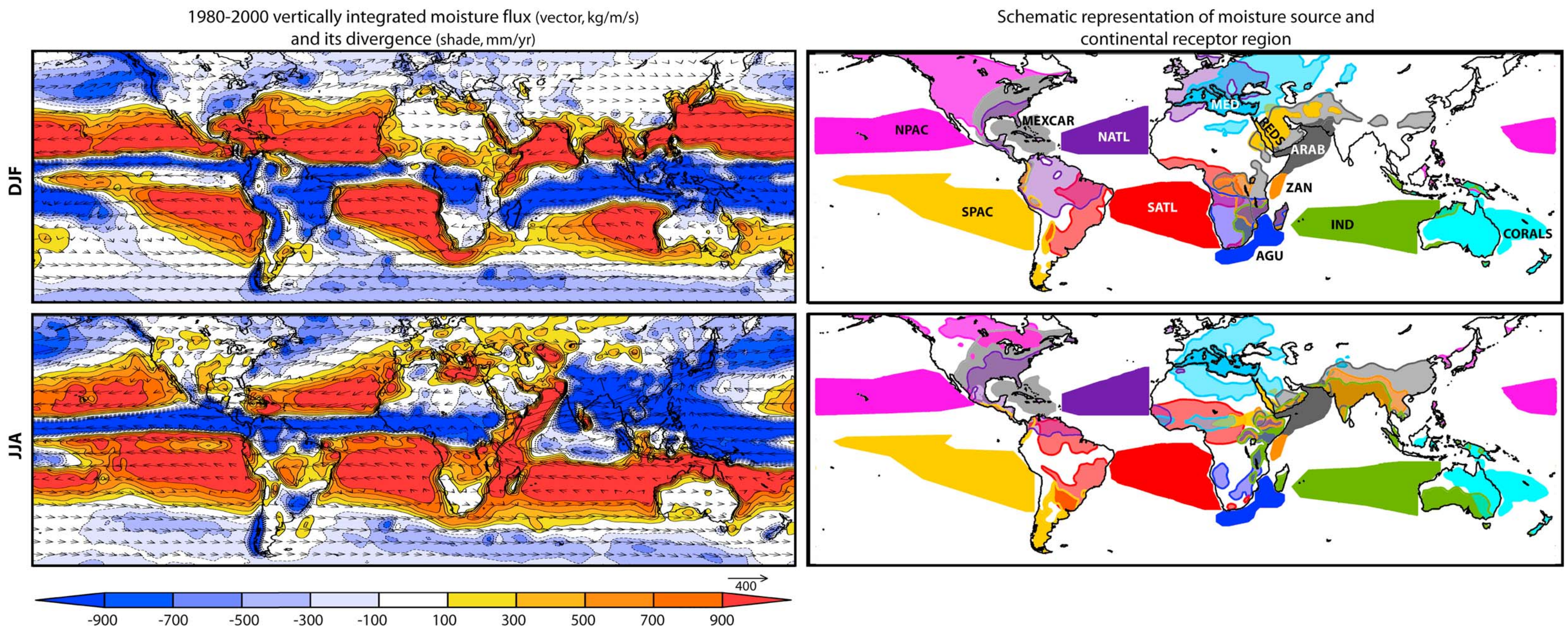

Figure 11. (left) The 1980–2000 vertically integrated moisture flux (vector; kg m^{-1} s^{-1}) and its divergence (contours; mm yr^{-1}) for JJA and DJF. Data: ERA40. (right) Schematic representation of moisture source and continental receptor regions for the period 1980–2000 for JJA and DJF. The sources of moisture (indicated in the bottom right panel) are as follows: NPAC, North Pacific; SPAC, South Pacific; NATL, North Atlantic; SATL, South Atlantic; MEXCAR, Mexico Caribbean; MED, Mediterranean Sea; REDS, Red Sea; ARAB, Arabian Sea; ZAN, Zanzibar Current; AGU, Agulhas Current; IND, Indian Ocean; CORALS, Coral Sea (as in *Gimeno et al.* [2010a]). Six of these source regions were defined using the threshold of 750 mm yr^{-1} of the annual vertically integrated moisture flux calculated for the period 1958–2001 using data from ERA40 for the oceanic sources. The Mediterranean Sea and the Red Sea were defined using their physical boundaries [from *Gimeno et al.*, 2010a]. Only negative values of *E-P* larger than -0.05 mm d^{-1} are plotted over the continents and are shown in the same colors as the corresponding oceanic source region. Overlapping continental regions are plotted with the appropriate shading mask. *E-P* fields are calculated by forward tracking from the moisture sources defined.

[60] Through net evaporation, the North Atlantic Ocean (NATL) is a relatively important source of water vapor, as evidenced by a higher surface salinity in this part of the Atlantic than in the Pacific [*Stohl and James*, 2005]. The subtropical NATL provides moisture for precipitation across an extremely large area that extends from Mexico to parts of Eurasia [*Drumond et al.*, 2011; *Gimeno et al.*, 2010b]. The NATL is also known to be an important source for many of the river basins that drain into it [e.g., *Nieto et al.*, 2008]. The NATL provides year-round moisture to both the continental area and the East Coast of North America, and is also of importance for western continental Europe and the British Isles. Because there are no large mountains along the Atlantic coast of western Europe, moisture is transported (mainly at low levels) deep into the interior of the Eurasian continent and also into the whole of the Mediterranean region during winter.

[61] The Mexican Caribbean Sea region (MEXCAR) is part of a complex and intriguing set of sources that contribute to precipitation over the Caribbean Islands, as well as to Central and North America. The MEXCAR is known for its importance in the transport of moisture to Central America [*Durán-Quesada et al.*, 2010], which is augmented by the presence of the Caribbean Low-Level Jet (CLLJ) [*Amador*, 2008; *Wang*, 2007]. The Gulf of Mexico is also under the influence of contributions of moisture from the MEXCAR, and this interaction between the air masses is of importance not only for the Gulf itself but also for the North American Great Plains. During late spring and summer, moisture from the MEXCAR, the Atlantic coast of Central America, the western Gulf of Mexico, and eastern Mexico and Texas all form an extended pattern that contributes moisture to extreme precipitation and flood events over the Midwestern United States [*Dirmeyer and Kinter*, 2009, 2010]. This fetch of moisture has been termed the Maya Express [*Dirmeyer and Kinter*, 2009] and is related to anticyclonic circulation around the Atlantic subtropical gyre.

[62] The South Atlantic (SATL) contributes to the moisture found over the South American east coast. Of particular importance here are the contributions to the northeastern part of Brazil, where regimes of extreme precipitation are observed [*Drumond et al.*, 2010; *Yoon and Zeng*, 2010]. The transport of moisture from the SATL to the Argentinean plains has also been shown to play an important role in the continental precipitation that occurs in this region [*Drumond et al.*, 2008]. Moisture from the SATL accounts for the development and maintenance of major cyclones in South America, where the precipitation associated with these systems primarily influences southern Brazil, Uruguay, and Argentina [*Reboita et al.*, 2010]. It is important to stress that the SATL is also a source of moisture for Antarctica [*Sodemann and Stohl*, 2009].

[63] Moisture from the North Pacific (NPAC) makes a seasonal contribution to the West Coast of North America. Contributions from the South Pacific (SPAC) contribute to moisture over the west coast of South America. However, the influence of the Pacific Ocean in the Americas is somewhat limited due to the presence of the Rocky Mountains (Andes) parallel to the West Coast of North (west coast of South) America that prevent moisture from the Pacific Ocean from penetrating very far into the American continent [*Peixoto and Oort*, 1992].

[64] Together with the Indian Ocean (IND), the Coral Sea (CORALS) represents the principal source of moisture for both Australia and Indonesia. The analysis of the dynamics of the moisture from the IND is not straightforward. It is presently suggested that the IND contributes moisture to East Africa, Australia, and Southern Asia. The contributions from the IND are involved in one of the most important of all tropical climate systems, namely the Indian Monsoon [*Krishnamurthy and Shukla*, 2000].

[65] Of key importance is the role of the Mediterranean (MED) as a moisture source for North Africa and specifically for the Saharan region. The Sahara and Sahel regions are under the influence of a complex system of transport to which both the Atlantic [*Knippertz and Martin*, 2005] and the MED contribute some moisture. In this case, the contributions are more significant at a seasonal scale, which is related to the onset of the West African Monsoon [*Cook*, 1999].

[66] Figure 11 also shows some interesting details. First, the highest net evaporation in an oceanic basin occurs in the Red Sea (REDS) [*Stohl and James*, 2005], providing large quantities of moisture that fall as precipitation (see also Figure 2) between the Gulf of Guinea and Indochina (from June to August, JJA) and between the African Great Lakes and Asia (from December to February, DJF). Second, there are vast regions of the globe where the influence of these major oceanic source regions is somewhat limited. Therefore, even though South Africa is situated adjacent to the Atlantic and Indian Oceans and is also located near the immense Southern Ocean, the only air masses that cause net precipitation here are those that reach it from the IND [*Stohl and James*, 2005], including the Agulhas Current (AGU). Another good example of large areas where major oceanic sources have a limited influence is Australia, where net precipitation during DJF occurs only from air masses that originate in the CORALS in the Pacific Ocean, but not from air masses that arrive from the IND, which contribute only during JJA over southern Australia.

[67] Regional results on sources of moisture extracted from the general picture shown in Figure 11 should be contextualized in the fact that they are based only on major oceanic source regions (fractions of the oceans). For a study that includes both major and also smaller source regions, it is necessary to identify the moisture that arrives in the selected target area. Figure 12 shows the moisture sources for selected continental areas, including the Sahel [*Nieto et al.*, 2006], Central Brazil [*Drumond et al.*, 2008], northeastern Brazil [*Drumond et al.*, 2010], Central America [*Durán-Quesada et al.*, 2010], the area over the Vostok ice core in the Antarctic [*Sodemann and Stohl*, 2009; *Nieto et al.*, 2010], the great Mississippi River [*Stohl and James*, 2005], the Norwegian west coast [*Stohl et al.*, 2008], the Indian Peninsula [*Ordóñez et al.*, 2012], and the Iberian Peninsula [*Gimeno et al.*, 2010b], as obtained using a backward tracking Lagrangian approach [*Stohl and James*, 2004]. The *E-P*

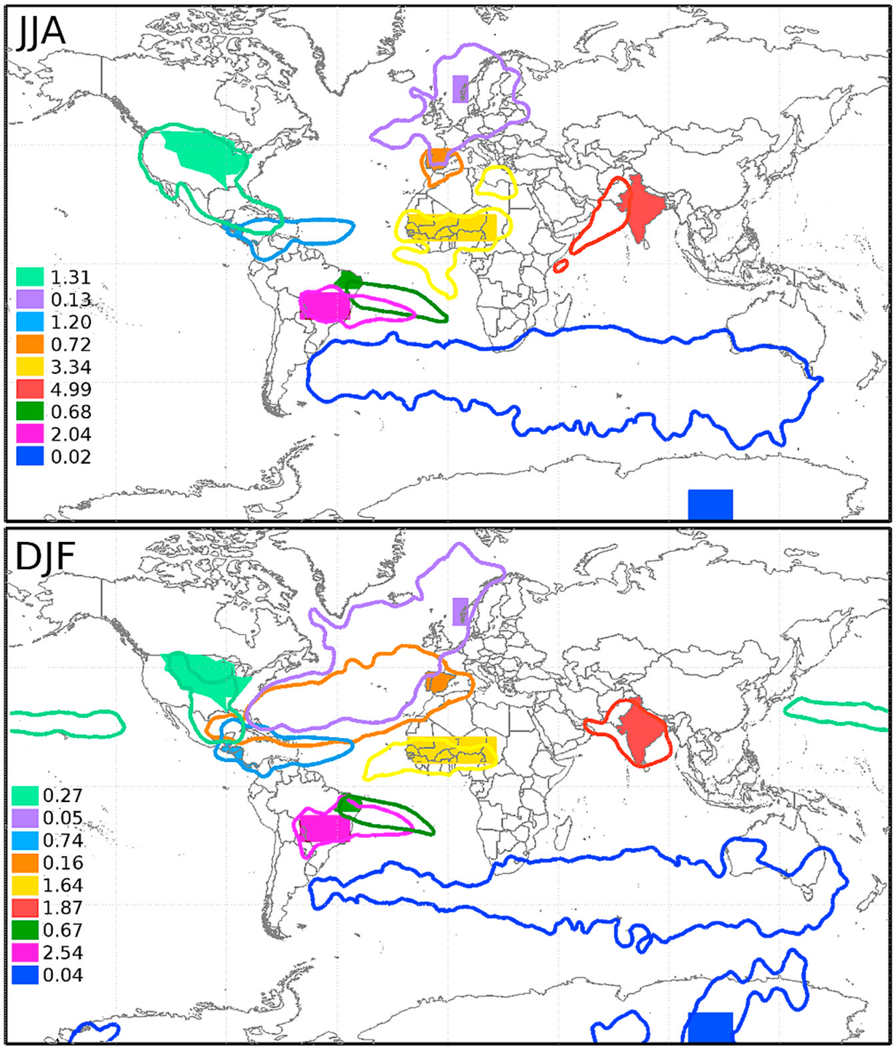

Figure 12. Mean 10 day backward vertical integrated net freshwater flux $(E\text{-}P)^{-10}$ in mm d^{-2} (contours) for selected target regions (continental areas in solid colors) for 2000–2004 based on global FLEXPART runs using ECMWF operational analysis (the same data as in the global study by *Gimeno et al.* [2010a, 2011]) for (top) JJA (June, July, August) and (bottom) DJF (December, January, February). Each contour surrounds the area covered by 95% of the moisture particles that reach the corresponding target region.

fields were computed using the FLEXPART model for the period 2000–2004 with data from the ECMWF operational analysis. Each color contour line indicates the source of 95% of the particles that transport the moisture to the respective target region for boreal summer and winter. Smaller sources can be also be estimated (and contrasted) from other analyses (e.g., the atlas "Moisture Sources by Nation" and "Moisture Sources by Basin" based on *Dirmeyer and Brubaker* [2007], http://www.iges.org/wcr).

[68] It is clear that some landmasses receive moisture from evaporation in the same hemisphere (e.g., northern Europe and eastern North America), while others receive moisture from both hemispheres with large seasonal variations (e.g., northern South America). The monsoonal regimes in India, tropical Africa and North America are provided with moisture from a large number of regions, highlighting the complexity of global patterns of precipitation. Moisture for the monsoonal regimes in these areas is provided mainly from local recycling over the continent and moisture inflow from the surrounding oceanic regions. Apart from the importance of the sources of moisture themselves, their understanding allows further assessment of the dynamical aspects of such circulations. The identification of the sources of moisture associated with the onset of the monsoon has been a primary need, as pointed out by *Bosilovich et al.* [2003], who used WVT to study the sources of moisture for the North American Monsoon. The case of the West African Monsoon, for which an intense moisture flux convergence in the boundary layer leads the moisture supply for the development of the monsoon, is also relevant here [see, e.g., *Hagos and Cook*, 2007]. Recent work [*Schewe et al.*, 2011] points to the importance of the moisture supply from the adjacent oceanic regions to monsoon systems in terms of moisture-advection feedback mechanisms. However, *Dirmeyer and Brubaker* [2007] pointed out the categorization of erroneous sources where there are sharp moisture gradients, e.g., the Mediterranean

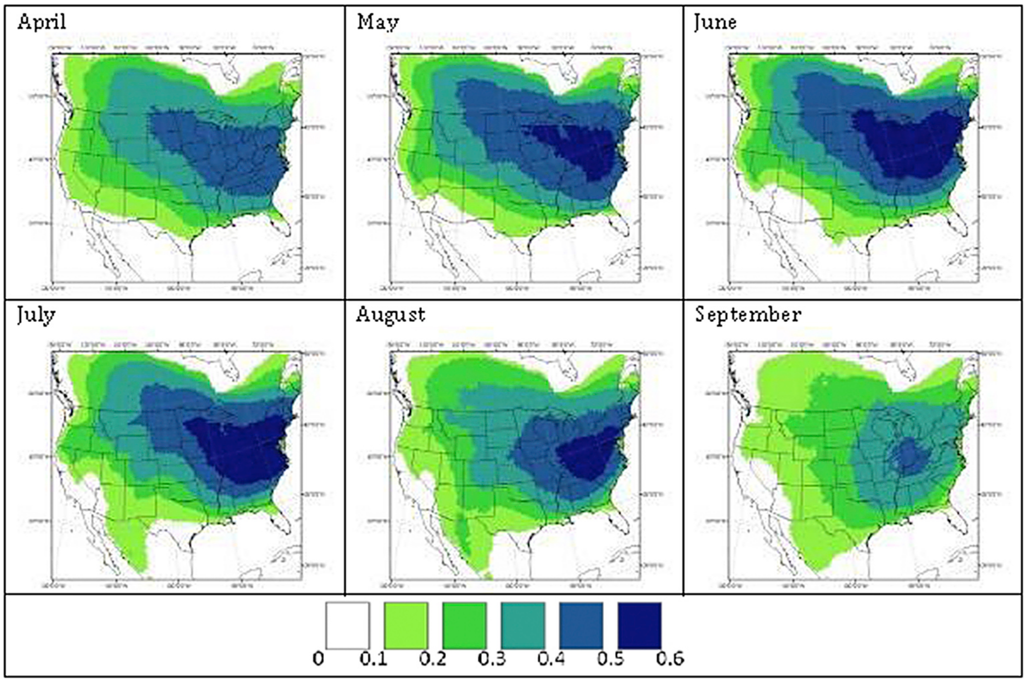

Figure 13. Fraction of total precipitation originating as ET from North America (shaded region) during the months of April–September, calculated using the Dynamic Recycling Model [*Dominguez et al.*, 2006] and NARR product from 1996 to 2006.

and Red Seas. This is a consequence of the inability to discern the exact location of water vapor parcels at sub-grid spatial or sub-output timescales at rain events, which is highly problematic in convergence zones between humid and arid air masses like in the Sahel. Thus, too much moisture is assigned to the dry side and is then tracked across arid regions. There are large areas without substantial direct transport of moisture from any of the major oceans, including in particular some of the driest inland regions (e.g., inner Asia). Precipitation only occurs in such regions when the recycling of continental moisture compensates (even partly) for the lack of a direct oceanic source of moisture (e.g., in eastern Siberia) [*Gimeno et al.*, 2010a].

[69] It is important to stress that not all oceanic regions can always be considered to be sources of moisture. The air masses that originate in the high-latitude oceans (Hudson Bay, the Arctic and the Southern Ocean), for instance, provide almost no moisture to landmasses at lower latitudes but instead take up more moisture from these regions [*Stohl and James*, 2005]. Furthermore, air masses from the Atlantic, Pacific, and Indian Oceans are a significant source of moisture for the Arctic and Southern Oceans. Even the air masses that originate in the MED, which are such an important source of water for all the Eurasian rivers that lie to the north of it, also receive net moisture input from river basins in Africa and India (Niger, Nile, Indus), especially during JJA.

3.2.2. Terrestrial Sources

[70] There is very strong seasonal cycling of precipitation of terrestrial origin, less occurring in winter than in summer when the rate of evapotranspiration is higher [*Dirmeyer and Brubaker*, 2007]. In the following discussion, the principal findings are given relating to precipitation of terrestrial origin in different regions of the world.

[71] Over Eurasia, precipitation in winter is predominantly oceanic in origin, but in summer evapotranspiration from land is the dominant source of moisture [*Numaguti*, 1999; *Kurita et al.*, 2004; *Dirmeyer and Brubaker*, 2007]. Westerly winds dominate the whole continent, and evapotranspiration from eastern Eurasia contributes to about 80% of the precipitation in China [*van der Ent et al.*, 2010] and to more than half the precipitation in Siberia [*Kurita et al.*, 2004]. The Yangtze River Basin, however, is affected by the East Asian Monsoon and experiences large seasonal variations [*Wei et al.*, 2012]. During June to July, when the monsoon is strong, moisture that originates from the Bay of Bengal (southwest) and from the South China Sea (south) crosses intermediate areas of land and contributes to precipitation over the basin. Local recycling over the Yangtze is lower during the rainy season but is important during the rest of the year [*Wei et al.*, 2012]. This is similar to the case of continental India, where most of the precipitation during JJA originates in the western and southern IND, but recycling is very limited [*Bosilovich and Schubert*, 2002]. Very similar conclusions are found by *Tuinenburg et al.* [2012], who focused on the Ganges River basin. The authors found that during the peak monsoon season, recycling within the Ganges basin is 5% of precipitation, while recycling before and after the monsoon is roughly 10%. Interestingly, 50–60% of the evaporation is recycled within the basin; however, the contribution of maritime origin is so large that it dwarfs the local signal [*Tuinenburg et al.*, 2011].

[72] At a smaller spatial scale, *Bisselink and Dolman* [2008, 2009] found that in Europe it is externally advected moisture that forms the major part of the precipitation; recycling is only significant in summer at times when the advection of moisture is limited.

[73] North America also sees a characteristic increase in precipitation recycling during the summer and very strong precipitation of terrestrial origin in the eastern part of the continent due to the predominance of westerly winds. During the peak of the summer more than 60% of the precipitation in the northeastern United States comes from terrestrial evapotranspiration (ET) from within the continent. Figure 13 shows the "continental recycling ratio" over the conterminous United States calculated using the DRM [*Dominguez et al.*, 2006], which is analogous to the results of *van der Ent et al.* [2010], who used the numerical budget method. Interestingly, this moisture can sometimes cross the Atlantic Ocean and contribute to roughly 30% of the precipitation in Europe [*van der Ent et al.*, 2010]. *Dominguez et al.* [2006] and *Dirmeyer and Brubaker* [2007] present a different metric for the contribution of local evapotranspiration to precipitation within the same region (which is the original definition of recycling). The regions of strong recycling during the warm season are the southeastern United States, the western United States, and the Rocky Mountain region. Within the continent itself, perhaps the most widely studied region is the Mississippi River basin [*Brubaker et al.*, 1993; *Dirmeyer and Brubaker*, 1999; *Bosilovich and Schubert*, 2001; *Brubaker et al.*, 2001; *Bosilovich and Schubert*, 2002; *Sudradjat et al.*, 2003; *Dominguez et al.*, 2006; *Zangvil et al.*, 2004, *Bosilovich and Chern*, 2006; *Dominguez and Kumar*, 2008; *Dirmeyer and Kinter*, 2010]. The quantification of recycling here is scale dependent [*Dirmeyer and Brubaker*, 2007] and shows strong spatial and temporal variability. Recycling ranges from about 14% in the Midwest [*Bosilovich and Schubert*, 2002] to about 32% for the entire basin [*Brubaker et al.*, 2001]. However, oceanic sources of moisture are dominant, and recycling only becomes important during drier periods when the amount of external moisture is reduced (such as during the drought of 1988). The recycling of moisture in the region of the North American Monsoon in northwestern Mexico and southwestern United States has also been the focus of extensive studies. During the monsoon, there is an abrupt increase in levels of vegetation and the rate of evapotranspiration increases, eventually leading to precipitation and thereby creating a positive feedback. Precipitation of terrestrial origin contributes between 15 and 30% of the total rainfall within the domain [*Bosilovich et al.*, 2003; *Dominguez et al.*, 2008]. In addition, the moisture from recycled monsoonal precipitation contributes (albeit modestly) to precipitation throughout the whole of North America [*Dominguez et al.*, 2009].

[74] Precipitation recycling is also important throughout South America [*Dirmeyer and Brubaker*, 2007]. Early studies that used stable water isotopes revealed that the Amazon basin has one of the smallest gradients of depletion of heavy isotopes in the world, and this fact enabled *Salati et al.* [1979] to estimate that about 50% of the rainfall in the region is recycled in origin. Notably, transpiration from plants dominates evapotranspiration, making the forests of Amazonia a very large contributor to precipitation [*Moreira et al.*, 1997]. Calculations of recycling within the western Amazon basin (the Large-scale Biosphere-Atmosphere Experiment for the Amazon–LBA region) vary depending on the area and methodology used, ranging from between 17.5% using the bulk method of *Brubaker et al.* [1993] to 27.2% using numerical water vapor tracers [*Bosilovich and Chern*, 2006]. *Lettau et al.* [1979] emphasized the role of "fast recycling" in the Amazon region, which refers to local showers that occur before all the cloud water is mixed. This means that a bulk recycling analysis that assumes a completely mixed atmosphere like that of *Brubaker et al.* [1993] would yield smaller results than the water vapor tracer method of *Bosilovich and Chern* [2006], which makes no such assumption. The moisture yielded by evapotranspiration from the Amazon moves with the predominant winds, and precipitation of terrestrial origin increases from northeast to southwest [*Eltahir and Bras*, 1994]. Moisture is eventually blocked by the Andes Mountains, and in the region downwind of the Rio de la Plata about 70% of the precipitation is of terrestrial origin, which means that in this region evapotranspiration increases the fresh water resources by a factor of three [*van der Ent et al.*, 2010]. In fact, water-limited, rain-fed agricultural regions in Argentina depend to a large extent on evapotranspiration from upwind terrestrial areas including the forests of Amazonia, making them vulnerable to potential changes due to deforestation or land degradation in the Amazon [*Keys et al.*, 2012].

[75] The dominant patterns of easterly wind also affect the geographical distribution of recycling over Africa. It has been estimated that more than 70% of the precipitation in West Africa originates from local sources or from regions to the east and south [*Savenije*, 1995; *Gong and Eltahir*, 1996]. In light of this fact, it has been found that the moisture that evaporates in East Africa is the main source of the rainfall in the Congo basin, and in turn, the Congo constitutes the major source of moisture for the Sahel [*van der Ent et al.*, 2010].

4. EXTREME EVENTS

[76] The analysis in the previous section shows that most large continental areas obtain moisture from just one or two sources, albeit with significant seasonal variations. In contrast, continental areas affected by monsoon regimes (e.g., India and tropical Africa) receive water from a large number of source regions. Continental regions that rely on moisture from only one or two source region(s) are bound to be exposed to more extreme drought events (due either to a changing climate or to natural variability) than regions that draw on multiple moisture sources.

[77] Reliable and steady moisture supply from the oceans to the continents is essential for humans and terrestrial ecosystems. Deviations from the "normal" case can lead to droughts when the moisture supply is interrupted or to

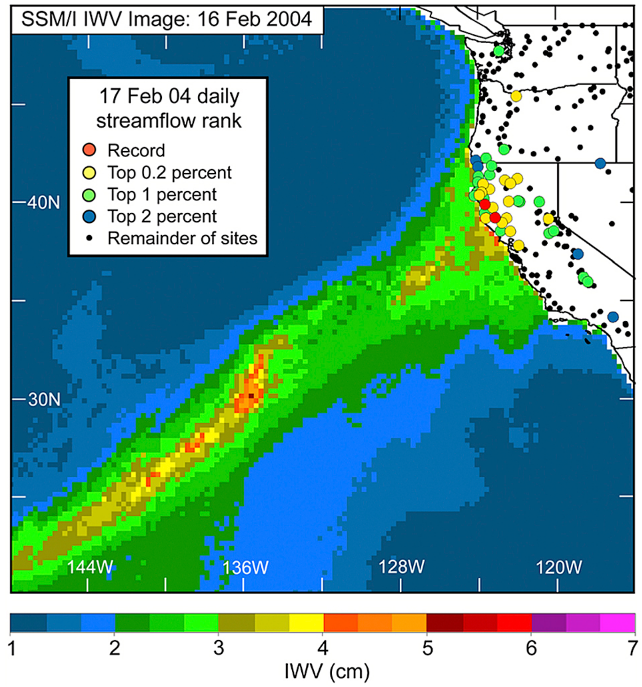

Figure 14. Satellite observation of vertically integrated water vapor on 16 February 2004 and ranking of daily streamflows (percent; see inset key) on 17 February for those gauges that have recorded data for more than 30 years. Taken from *Ralph et al.* [2006].

flooding when the supply of moisture for precipitation is too great. Often, drought or wet conditions triggered by abnormal moisture transport can be enhanced and prolonged by evaporation feedback from the local land surface [*Trenberth and Guillemot*, 1996].

[78] Often associated with extreme precipitation events are the atmospheric rivers discussed earlier in this review [*Ralph and Dettinger*, 2011]. They transport particularly moist air into the warm sector of extratropical cyclones [*Bao et al.*, 2006], from where it converges along the trailing cold front [*Ralph et al.*, 2005] and subsequently feeds the precipitation-producing warm conveyor belts associated with the cold front of the cyclone [*Eckhardt et al.*, 2004]. The precipitation associated with such events is increased further when the AR impinges on a coastal mountain range, such as in California [*Ralph et al.*, 2004, 2006] or Norway [*Stohl et al.*, 2008]. An example is shown in Figure 14 where, as the flow is blocked by the mountain range, orographic lifting forces the moist air upward, and this can lead to extreme orographic precipitation. It also enhances the ascent associated with the warm conveyor belt.

[79] Most studies of ARs have to date been performed for the North Pacific and have assessed their impact on the North American west coast. The so-called "Pineapple Express" delivers tropical moisture from the region around Hawai'i to western North America [e.g., *Higgins et al.*, 2000; *Cavazos and Rivas*, 2004; *Ralph et al.*, 2004, 2005; *Bao et al.*, 2006]. *Neiman et al.* [2002] and *Andrews et al.* [2004] showed that when the AR is oriented almost perpendicular to mountain ranges in California, there are intense storms of orographically enhanced precipitation. *Dettinger* [2004] showed that flows that follow the Pineapple Express are formed of ARs in the Merced River near the Yosemite Valley (located in California); these have increased by an order of magnitude more than those that follow other winter storms over the last 50 years. *Ralph et al.* [2006] showed that all flood events in a Californian river system were associated with AR flows and the resulting particularly strong cyclonic precipitation. However, ARs can also tap the reservoir of tropical moisture in many other regions [*Knippertz and Wernli*, 2010], and tropical plumes of moisture can also lead to extremes of precipitation in subtropical regions, for instance in West Africa [*Knippertz and Martin*, 2005]. *Stohl et al.* [2008] identified a special case where two former tropical cyclones diverted tropical and subtropical moisture to the very high latitude of 60°N and caused severe flooding in western Norway. *Schumacher and Galarneau* [2012] analyzed two recurving tropical cyclones, Erin (2007) and Ike (2008), and demonstrated that tropical cyclone-related moisture transport can increase the total water vapor in the atmosphere over North America by 20 mm or more, and that the moisture transport takes place both in the boundary layer and above it. *Reale et al.* [2001] found out the additional contribution of eastern Atlantic tropical systems in terms of moisture advection for a series of floods that affected the Mediterranean region during autumn 1998. Recently, *Lavers et al.* [2011] showed that the ten largest winter floods in the UK since 1970 were all associated with ARs.

[80] The intensity of precipitation in monsoon regions also depends strongly on the transport of water vapor from oceanic source regions. Almost analogous to the situation in the midlatitudes, strong moisture transport, synoptically forced ascent, and topographically enhanced precipitation can lead to extreme events, such as over Mumbai [*Kumar et al.*, 2008]. Increased cross-equatorial moisture transport can increase the precipitation associated with the South American summer monsoon [*Carvalho et al.*, 2010]. Regarding the North American Monsoon system, increases in the moisture supply from the Caribbean and the Gulf of Mexico can lead to increased rainfall in western Mexico [*Douglas et al.*, 1993] and southwestern United States [*Schmitz and Mullen*, 1996; *Hu and Feng*, 2002] and can produce large-scale floods in the United States and Canada [*Dirmeyer and Brubaker*, 1999; *Brimelow and Reuter*, 2005]. According to *Chan and Misra* [2010], an increase in moisture transport from the Atlantic warm pool is also related to wetter-than-normal summers in the southeastern United States.

[81] Droughts, on the other hand, are often caused by a diminished supply of water vapor from oceanic moisture source regions. For example, a reduced intensity in northeast trade wind moisture transport into southern Amazonia was an important factor in the severe drought in Amazonia in 2005 [*Marengo et al.*, 2008]; reduced tropical moisture transport is responsible for bad droughts in southeast Australia [*Ummenhofer et al.*, 2009]; and a reduction in moisture transport from the Arabian Sea was found to be linked with an intense drought in India in 2002 [*Valsala and

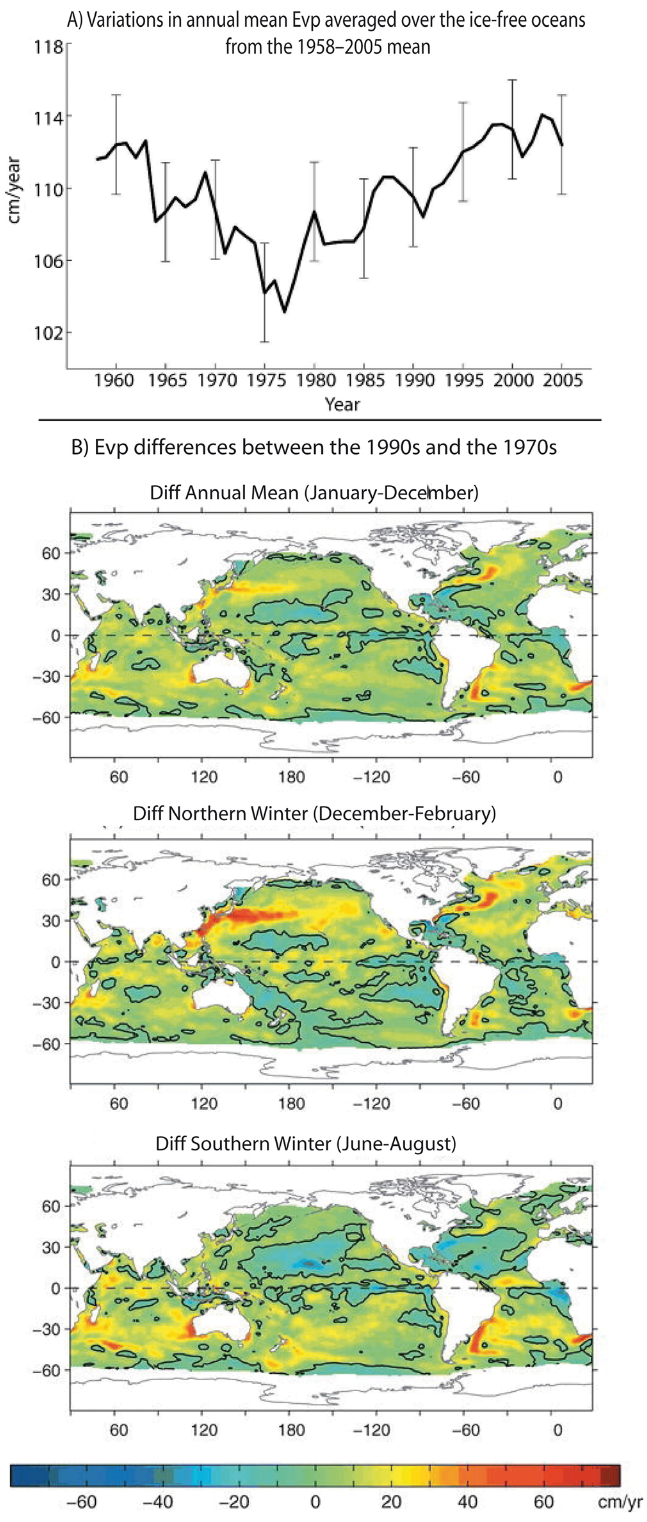

Figure 15. (a) Variations in annual mean evaporation averaged over the ice-free oceans. The error bars indicate 1 SD from the 1958–2005 mean; (b) differences in evaporation between the 1990s and the 1970s in (top) annual mean, (middle) northern winter (December–February), and (bottom) southern summer (June–August). Zero contours are shown by thin black lines. From *Yu* [2007].

Ikeda, 2005]. For northeast China, it was shown that evaporation from the Yellow Sea is important for the variations in moisture inflow observed between years that are wetter or drier than normal [*Simmonds et al.*, 1999].

[82] Land-atmosphere coupling via moisture recycling has also been found to be important for heat waves and droughts. In Europe, heat waves are usually preceded by a strong precipitation deficit in spring, which depletes the soil moisture and then later reduces latent cooling and cloud formation [*Fischer et al.*, 2007], thereby producing heat and drought. Similar relationships have been found in other regions. For instance, the soil moisture provides a feedback mechanism for the Asian Summer Monsoon [*Meehl*, 1994] and can reinforce drought conditions in the Sahel [*Nicholson*, 2000]. This emphasizes the importance of the relationships between soil moisture and climate (see *Seneviratne et al.* [2010] for a review of moisture-climate interactions), especially with respect to extreme conditions.

5. IMPLICATIONS OF CLIMATE CHANGE

[83] It has now become well established that water vapor plays a major role in the climate of the planet [*IPCC*, 2007]. In particular, water vapor accounts for roughly 60% of the natural greenhouse effect under clear skies [*Kiehl and Trenberth*, 1997], presenting also the largest positive feedback in the climate change scenarios developed using GCMs [*Held and Soden*, 2000]. Climate change scenarios suggest that the high sensitivity of saturation vapor pressure to temperature will result in an intensified hydrological cycle, with higher rates of evaporation and precipitation in a warmer world [*Held and Soden*, 2006]. This result follows directly from the C-C relationship. However, the response of the hydrological cycle is slightly more complex, and thermodynamics alone cannot explain all of the predicted changes in certain characteristics of the hydrological cycle. In fact, exclusive attention to thermodynamics, such as in *Held and Soden* [2006], suggests that *E-P* would decrease everywhere over land, but this is not what GCM models suggest; likewise it is not possible to explain thermodynamically the expected changes in the latitudinal boundary between regions of positive and negative *E-P* [*Seager et al.*, 2010]. This means that changes in atmospheric circulation induced by global warming will redirect moisture and cause source-sink relationships of atmospheric water vapor that differ from the present case. Those continental regions that receive moisture from only one or two source region(s) may be more sharply exposed to changes in water cycle due to changing climate than regions that draw on multiple moisture sources.

[84] A brief summary is given in the following two subsections of the observed and expected changes related to the atmospheric transport of moisture.

5.1. Observed Changes

[85] Current best estimates of oceanic evaporation, such as those derived from the OAFlux data [*Yu and Weller*, 2007], show that a strong increase in the overall rate of evaporation from the oceans has been occurring since 1978 (see Figure 15) and that this increase was most pronounced during

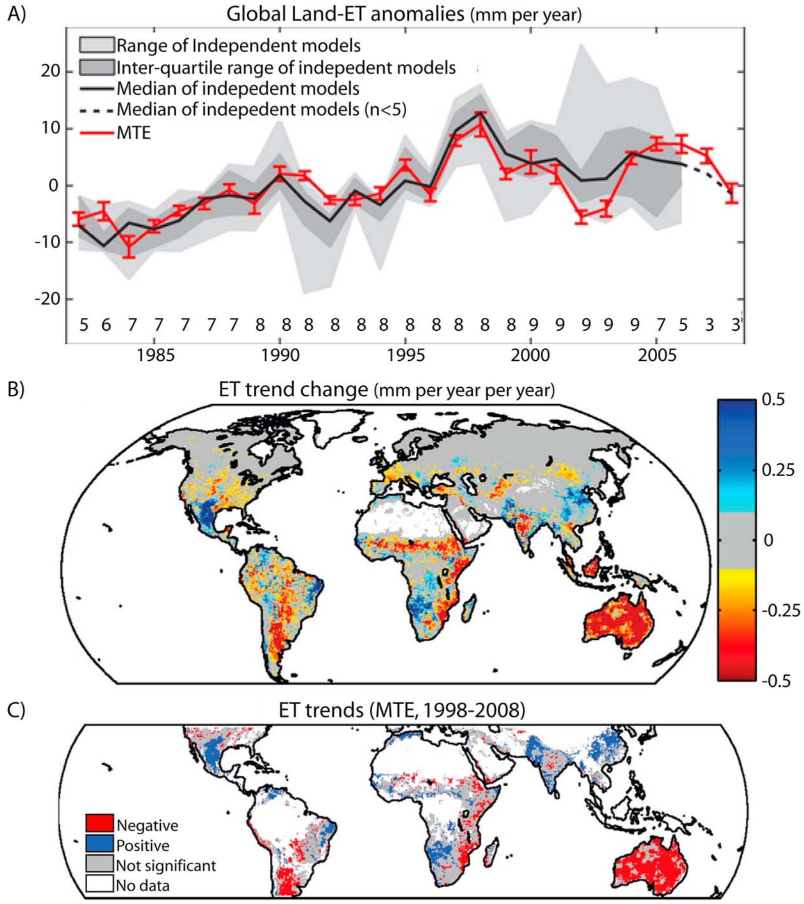

Figure 16. Global land-ET variability according to MTE (the model tree ensemble) and independent models. (a) Annual global land ET anomalies based on MTE and an ensemble of up to nine independent process-oriented models. Error bars indicate 1 SD within the MTE. Numbers at the bottom show the number of models available each year. (b) Map of the change in ET trend between 1982 and 1997 and 1998 and 2008 in millimeters per year. Small trend changes of ± 0.1 mm yr^{-1} are shown in gray to enhance clarity. (c) Significant ($P < 0.1$) ET trends derived from MTE. Regions without data in MTE (nonvegetated areas) are blanked in the map. From *Jung et al.* [2010].

the 1990s. While the increase in evaporation has occurred at a global scale [*Yu*, 2007], the spatial structures of the increase are more coherent in winter than in summer. The most significant of these are the reduction in evaporation in the subtropics, the strong increase in evaporation along the paths of the global western boundary currents, and the increase over the Indo-Pacific warm pools (Figure 15b) [*Yu*, 2007]. Changes in evapotranspiration may also have been produced, but there are constraints on this at the global scale. Results from in situ observations (FLUXNET network) and satellite remote sensing were used in a recent comprehensive study that assessed the spatial and temporal changes in evapotranspiration during the last three decades [*Jung et al.*, 2010]. These authors suggested that global annual evapotranspiration increased on average by 7.1 ± 1.0 mm per year per decade from 1982 to 1997, this last year being coincident with a major El Niño event (Figure 16a). After that, the global increase in evapotranspiration seems to have ceased until 2008, most probably due to the limitation of moisture in the Southern Hemisphere, particularly in Africa and Australia (Figures 16b and 16c). Paradoxically, terrestrial observations over the past 50 years show that the decrease in pan evaporation is consistent with what one would expect from the observed large and widespread decreases in sunlight resulting from increasing cloud coverage and aerosol concentration [*Roderick and Farquhar*, 2002].

[86] A number of studies in the last decade have provided convincing evidence that water vapor is on the increase over a number of regions, namely the United States [*Robinson*, 2000], central Europe [*Philipona et al.*, 2004], and China [*Wang and Gaffen*, 2001]. It has now been proved objectively that changes in vertical integrated water vapor in central Europe are mostly associated with corresponding changes in surface temperature, i.e., warming (cooling) regions are linked with positive (negative) trends of moisture [*Philipona et al.*, 2005; *IPCC*, 2007]. Using a large number of stations, *Dai et al.* [2006] studied the trends in relative and specific humidity for the period 1976–2005. While the global trend in surface relative humidity is very small, specific humidity increases by 4.9% per 1°C [*IPCC*, 2007]. The evolution of vertically integrated water vapor (precipitable water) has been derived from a number of different satellite

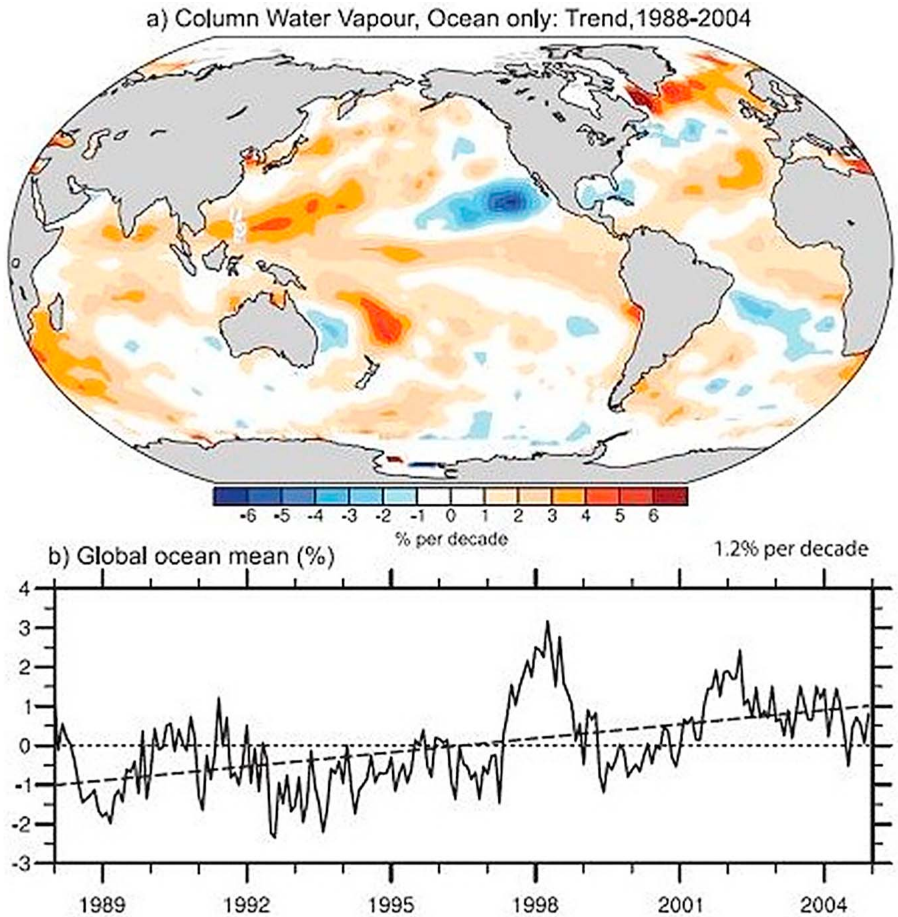

Figure 17. (top) Linear trends in precipitable water (total column water vapor) in percent per decade and (bottom) monthly time series of anomalies relative to 1988–2004 in percent over the global ocean plus linear trend, from RSS SSM/I [from *IPCC*, 2007, chapter 3].

data sets (e.g., TIROS Operational Vertical Sounder (TOVS), Scanning Multichannel Microwave Radiometer (SMMR), SSM/I). According to *Trenberth et al.* [2005], the linear trend for the period 1988–2004 over the oceans was of the order of 1.2% per decade (Figure 17). However, the relatively short periods with available data, and strong interannual variability (often associated with El Niño events or large volcanic eruptions), affect the statistical significance of the trends. Nevertheless, the trends are predominantly positive over the oceans, and additionally suggest an El Niño–Southern Oscillation (ENSO) fingerprint. According to the latest Intergovernmental Panel on Climate Change (IPCC) report, there was an overall growth of 5% in water vapor throughout the entire twentieth century, mostly due to increases during the last three decades [*Trenberth et al.*, 2007b].

[87] However, it should also be noted that changing circulation patterns will lead to large regional changes in the moisture budget. Evaporation rates depend on changes in temperature of both the sea and the air, as well as on changes in wind conditions (Figure 11, left). It is likely that there will be a significant impact over the continental areas that are more severely affected by changes in the wind field associated with these different circulation patterns (see Figure 11, right).

[88] Some regional changes are already being observed. For example, changes in atmospheric circulation patterns are partially responsible for declining precipitation over regions such as the Iberian Peninsula [*Paredes et al.*, 2006] and southwestern United States [*Seager et al.*, 2007], areas predicted to be prone to a higher frequency of droughts in future according to climate projections [e.g., *IPCC*, 2007]. *Dirmeyer and Brubaker* [2007] found trends in recycling ratio over large areas at high latitudes.

[89] Interestingly, there have been also changes in precipitation, aridity and soil moisture. Dry or drought conditions are deemed to occur in an area if the PDSI (Palmer Drought Severity Index, an approximate measure of the cumulative effect of atmospheric moisture supply and demand) is less than -0.5, and very dry areas (severe or extreme drought) are defined for a PDSI of less than -3 [*Palmer*, 1965]. Another index used for the same purpose is the Standardized Precipitation Evapotranspiration Index (SPEI). This index combines the sensitivity of the PDSI to changes in evaporation demand (caused by temperature fluctuations and trends) with the multitemporal nature of the Standardized Precipitation Index (SPI). Further details on the drought indicator have been provided by *Vicente-Serrano et al.* [2010]. A value of SPEI of less than -0.84,

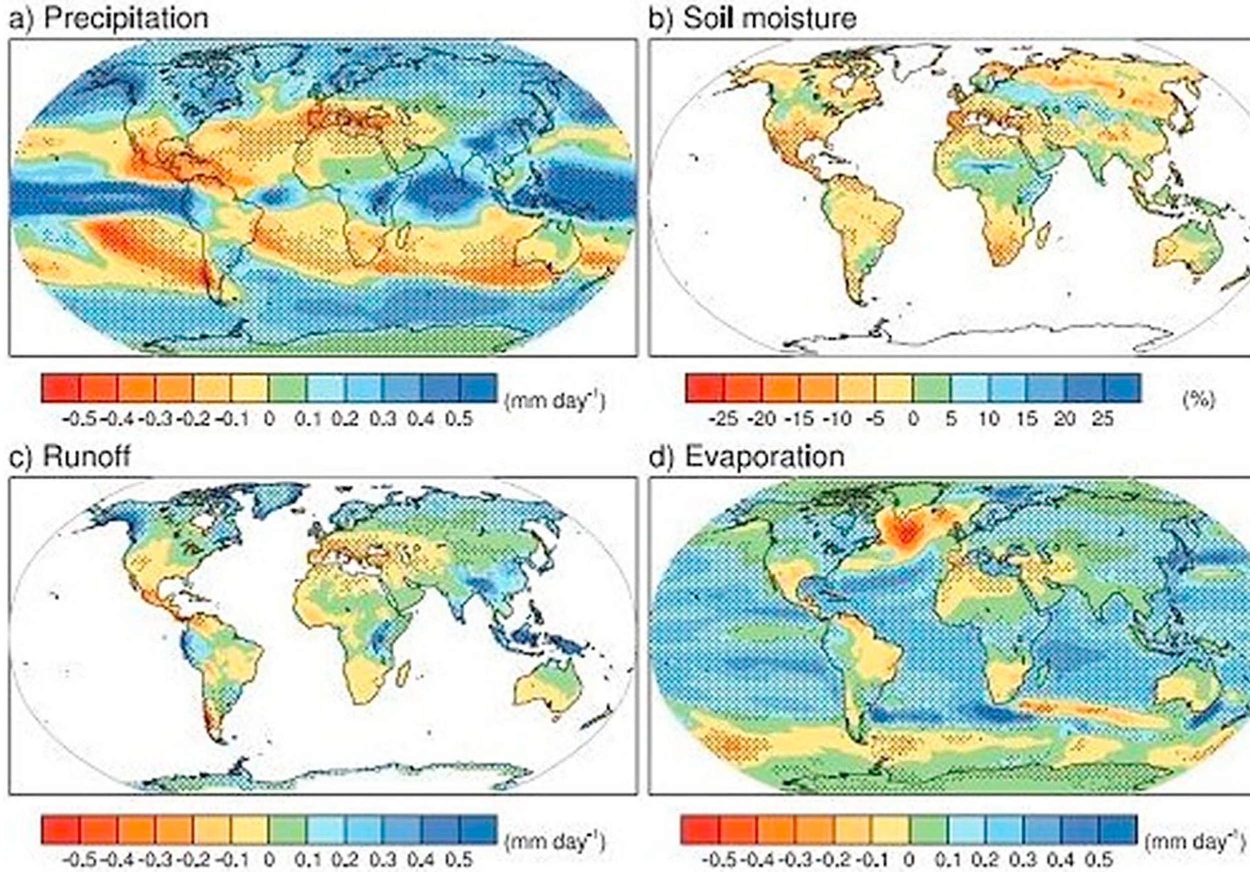

Figure 18. Multimodel mean changes in (a) precipitation (mm d^{-1}), (b) soil moisture content (%), (c) runoff (mm d^{-1}), and (d) evaporation (mm d^{-1}). To indicate consistency in the sign of change, regions are stippled where at least 80% of models agree on the sign of the mean change. Changes are annual means for the SRES A1B scenario for the period 2080–2099 relative to 1980–1999. Soil moisture and runoff changes are shown at land points with valid data from at least 10 models [from *IPCC*, 2007, chapter 10].

which represents 20% on the normal distribution of SPEI values, indicates drought conditions. According to recent analysis the global prevalence of dry areas has increased significantly (1.74% per decade) since the 1950s [*Dai*, 2011]. Some of this drying has occurred in highly populated areas of the world, such as the Mediterranean [*López-Moreno et al.*, 2009; *Sousa et al.*, 2011], the Fertile Crescent in the Middle East [*Trigo et al.*, 2010], and southwestern United States [*Seager et al.*, 2007]. However, sparsely populated regions such as the Amazon [*Lewis et al.*, 2011] and Australia [*Dai*, 2011] have also been affected by an increasing frequency of extreme drought events. Of particular social interest is the case of Africa, where drought is a natural hazard that affects a large number of people with disastrous consequences, being responsible for famine, epidemics, and land degradation [*United Nations* (*UN*), 2008]. Among the most significant natural disasters affecting the world for the period 1974–2007, the two that resulted in the greatest number of deaths were the droughts that killed 450,000 and 325,000 people in Ethiopia/Sudan and the Sahel region in 1984 and 1974, respectively [*UN*, 2008]. Interestingly, these very same areas are expected to become even drier in the coming decades according to the latest results published in IPCC AR4 [*IPCC*, 2007].

5.2. Expected Changes

[90] Figure 18 shows changes in annual precipitation, evaporation, soil moisture, and runoff at the global scale and for the A1B scenario, obtained using the multimodel approach adopted in IPCC AR4. Large increases in precipitation are expected at high latitudes but also in the equatorial band (Figure 18a) as a consequence of an increasing atmospheric convergence of moisture. In contrast, significant decreases (of up to 20%) can be expected in the Mediterranean region, the Caribbean region and more generally at subtropical latitudes, including most continental west coasts [*IPCC*, 2007]. On the whole, precipitation over the land (ocean) will increase slightly by 2100, by about 5% (4%) but with large regional asymmetries. It should be noted that increases in precipitation in high latitudinal bands are expected to occur throughout the year, while increases in more tropical regions will be restricted to particular seasons such as JJA for the South Asian Monsoon or DJF for the Australian Monsoon.

[91] Changes in annual mean evaporation (Figure 18d) resemble the pattern of changes in temperature, with

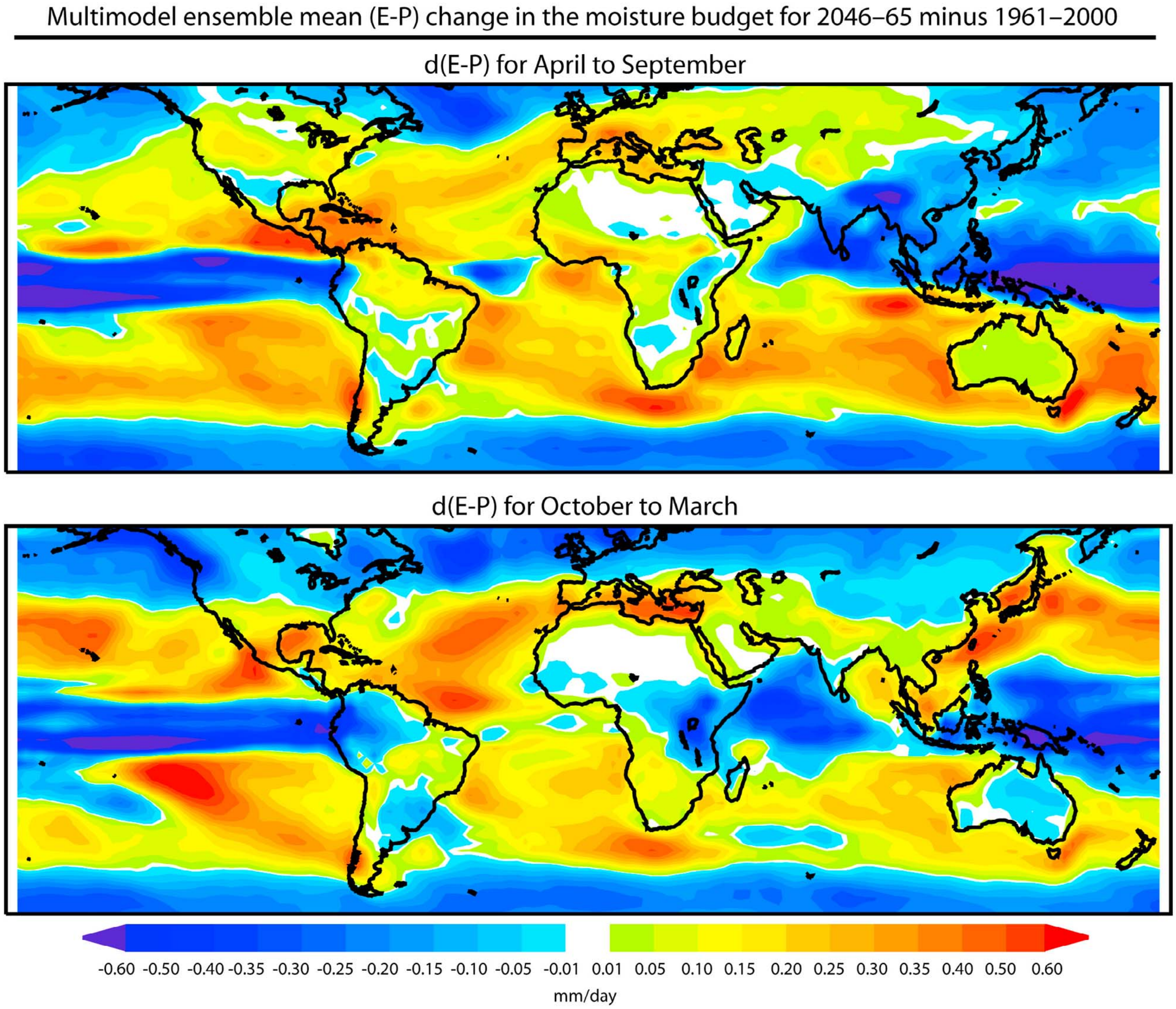

Figure 19. The climatological multimodel ensemble mean change in the moisture budget for the difference between evaporation and precipitation for (top) April to September and (bottom) October to March 2046–2065, relative to 1961–2000. Units are mm d^{-1}. Data provided by *Seager et al.* [2010].

increases over most of the ocean, with a few exceptions such as to the south of Greenland, where decreasing evaporation is matched by decreasing temperature (Figure 18d). Changes in runoff are bound to reflect the changes described above in precipitation and evaporation, being characterized by significant reductions in the Mediterranean basin and Central America but also by increases in Southeast Asia, the African Great Lakes, and at high latitudes (Figure 18c).

[92] As far as future scenarios are concerned, GCMs tend to agree on the tendency toward a markedly hotter and drier Mediterranean basin [*Mariotti et al.*, 2008] and southwestern United States [*Seager et al.*, 2007]. For these two areas, it is possible to predict that the combined effects of a decrease in precipitation and an increase in surface temperature will lead to changes in the water cycle that could have serious implications.

[93] Of particular interest here is an assessment of the predictions of CGMs in relation to the major sources of moisture as estimated by the means of areas of high *E-P*. Using data from 15 of the models that comprised the Third Coupled Model Intercomparison Project (CMIP3) [*Seager et al.*, 2010], the projected changes to the overall *E-P* budget were calculated (Figure 19). The general distribution of *E-P* shows a poleward expansion of the dry subtropical regions and wetter middle-to-high latitudes associated with two distinct aspects of global circulation, namely the expansion of the Hadley cell [*Lu et al.*, 2007] and the poleward shift in the midlatitude storm tracks [*Bengtsson et al.*, 2006]. Changes in *E-P* thus correspond largely to what might be expected according to these two changes in global circulation, i.e., the tropics, along with the middle to high latitudes, become wetter (a decrease in *E-P*), and the subtropics become drier (an increase in *E-P*). This evolution suggests that the major oceanic sources of moisture as indicated in Figure 11 will probably increase in intensity, thereby providing more moisture for precipitation. These

results seem to show how changes in mean circulation appear to cause a decrease in *E-P* in the equatorial regions between 160° E and 70°W. The increase in *E-P* to the north and south of this band are thought to be related to a shift in the ITCZ [*Seager et al.*, 2010]. The weakening of the tropical circulation [*Seager et al.*, 2010] results in a poleward decrease of *E-P* in the region of the trade winds.

[94] Despite the level of agreement among GCMs, it is not clear how well these models reproduce the moisture source areas at global [*Gimeno et al.*, 2010a] and regional scales. In particular, additional work is needed to assess the ability of GCMs to reproduce the main source areas for highly sensitive areas such as the Mediterranean and the Iberian Peninsulas, as identified in recent work [*Gimeno et al.*, 2010b].

6. FUTURE CHALLENGES

[95] The identification of moisture sources as part of the analysis of extreme events has become a major research area (e.g., for flooding and droughts), but it is also increasingly important for regional and global climatic assessments, including paleoclimatic reconstructions and future climate change scenarios. As moisture source diagnostics become more widely used, it will be advisable to assess their validity in more detail and evaluate the fundamental assumptions made. Consistency among methods using water tracers still remains to be established. The use of stable water isotopes constitutes one promising means of obtaining source-related information [*Pfahl and Wernli*, 2009]. Unfortunately, there is still some way to go in terms of understanding the relationship between water isotope signatures and precipitation sources, particularly since isotopic fractionation during air mass transport may overwrite source signatures [*Sodemann et al.*, 2008]. In this regard it is crucial to improve our understanding of how moisture sources affect precipitation isotopes, in order to allow the correct interpretation of most paleoclimatic archives, such as ice cores and cave sediments. Therefore, future research must combine moisture source diagnostics with all other available information, including stable water isotopes and other measurements.

[96] Another pressing issue relates to the necessity of using longer data sets. Most studies based on Lagrangian methods to diagnose moisture sources have used short time series with less than 10 years. This length of time is far too short to establish statistically significant trends, to assess the impact of major modes of climate variability, such as ENSO or NAO (North Atlantic Oscillation), or to characterize changes in the precipitation regime at the decadal scale (such as during the 1960s and 1970s in the Sahel or in the 2000s in Australia and southwestern United States).

[97] Traditionally, the motivation for delineating source-sink regions of precipitation, particularly over terrestrial areas (precipitation recycling), has been the understanding of how precipitation in one region could be affected by potential land use/land cover changes in nearby regions [*Brubaker et al.*, 1993; *Eltahir and Bras*, 1996]. However, changes in land cover over a region will not only affect climate through recycling but also through the modification of the local structure of the atmosphere through thermodynamic processes and through large-scale effects on atmospheric circulation [*Goessling and Reick*, 2011]. In some cases, local thermodynamic processes have dominated the soil-precipitation interactions and have been shown to be more important than recycling [*Schär et al.*, 1999]. In other numerical experiments, with global modifications to terrestrial evaporation, the effect can be attributed primarily to changes in large-scale circulation and not to recycling [*Goessling and Reick*, 2011].

[98] It should also be stressed that it is likely that changes in soil moisture content will lead to a greater incidence of heatwaves in densely populated areas such as Europe. In fact, it has been shown that large summer heatwaves in Europe in the last 30 years have been amplified by dry conditions in winter/spring in the Mediterranean area [*Vautard et al.*, 2007]. On the other hand, using global and regional models it has been shown that land-atmosphere coupling (through soil moisture) is of paramount importance in explaining the increased likelihood of heatwaves in central and eastern Europe [*Seneviratne et al.*, 2006] and that the severe 2010 heatwave in Russia corresponds to a more typical extreme event for the late twenty-first century [*Barriopedro et al.*, 2011].

[99] Finally, it must be borne in mind that a reliable and robust assessment of source-sink relationships in the atmospheric water cycle is a requirement for understanding a major driving factor for extreme weather events. It has been shown that the convergence and transport (the ARs) from regions of high water vapor can trigger rainfall extremes and cause floods in both the United States [*Ralph et al.*, 2006] and Europe [*Stohl et al.*, 2008]. The ability of global and regional models to reproduce the atmospheric thermodynamics that drive these ARs has been tested both for short-term forecasting [*Leung and Qian*, 2009] and within the framework of climate change studies [*Dettinger*, 2011]. The former authors showed how their simulation realistically captured the mean and extreme precipitation, and the precipitation/temperature anomalies of all the AR events from 1980 to 1999. The latter concluded that average AR statistics for California do not change much in most climate models under an A2 greenhouse gas emissions scenario. However, extremes change notably, for instance years with many AR episodes become more frequent and those episodes with water vapor transport rates higher than historical. In contrast, the absence of moisture transport to continental regions is bound to play a major role in the buildup and persistence of continental drought [*Seneviratne et al.*, 2006; *Hoerling and Kumar*, 2003].

[100] In summary, the present review has discussed the most important sources of atmospheric moisture at the global scale (both oceanic and terrestrial) and their influence on precipitation over continental regions. Furthermore, the methods used to establish source-sink relationships of atmospheric water vapor have been discussed, together with the advantages and caveats associated with each technique. Moreover, the present review has also stressed the role played by the highly concentrated transport of moisture as

being the most responsible for meteorological extremes, such as flooding (through structures known as atmospheric rivers) and such climate extremes as droughts, through the prolonged diminished supply of water vapor from moisture source regions. Finally, some consideration has been given to the implications of climate change for the transport of moisture and its role in the hydrological cycle.

[101] Despite having covered the foregoing important issues, a number of questions nevertheless remain within the current scientific state-of-the-art knowledge, namely the following: (1) Have the moisture source regions been stationary throughout the years, or have they changed location significantly over the last three decades? (2) How can changes in intensity (more evaporation) and position of the sources affect the distribution of continental precipitation? (3) What is the role of the main modes of climate variability such as NAO or ENSO in the variability of the moisture source regions? (4) How much moisture is there, and where is it being transported, by low-level jets and atmospheric rivers and what is the role of these in extreme events? (5) Do droughts result mainly from a lack of evaporation over the identified main moisture source areas and/or circulation anomalies in the transport? (6) What is the role of the warm pools (oceanic regions of intense evaporation) in the supply of moisture? (7) How will climate change alter the location and significance of source regions and the transport of moisture from these toward continental areas in the future? All these important scientific questions require further study in order to be addressed in depth in future years.

NOTATION

A	area
ADEOS	Advanced Earth Observing Satellite
AGCM	Atmospheric general circulation model
AGU	Agulhas Current
AIRS	Atmospheric Infrared Sounder
AR	atmospheric river
AVHRR	advanced very high resolution radiometer
BR	Bowen ratio
C-C	Clausius-Clapeyron equation
CCN	cloud condensation nuclei
c_e	turbulent exchange coefficient
CLLJ	Caribbean Low-Level Jet
CMAP	CPC Merged Analysis of Precipitation
CMIP3	Third Coupled Model Intercomparison Project
CMORPH	CPC MORPHing technique
CORALS	Coral Sea
c_p	specific heat of air
CPC	Climate Prediction Center
D	deuterium
DJF	period from December to February
DMSP	Defense Meteorological Satellite Program
dq	difference between q_s and q_a
DRM	Dynamic Recycling Model
e	vapor pressure above the surface
E	rate of evaporation
EC	eddy covariance
ECMWF	European Centre for Medium-Range Weather Forecasts
ENSO	El Niño–Southern Oscillation
Envisat	environmental satellite
$(e\text{-}p)_k$	the rates of moisture increase and decrease along the trajectory of each particle
E-P	surface freshwater flux
ERA-40	ECMWF Re-Analysis 40
$e_s(T_0)$	saturation vapor pressure at the surface temperature T_0
ET	evapotranspiration
FLUXNET	global network of micrometeorological towers that use eddy covariance methods to measure the exchanges of carbon dioxide, water vapor, and energy between the biosphere and atmosphere
g	acceleration due to gravity
GCIP	GEWEX Continental-scale International Project
GCM	general circulation model
GEWEX	Global Energy and Water-Cycle Experiment
GNIP	Global Network of Isotopes in Precipitation
GOME	Global Ozone Monitoring Experiment
GPCP	Global Precipitation Climatology Project
GPS	Global Positioning System
GRACE	Gravity and Climate Experiment
HDO	“heavy water” where one proton has been replaced by deuterium
HIRS	High-Resolution Infrared Radiation Sounder
IAEA	International Atomic Energy Agency
IMG	Interfermetric Monitor for Greenhouse gases sensor
IND	Indian Ocean
IPCC	Intergovernmental Panel on Climate Change
ISS	isotopic steady state
ITCZ	Intertropical Convergence Zone
JJA	period from June to August
L_v	latent heat of vaporization
MED	Mediterranean
MERRA	Modern Era Retrospective-Analysis for Research and Applications
MEXCAR	Mexico Caribbean Sea region
MIPAS	Michelson Interferometer for Passive Atmospheric Sounding
MISR	Multiangle Imaging Spectroradiometer
NAO	North Atlantic Oscillation
NATL	North Atlantic
NCEP	National Centers for Environmental Prediction
NPAC	North Pacific
OAFlux	Objectively Analyzed air-sea Flux project
p	pressure
P	precipitation rate
PDSI	Palmer Drought Severity Index
PERSIANN	Precipitation Estimation from Remotely Sensed Information using Artificial Neural Networks

p_s pressure at the surface
q specific humidity
q_a near-surface atmospheric specific humidity
q_s saturation specific humidity at the sea surface temperature
QuikSCAT QuikScatterometer
R local recycling ratio
r_a bulk aerodynamic resistance
RCM regional model
REDS Red Sea
RH relative humidity
$R_{i,k}(x, y)$ the evaporative contribution of surface grid (x, y) to the precipitable water that contributes to rain in grid box (i) from parcel (k)
R_n net incoming radiation
r_s the canopy-averaged leaf stomatal resistance using the big-leaf approximation
SATL South Atlantic
SCIAMACHY Scanning Imaging Absorption Spectrometer for Atmospheric Chartography
SD standard deviation
SMMR Scanning Multichannel Microwave Radiometer
SMOW standard mean ocean water
SPAC South Pacific
SPCZ South Pacific Convergence Zone
SPEI Standardized Precipitation Evapotranspiration Index
SPI Standardized Precipitation Index
SSM/I Special Sensor Microwave Imager
SST sea surface temperature
SWING stable water isotope modeling intercomparison group
T temperature of the atmosphere close to the surface
T_a air temperature
TCWV total column water vapor
TES Tropospheric Emission Spectrometer
TMPA TRMM Multisatellite Precipitation Analysis
TOVS TIROS Operational Vertical Sounder
TRMM Tropical Rainfall Measuring Mission
u vertically integrated zonal water vapor flux divided by w (equivalent to a water vapor–weighted zonal wind)
U near-surface wind speed
UN United Nations
UMORA Unified Microwave Ocean Retrieval Algorithm
v water vapor weighted meridional wind
$\mathbf{V}$ vector representing the horizontal wind at a given level
w amount of water vapor contained in a unit area column of air
W precipitable water
WCRPs World Climate Research Programs
WEBS water and energy budget synthesis
WMO World Meteorological Organization
WVT water vapor tracers
ρ air density
Δ slope of the saturation vapor pressure versus temperature curve at temperature T
$\nabla \cdot \Theta$ divergence of the vertically integrated total horizontal flux of water vapor
Θ vertically integrated total horizontal flux of water vapor

GLOSSARY

Atmospheric river (AR): Relatively narrow conduits in the atmosphere responsible for up to 90% of the horizontal transport of water vapor outside the tropics, resulting from the combination of strong low-level winds and high concentrations of water vapor. These conduits were termed "atmospheric rivers" by *Newell et al.* [1992] because the mass transport rates of water are comparable to those of world's largest terrestrial rivers.

Clausius-Clapeyron (C-C) equation: Equation that gives the saturation vapor pressure (SVP) of air over liquid water as a function of temperature and that involves the specific latent heat of evaporation (L_v). This relationship with L_v implies a nonlinear (exponential) function between both magnitudes as the L_v depends also on temperature.

El Niño–Southern Oscillation (ENSO): The El Niño–Southern Oscillation is a quasiperiodic climatic phenomenon observed over the tropical Pacific Ocean. It is composed of an oceanic component characterized by variations in the temperature of the surface of the tropical Pacific Ocean (El Niño), coupled with an atmospheric component seen in variations in surface air pressure in the tropical Pacific (the Southern Oscillation). An El Niño (La Niña) event is characterized by warmer (colder) water than normal over the eastern tropical Pacific accompanied by higher (lower) surface air pressure in the western Pacific.

Evapotranspiration: The combined processes through which water is transferred to the atmosphere from open water and ice surfaces, bare soil, and vegetation that make up the Earth's surface (taken from the AMS glossary of Meteorology).

Hadley circulation: A pattern of circulation observed in the tropical atmosphere, consisting of rising motion near the equator, a poleward flow at the upper troposphere, descending motion in the subtropics, and equatorward flow near the surface.

Indo-Pacific warm pool: Area enclosed by the region that extends from the western tropical Pacific Ocean through the Indonesian archipelago where it crosses the eastern tropical Indian Ocean, with mean SSTs greater than 28°C; known to be the warmest body of open oceanic water on the planet.

Intertropical Convergence Zone (ITCZ): The dividing line between the southeast trades and the northeast trades (of the Southern and Northern Hemispheres, respectively), associated with a band of cloudiness and precipitation. It encompasses the rising branch of the Hadley cell.

Low-level jet (LLJ): Also known as the low-level jet stream. A jet stream (region of strong winds concentrated in a narrow band) typically found in the lower 2–3 km of the troposphere, which commonly transports substantial amounts of moisture in the tropics, midlatitudes and regions between them (taken from the AMS glossary of Meteorology).

Monsoon: A thermally driven wind that arises from differential heating between a landmass and the adjacent ocean, which reverses its direction seasonally (taken from the NWS/NOAA glossary of Meteorology).

Pan evaporation: Measured water loss from free water surface of class-A evaporation pan. It is a measurement that combines the effects of several climate elements: temperature, humidity, rain fall, drought dispersion, solar radiation, and wind.

Precipitable water: The total atmospheric water vapor contained in a vertical column of unit cross-sectional area extending between any two specified levels.

Precipitation: Any product of the condensation of atmospheric water vapor that falls under gravity (taken from the AMS glossary of Meteorology).

Rawinsonde: A radiosonde tracked from the ground by a direction-finding antenna, used to measure variations in horizontal wind direction and the variation of wind speed with altitude (taken from the AMS glossary of Meteorology).

South Pacific Convergence Zone (SPCZ): A band of low-level convergence, cloudiness, and precipitation extending southeastward from the Indo-Pacific warm pool.

Surface freshwater flux: The difference between rates of evaporation and precipitation per unit area.

Teleconnection pattern: A linkage between the changes in weather that occur in widely separated regions of the globe (taken from the AMS glossary of Meteorology).

Total column of water vapor (TCWV): Vertical integral from the ground to the nominal top of the atmosphere, expressing the total amount of water vapor. Equivalent to precipitable water for the case where the lower and upper levels are the Earth's surface and the top of the atmosphere, respectively.

[102] **ACKNOWLEDGMENTS.** Authors thank comments by P. A. Dirmeyer and an anonymous reviewer for the first version of the manuscript. Luis Gimeno would like to thank the Spanish Ministry of Science and FEDER for their partial funding of this research through the project MSM. A. Stohl was supported by the Norwegian Research Council within the framework of the WATER-SIP project. The work of Ricardo Trigo was partially supported by the FCT (Portugal) through the ENAC project (PTDC/AAC-CLI/103567/2008).

[103] The Editor on this paper was Mark Moldwin. He thanks Paul Dirmeyer and one anonymous reviewer.

REFERENCES

Adler, R. F., et al. (2003), The version-2 Global Precipitation Climatology Project (GPCP) monthly precipitation analysis (1979-present), *J. Hydrometeorol.*, *4*(6), 1147–1167, doi:10.1175/1525-7541(2003)004<1147:TVGPCP>2.0.CO;2.

Allan, R. P. (2009), Examination of relationships between clear-Sky longwave radiation and aspects of the atmospheric hydrological cycle in climate models, reanalyses, and observations, *J. Clim.*, *22*, 3127–3145, doi:10.1175/2008JCLI2616.1.

Amador, J. A. (2008), The Intra Americas Seas Low-Level Jet (IALLJ): Overview and future research, in *Trends and Directions in Climate Research*, edited by L. Gimeno, R. Garcia, and R. Trigo, *Ann. N. Y. Acad. Sci.*, *1146*, 153–188.

Andersson, A., C. Klepp, K. Fennig, S. Bakan, H. Grassl, and J. Schulz (2011), Evaluation of HOAPS-3 ocean surface freshwater flux components, *J. Appl. Meteorol. Climatol.*, *50*, 379–398, doi:10.1175/2010JAMC2341.1.

Andersson, E., et al. (2005), Assimilation and modeling of the atmospheric hydrological cycle in the ECMWF forecasting system, *Bull. Am. Meteorol. Soc.*, *82*, 387–402, doi:10.1175/BAMS-86-3-387.

Andrews, E. D., R. C. Antweiler, P. J. Neiman, and F. M. Ralph (2004), Influence of ENSO on flood frequency along the California Coast, *J. Clim.*, *17*, 337–348, doi:10.1175/1520-0442(2004)017<0337:IOEOFF>2.0.CO;2.

Baldocchi, D., et al. (2001), FLUXNET: A new tool to study the temporal and spatial variability of ecosystem-scale carbon dioxide, water vapor, and energy flux densities, *Bull. Am. Meteorol. Soc.*, *82*, 2415–2434, doi:10.1175/1520-0477(2001)082<2415:FANTTS>2.3.CO;2.

Bales, R. C. (2003), Hydrology, overview, in *Encyclopedia of Atmospheric Sciences*, 2nd ed., pp. 968–973, Academic, Amsterdam.

Bao, J. W., S. A. Michelson, P. J. Neiman, F. M. Ralph, and J. M. Wilczak (2006), Interpretation of enhanced integrated water vapor bands associated with extratropical cyclones: Their formation and connection to tropical moisture, *Mon. Weather Rev.*, *134*, 1063–1080, doi:10.1175/MWR3123.1.

Barriopedro, D., E. M. Fischer, J. Luterbacher, R. M. Trigo, and R. García-Herrera (2011), The hot summer of 2010: Redrawing the temperature record map of Europe, *Science*, *332*, 220–224, doi:10.1126/science.1201224.

Bates, J. J., D. L. Jackson, F. M. Breon, and Z. D. Bergen (2001), Variability of tropical upper tropospheric humidity, *J. Geophys. Res.*, *106*(D23), 32,271–32,281, doi:10.1029/2001JD000347.

Bengtsson, L., K. I. Hodges, and E. Roeckner (2006), Storm tracks and climate change, *J. Clim.*, *19*, 3518–3543, doi:10.1175/JCLI3815.1.

Benson, L., and H. Klieforth (1989), Stable isotopes in precipitation and ground water in the Yucca Mountain Region, southern Nevada: Paleoclimatic implications, in *Aspects of Climate Variability in the Pacific and the Western Americas*, *Geophys. Monogr. Ser.*, vol. 55, edited by D. H. Peterson, pp. 41–59, AGU, Washington, D. C., doi:10.1029/GM055p0041.

Benton, G. S., and M. A. Estoque (1954), Water vapor transfer over the North American continent, *J. Meteorol.*, *11*(6), 462–477, doi:10.1175/1520-0469(1954)011<0462:WVTOTN>2.0.CO;2.

Bielli, S., and R. Roca (2010), Scale decomposition of atmospheric water budget over West Africa during the monsoon 2006 from NCEP/GFS analyses, *Clim. Dyn.*, *35*(1), pp. 143–157, doi:10.1007/s00382-009-0597-5.

Bingham, F. M., G. R. Foltz, and M. J. McPhaden (2010), Seasonal cycles of surface layer salinity in the Pacific Ocean, *Ocean Sci.*, *6*, 775–787, doi:10.5194/os-6-775-2010.

Bisselink, B., and A. Dolman (2008), Precipitation recycling: Moisture sources over Europe using ERA-40 data, *J. Hydrometeorol.*, *9*(5), 1073–1083, doi:10.1175/2008JHM962.1.

Bisselink, B., and A. Dolman (2009), Recycling of moisture in Europe: Contribution of evaporation to variability in very wet and dry years, *Hydrol. Earth Syst. Sci.*, *13*(9), 1685–1697, doi:10.5194/hess-13-1685-2009.

Bloom, S. C., L. L. Takacs, A. M. da Silva, and D. Ledvina (1996), Data assimilation using incremental analysis updates, *Mon. Weather Rev.*, *124*, 1256–1271, doi:10.1175/1520-0493(1996)124<1256:DAUIAU>2.0.CO;2.

Blossey, P. N., Z. Kuang, and D. M. Romps (2010), Isotopic composition of water in the tropical tropopause layer in cloud-resolving simulations of an idealized tropical circulation, *J. Geophys. Res.*, *115*, D24309, doi:10.1029/2010JD014554.

Bosilovich, M., and J. Chern (2006), Simulation of water sources and precipitation recycling for the MacKenzie, Mississippi, and Amazon River basins, *J. Hydrometeorol.*, *7*, 312–329, doi:10.1175/JHM501.1.

Bosilovich, M. G., and S. D. Schubert (2001), Precipitation recycling in the GEOS-1 data assimilation system over the central United States, *J. Hydrometeorol.*, *2*, 26–35, doi:10.1175/1525-7541(2001)002<0026:PROTCU>2.0.CO;2.

Bosilovich, M. G., and S. D. Schubert (2002), Water vapor tracers as diagnostics of the regional hydrologic cycle, *J. Hydrometeorol.*, *3*, 149–165, doi:10.1175/1525-7541(2002)003<0149:WVTADO>2.0.CO;2.

Bosilovich, M. G., Y. C. Sud, S. D. Schubert, and G. K. Walker (2003), Numerical simulation of the large-scale North American Monsoon water sources, *J. Geophys. Res.*, *108*(D16), 8614, doi:10.1029/2002JD003095.

Bosilovich, M., S. Schubert, G. Kim, R. Gelaro, M. Rienecker, M. Suarez, J. Bacmeister, R. Todling, and J. Chen (2006), NASA's Modern Era Retrospective-analysis for Research and Applications (MERRA), *Eos Trans. AGU*, *87*(52), Fall Meet. Suppl., Abstract H32A-03.

Bowen, G. J. (2009), Gridded maps of the isotopic composition of meteoric precipitation, Purdue Univ., West Lafayette, Indiana. [Available at http://www.waterisotopes.org.]

Bowen, G. J., and J. Revenaugh (2003), Interpolating the isotopic composition of modern meteoric precipitation, *Water Resour. Res.*, *39*(10), 1299, doi:10.1029/2003WR002086.

Brimelow, J. C., and G. W. Reuter (2005), Transport of atmospheric moisture during three extreme rainfall events over the Mackenzie River Basin, *J. Hydrometeorol.*, *6*, 423–440, doi:10.1175/JHM430.1.

Brubaker, K. L., D. Entekhabi, and P. S. Eagleson (1993), Estimation of continental precipitation recycling, *J. Clim.*, *6*(6), 1077–1089, doi:10.1175/1520-0442(1993)006<1077:EOCPR>2.0.CO;2.

Brubaker, K. L., P. A. Dirmeyer, A. Sudradjat, B. S. Levy, and F. Bernal (2001), A 36-yr climatological description of the evaporative sources of warm-season precipitation in the Mississippi River basin, *J. Hydrometeorol.*, *2*, 537–557, doi:10.1175/1525-7541(2001)002<0537:AYCDOT>2.0.CO;2.

Budyko, M. I. (1974), *Climate and Life*, 508 pp., Academic, New York.

Budyko, M. I., and O. A. Drozdov (1953), Zakonomernosti vlagooborota v tmosphere (regularities of the hydrologic cycle in the atmosphere), *Izv. Akad. Nauk SSSR Ser. Geogr.*, *4*, 5–14.

Burde, G. I., and A. Zangvil (2001a), The estimation of regional precipitation recycling. Part I: Review of recycling models, *J. Clim.*, *14*, 2497–2508, doi:10.1175/1520-0442(2001)014<2497:TEORPR>2.0.CO;2.

Burde, G. I., and A. Zangvil (2001b), The estimation of regional precipitation recycling. Part II: A new recycling model, *J. Clim.*, *14*, 2509–2527, doi:10.1175/1520-0442(2001)014<2509:TEORPR>2.0.CO;2.

Burde, G. I., et al. (2006), Bulk recycling models with incomplete vertical mixing. Part I: Conceptual framework and models, *J. Clim.*, *19*, 1461–1472, doi:10.1175/JCLI3687.1.

Cadet, D. L., and N. O. Nnoli (1987), Water vapour transport over Africa and the Atlantic Ocean during summer 1979, *Q. J. R. Meteorol. Soc.*, *113*, 581–602, doi:10.1002/qj.49711347609.

Carvalho, L. M. V., A. E. Silva, C. Jones, B. Liebmann, P. L. Silva Dias, and H. R. Rocha (2010), Moisture transport and intraseasonal variability in the South America Monsoon system, *Clim. Dyn.*, *46*, 1865–1880.

Cavazos, T., and D. Rivas (2004), Variability of extreme precipitation events in Tijuana, Mexico, *Clim. Res.*, *25*, 229–243, doi:10.3354/cr025229.

Chan, S. C., and V. Misra (2010), A diagnosis of the 1979–2005 extreme rainfall events in the southeastern United States with isentropic moisture tracing, *Mon. Weather Rev.*, *138*, 1172–1185, doi:10.1175/2009MWR3083.1.

Chou, S., E. Nelkin, J. Ardizzone, R. Atlas, and C. Shie (2003), Surface turbulent heat and momentum fluxes over global oceans based on the Goddard satellite retrievals, Version 2(GSSTF2), *J. Clim.*, *16*, 3256–3273, doi:10.1175/1520-0442(2003)016<3256:STHAMF>2.0.CO;2.

Christensen, J. H., and O. B. Christensen (2003), Severe summertime flooding in Europe, *Nature*, *421*, 805–806, doi:10.1038/421805a.

Cook, K. H. (1999), Generation of the African easterly jet and its role in determining West African precipitation, *J. Clim.*, *12*, 1165–1184, doi:10.1175/1520-0442(1999)012<1165:GOTAEJ>2.0.CO;2.

Coplen, T. B., P. J. Neiman, A. B. White, J. M. Landwehr, F. M. Ralph, and M. D. Dettinger (2008), Extreme changes in stable hydrogen isotopes and precipitation characteristics in a landfalling Pacific storm, *Geophys. Res. Lett.*, *35*, L21808, doi:10.1029/2008GL035481.

Craig, H., and L. I. Gordon (1965), Deuterium and oxygen-18 variations in the ocean and marine atmosphere, in *Proceedings of Conference on Stable Isotopes in Oceanic Studies and Paleotemperatures*, edited by E. Tongiorgi, pp. 9–130, Lab. Geol. and Nuclear Sci., Spoleto, Italy.

Curry, J. A., et al. (2004), SEAFLUX, *Bull. Am. Meteorol. Soc.*, *85*, 409–424, doi:10.1175/BAMS-85-3-409.

D'Abreton, P. C., and P. D. Tyson (1995), Divergent and non-divergent water vapor transport over southern Africa during wet and dry conditions, *Meteorol. Atmos. Phys.*, *55*(1–2), 47–59, doi:10.1007/BF01029601.

Dai, A. (2011), Drought under global warming: A review, *Wiley Interdiscip. Rev. Clim. Change*, *2*(1), 45–65, doi:10.1002/wcc.81.

Dai, A., and K. E. Trenberth (2002), Estimates of freshwater discharge from continents: Latitudinal and seasonal variations, *J. Hydrometeorol.*, *3*, 660–687, doi:10.1175/1525-7541(2002)003<0660:EOFDFC>2.0.CO;2.

Dai, A., et al. (2006), Recent trends in cloudiness over the United States: A tale of monitoring inadequacies, *Bull. Am. Meteorol. Soc.*, *87*, 597–606, doi:10.1175/BAMS-87-5-597.

Dai, A., J. Wang, P. W. Thorne, D. E. Parker, L. Haimberger, and X. L. Wang (2011), A new approach to homogenize radiosonde humidity data, *J. Clim.*, *24*, 965–991, doi:10.1175/2010JCLI3816.1.

Dansgaard, W. (1964), Stable isotopes in precipitation, *Tellus*, *16*, 436–468, doi:10.1111/j.2153-3490.1964.tb00181.x.

Dee, D. P., et al. (2011), The ERA-Interim reanalysis: Configuration and performance of the data assimilation system, *Q. J. R. Meteorol. Soc.*, *137*, 553–597, doi:10.1002/qj.828.

Dettinger, M. D. (2004), Fifty-two years of Pineapple-Express storms across the West Coast of North America, *PIER Proj. Rep. CEC-500-2005-004*, 15 pp., Calif. Energy Comm., Sacramento, Calif.

Dettinger, M. (2011), Climate change, atmospheric rivers, and floods in California—A multimodel analysis of storm frequency and magnitude changes, *J. Am. Water Resour. Assoc.*, *47*(3), 514–523, doi:10.1111/j.1752–1688.2011.00546.x.

Di Baldassarre, G., and A. Montanari (2009), Uncertainty in river discharge observations: A quantitative analysis, *Hydrol. Earth Syst. Sci.*, *13*(6), 913–921, doi:10.5194/hess-13-913-2009.

Dirmeyer, P. A., and K. L. Brubaker (1999), Contrasting evaporative moisture sources during the drought of 1988 and the flood of 1993, *J. Geophys. Res.*, *104*, 19,383–19,397, doi:10.1029/1999JD900222.

Dirmeyer, P. A., and K. L. Brubaker (2006), Evidence for trends in the Northern Hemisphere water cycle, *Geophys. Res. Lett.*, *33*, L14712, doi:10.1029/2006GL026359.

Dirmeyer, P. A., and K. L. Brubaker (2007), Characterization of the global hydrologic cycle from a back-trajectory analysis of atmospheric water vapor, *J. Hydrometeorol.*, *8*(1), 20–37, doi:10.1175/JHM557.1.

Dirmeyer, P. A., and J. L. Kinter III (2009), The "Maya Express": Floods in the U.S. Midwest, *Eos Trans. AGU*, *90*(12), 101, doi:10.1029/2009EO120001.

Dirmeyer, P. A., and J. L. Kinter (2010), Floods over the U.S. Midwest: A regional water cycle perspective, *J. Hydrometeorol.*, *11*, 1172–1181, doi:10.1175/2010JHM1196.1.

Dominguez, F., and P. Kumar (2008), Precipitation recycling variability and eco climatological stability–A study using NARR Data. Part I: Central US Plains ecoregion, *J. Clim.*, *21*, 5165–5186, doi:10.1175/2008JCLI1756.1.

Dominguez, F., P. Kumar, X. Liang, and M. Ting (2006), Impact of atmospheric moisture storage on precipitation recycling, *J. Clim.*, *19*(8), 1513–1530, doi:10.1175/JCLI3691.1.

Dominguez, F., P. Kumar, and E. R. Vivoni (2008), Precipitation recycling variability and ecoclimatological stability—A study using NARR Data. Part II: North American Monsoon region, *J. Clim.*, *21*, 5187–5203, doi:10.1175/2008JCLI1760.1.

Dominguez, F., J. C. Villegas, and D. D. Breshears (2009), Spatial extent of the North American Monsoon: Increased cross-regional linkages via atmospheric pathways, *Geophys. Res. Lett.*, *36*, L07401, doi:10.1029/2008GL037012.

Douglas, M. W., R. A. Maddox, K. Howard, and S. Reyes (1993), The Mexican Monsoon, *J. Clim.*, *6*, 1665–1677, doi:10.1175/1520-0442(1993)006<1665:TMM>2.0.CO;2.

Dressler, A. E., Z. Zhang, and P. Yang (2008), Water-vapor climate feedback inferred from climate fluctuations, 2003–2008, *Geophys. Res. Lett.*, *35*, L20704, doi:10.1029/2008GL035333.

Drumond, A., R. Nieto, L. Gimeno, and T. Ambrizzi (2008), A Lagrangian identification of major sources of moisture over Central Brazil and La Plata Basin, *J. Geophys. Res.*, *113*, D14128, doi:10.1029/2007JD009547.

Drumond, A., R. Nieto, R. M. Trigo, T. Ambrizzi, E. Souza, and L. Gimeno (2010), A Lagrangian identification of the main sources of moisture affecting northeastern Brazil during its pre-rainy and rainy seasons, *PLoS ONE*, *5*(6), e11205, doi:10.1371/journal.pone.0011205.

Drumond, A., L. Gimeno, and R. Nieto (2011), On the contribution of the tropical Western Hemisphere warm pool source of moisture to the Northern Hemisphere precipitation through a lagrangian approach, *J. Geophys. Res.*, *116*, D00Q04, doi:10.1029/2010JD015397.

Druyan, L. M., and R. D. Koster (1989), Sources of Sahel precipitation for simulated drought and rainy seasons, *J. Clim.*, *2*, 1438–1446, doi:10.1175/1520-0442(1989)002<1438:SOSPFS>2.0.CO;2.

Durán-Quesada, A. M., L. Gimeno, J. A. Amador, and R. Nieto (2010), Moisture sources for Central America: Identification of moisture sources using a Lagrangian analysis technique, *J. Geophys. Res.*, *115*, D05103, doi:10.1029/2009JD012455.

Eckhardt, S., A. Stohl, H. Wernli, P. James, C. Forster, and N. Spichtinger (2004), A 15-year climatology of warm conveyor belts, *J. Clim.*, *17*, 218–237, doi:10.1175/1520-0442(2004)017<0218:AYCOWC>2.0.CO;2.

Eltahir, E. A. B., and R. L. Bras (1994), Precipitation recycling in the Amazon basin, *Q. J. R. Meteorol. Soc.*, *120*, 861–880, doi:10.1002/qj.49712051806.

Eltahir, E. A. B., and R. L. Bras (1996), Precipitation recycling, *Rev. Geophys.*, *34*, 367–378, doi:10.1029/96RG01927.

Fairall, C. W., E. F. Bradley, J. E. Hare, A. A. Grachev, and J. B. Edson (2003), Bilk parameterization of air-sea fluxes: Updates and verification for the COARE algorithm, *J. Clim.*, *16*(4), 571–591, doi:10.1175/1520-0442(2003)016<0571:BPOASF>2.0.CO;2.

Farquhar, G. D., and L. A. Cernusak (2005), On the isotopic composition of leaf water in the non-steady state, *Funct. Plant Biol.*, *32*, 293–303, doi:10.1071/FP04232.

Ferretti, D., E. Pendall, J. Morgan, J. Nelson, D. LeCain, and A. Mosier (2003), Partitioning evapotranspiration fluxes from a Colorado grassland using stable isotopes: Seasonal variations and ecosystem implications of elevated atmospheric CO_2, *Plant Soil*, *254*, 291–303, doi:10.1023/A:1025511618571.

Fischer, E. M., S. I. Seneviratne, D. Luthi, and C. Schaer (2007), Contribution of land-atmosphere coupling to recent European summer heat waves, *Geophys. Res. Lett.*, *34*, L06707, doi:10.1029/2006GL029068.

Fisher, J. B., K. P. Tu, and D. D. Baldocchi (2008), Global estimates of the landatmosphere water flux based on monthly AVHRR and ISLSCP-II data, validated at 16 FLUXNET sites, *Remote Sens. Environ.*, *112*(3), 901–919, doi:10.1016/j.rse.2007.06.025.

Fontaine, B., P. Roucou, and S. Trzaska (2003), Atmospheric water cycle and moisture fluxes in the West African Monsoon: Mean annual cycles and relationship using NCEP/NCAR reanalysis, *Geophys. Res. Lett.*, *30*(3), 1117, doi:10.1029/2002GL015834.

Frankenberg, C., et al. (2009), Dynamic processes governing the isotopic composition of water vapor as observed from space and ground, *Science*, *325*, 1374–1377, doi:10.1126/science.1173791.

Friedman, I., G. I. Smith, J. D. Gleason, A. Warden, and J. M. Harris (1992), Stable isotope composition of waters in southeastern California. 1. Modern precipitation, *J. Geophys. Res.*, *97*(D5), 5795–5812, doi:10.1029/92JD00184.

Friedman, I., J. M. Harris, G. I. Smith, and C. A. Johnson (2002), Stable isotope composition of waters in the Great Basin, United States 1. Air-mass trajectories, *J. Geophys. Res.*, *107*(D19), 4400, doi:10.1029/2001JD000565.

Fudeyasu, H., Y. Wang, M. Satoh, T. Nasuno, H. Miura, and W. Yanase (2008), Global cloud-system-resolving model NICAM successfully simulated the lifecycles of two real tropical cyclones, *Geophys. Res. Lett.*, *35*, L22808, doi:10.1029/2008GL036003.

Gat, J. R., and I. Carmi (1970), Evolution of the isotopic composition of the atmospheric water in the Mediterranean Sea area, *J. Geophys. Res.*, *75*(15), 3039–3048, doi:10.1029/JC075i015p03039.

Gimeno, L., A. Drumond, R. Nieto, R. M. Trigo, and A. Stohl (2010a), On the origin of continental precipitation, *Geophys. Res. Lett.*, *37*, L13804, doi:10.1029/2010GL043712.

Gimeno, L., R. Nieto, R. M. Trigo, S. M. Vicente-Serrano, and J. I. López-Moreno (2010b), Where does the Iberian Peninsula moisture come from? An answer based on a Lagrangian approach, *J. Hydrometeorol.*, *11*, 421–436, doi:10.1175/2009JHM1182.1.

Gimeno, L., R. Nieto, A. Drumond, A. M. Durán-Quesada, A. Stohl, H. Sodemann, and R. M. Trigo (2011), A close look at oceanic sources of continental precipitation, *Eos Trans. AGU*, *92*(23), 193–194, doi:10.1029/2011EO230001.

Goessling, H., and C. H. Reick (2011), What do moisture recycling estimates tell? Lessons from an extreme global land-cover change model experiment, *Hydrol. Earth Syst. Sci.*, *15*, 3217–3235, doi:10.5194/hess-15-3217-2011.

Gong, C. L., and E. A. B. Eltahir (1996), Sources of moisture for rainfall in West Africa, *Water Resour. Res.*, *32*(10), 3115–3121, doi:10.1029/96WR01940.

Goodberlet, M., C. Swift, and J. Wilkerson (1990), Ocean surface wind speed measurements of the Special Sensor Microwave/Imager (SSM/I), *IEEE Trans. Geosci. Remote Sens.*, *28*, 823–828, doi:10.1109/36.58969.

Gustafsson, M., D. Rayner, and D. Chen (2010), Extreme rainfall events in southern Sweden: Where does the moisture come from?, *Tellus, Ser. A*, *62*, 605–616, doi:10.1111/j.1600-0870.2010.00456.x.

Hagos, S. M., and K. H. Cook (2007), Dynamics of the West African Monsoon jump, *J. Clim.*, *20*, 5264–5284, doi:10.1175/2007JCLI1533.1.

Held, I. M., and B. J. Soden (2000), Water vapor feedback and global warming, *Annu. Rev. Energy Environ.*, *25*, 441–475, doi:10.1146/annurev.energy.25.1.441.

Held, I. M., and B. J. Soden (2006), Robust responses of the hydrological cycle to global warming, *J. Clim.*, *19*, 5686–5699, doi:10.1175/JCLI3990.1.

Helfand, H. M., and S. D. Schubert (1995), Climatology of the simulated Great Plains low-level jet and its contribution to the continental moisture budget of the United States, *J. Clim.*, *8*(4), 784–806, doi:10.1175/1520-0442(1995)008<0784:COTSGP>2.0.CO;2.

Henderson-Sellers, A., K. McGuffie, and H. Zhang (2002), Stable isotopes as validation tools for global climate model predictions of the impact of Amazonian deforestation, *J. Clim.*, *15*, 2664–2677, doi:10.1175/1520-0442(2002)015<2664:SIAVTF>2.0.CO;2.

Higgins, R. W., J. K. E. Schemm, W. Shi, and A. Leetma (2000), Extreme precipitation events in the western United States related to tropical forcing, *J. Clim.*, *13*, 793–820, doi:10.1175/1520-0442(2000)013<0793:EPEITW>2.0.CO;2.

Hilburn, K. A., and F. J. Wentz (2008), Intercalibrated passive microwave rain products from the Unified Microwave Ocean Retrieval Algorithm (UMORA), *J. Appl. Meteorol. Climatol.*, *47*, 778–794, doi:10.1175/2007JAMC1635.1.

Hoerling, M. P., and A. Kumar (2003), The perfect ocean for drought, *Science*, *299*, 691–694, doi:10.1126/science.1079053.

Houze, R. A. (1993), *Cloud Dynamics*, *Int. Geophys. Ser.*, vol. 53, Academic, San Diego.

Hsu, K., X. Gao, S. Sorooshian, and H. Gupta (1997), Precipitation estimation from remotely sensed information using artificial neural networks, *J. Appl. Meteorol.*, *36*, 1176–1190, doi:10.1175/1520-0450(1997)036<1176:PEFRSI>2.0.CO;2.

Hu, Q., and S. Feng (2002), Interannual rainfall variations in the North American Summer Monsoon region: 1900–98, *J. Clim.*, *15*, 1189–1202, doi:10.1175/1520-0442(2002)015<1189:IRVITN>2.0.CO;2.

Huffman, G. J., et al. (1997), The Global Precipitation Climatology Project (GPCP) combined precipitation dataset, *Bull. Am. Meteorol. Soc.*, *78*, 5–20, doi:10.1175/1520-0477(1997)078<0005:TGPCPG>2.0.CO;2.

Huffman, G. J., et al. (2007), The TRMM Multisatellite Precipitation Analysis (TMPA): Quasi-global, multiyear, combined-sensor precipitation estimates at fine scales, *J. Hydrometeorol.*, *8*, 38–55, doi:10.1175/JHM560.1.

Ingraham, N. L., and B. E. Taylor (1991), Light stable isotope systematics of large-scale hydrologic regimes in California and Nevada, *Water Resour. Res.*, *27*(1), 77–90, doi:10.1029/90WR01708.

Intergovernmental Panel on Climate Change (IPCC) (2007), *Climate Change 2007: The Physical Science Basis: Working Group I Contribution to the Fourth Assessment Report of the IPCC*, edited by S. Solomon et al., Cambridge Univ. Press, New York.

Joussaume, S., J. Jouzel, and R. Sadourny (1984), A general circulation model of water isotope cycles in the atmosphere, *Nature*, *311*, 24–29, doi:10.1038/311024a0.

Joyce, R. J., J. E. Janowiak, P. A. Arkin, and P. Xie (2004), CMORPH: A method that produces global precipitation estimates from passive microwave and infrared data at high spatial and temporal resolution, *J. Hydrometeorol.*, *5*, 487–503, doi:10.1175/1525-7541(2004)005<0487:CAMTPG>2.0.CO;2.

Jung, M., et al. (2010), Recent decline in the global land evapotranspiration trend due to limited moisture supply, *Nature*, *467*(7318), 951–954, doi:10.1038/nature09396.

Kanamitsu, M., W. Ebisuzaki, J. Woollen, S. Yang, J. Hnilo, M. Fiorino, and G. Potter (2002), NCEPDOE AMIP-II reanalysis (R-2), *Bull. Am. Meteorol. Soc.*, *83*, 1631–1643, doi:10.1175/BAMS-83-11-1631.

Kendall, C., and T. B. Coplen (2001), Distribution of oxygen-18 and deuterium in river waters across the United States, *Hydrol. Processes*, *15*, 1363–1393, doi:10.1002/hyp.217.

Keys, P. W., R. J. van der Ent, L. J. Gordon, H. Hoff, R. Nikoli, and H. G. G. Savenije (2012), Analyzing precipitationsheds to understand the vulnerability of rainfall dependent regions, *Biogeosciences*, *9*, 733–746, doi:10.5194/bg-9-733-2012.

Kiehl, J. T., and K. E. Trenberth (1997), Earth's annual global mean energy budget, *Bull. Am. Meteorol. Soc.*, *78*, 197–208, doi:10.1175/1520-0477(1997)078<0197:EAGMEB>2.0.CO;2.

Kistler, R., et al. (2001), The NCEP-NCAR 50-year reanalysis: Monthly means CD-ROM and documentation, *Bull. Am. Meteorol. Soc.*, *82*, 247–267, doi:10.1175/1520-0477(2001)082<0247:TNNYRM>2.3.CO;2.

Knippertz, P., and J. E. Martin (2005), Tropical plumes and extreme precipitation in subtropical and tropical West Africa, *Q. J. R. Meteorol. Soc.*, *131*, 2337–2365, doi:10.1256/qj.04.148.

Knippertz, P., and H. Wernli (2010), A Lagrangian climatology of tropical moisture exports to the Northern Hemispheric extratropics, *J. Clim.*, *23*, 987–1003, doi:10.1175/2009JCLI3333.1.

Koster, R., J. Jouzel, R. Souzzo, G. Russel, D. Rind, and P. S. Eagleson (1986), Global sources of local precipitation as determined by the NASA/GISS GCM, *Geophys. Res. Lett.*, *13*, 121–124, doi:10.1029/GL013i002p00121.

Krishnamurthy, V., and J. Shukla (2000), Intraseasonal and interannual variability of rainfall over India, *J. Clim.*, *13*, 4366–4377, doi:10.1175/1520-0442(2000)013<0001:IAIVOR>2.0.CO;2.

Kubota, M., and H. Tomita (2007), Introduction of J-OFURO latent heat flux version 2, paper presented at Joint EUMETSAT Meteorological Satellite Conference and 15th Satellite Meteorology and Oceanography Conference, Am. Meteorol. Soc., Amsterdam.

Kumar, A., J. Dudhia, R. Rotunno, D. Niyogi, and U. C. Mohanty (2008), Analysis of the 26 July 2005 heavy rain event over Mumbai, India using the Weather Research and Forecasting (WRF) model, *Q. J. R. Meteorol. Soc.*, *134*, 1897–1910, doi:10.1002/qj.325.

Kurita, N., N. Yoshida, G. Inoue, and E. A. Chayanova (2004), Modern isotope climatology of Russia: A first assessment, *J. Geophys. Res.*, *109*, D03102, doi:10.1029/2003JD003404.

Lagerloef, G., R. Schmitt, J. Schanze, and H. Y. Kao (2010), The ocean and the global water cycle, *Oceanography*, *23*(4), 82–93, doi:10.5670/oceanog.2010.07.

Large, W. G., and S. G. Yeager (2009), The global climatology of an interannually varying air-sea flux data set, *Clim. Dyn.*, *33*, 341–364, doi:10.1007/s00382-008-0441-3.

Lavers, D. A., R. P. Allan, E. F. Wood, G. Villarini, D. J. Brayshaw, and A. J. Wade (2011), Winter floods in Britain are connected to atmospheric rivers, *Geophys. Res. Lett.*, *38*, L23803, doi:10.1029/2011GL049783.

Lee, X., R. Smith, and J. Williams (2006), Water vapor $^{18}O/^{16}O$ isotope ratio in surface air in New England, USA, *Tellus*, *588*, 293–304.

Legates, D. R., H. F. Lins, and G. J. McCabe (2005), Comments on "Evidence for global runoff increase related to climate warming" by Labat et al., *Adv. Water Resour.*, *28*(12), 1310–1315, doi:10.1016/j.advwatres.2005.04.006.

Lettau, H., K. Lettau, and L. C. Molion (1979), Amazonia's hydrological cycle and the role of atmospheric recycling in assessing deforestation effects, *Mon. Weather Rev.*, *107*, 227–238, doi:10.1175/1520-0493(1979)107<0227:AHCATR>2.0.CO;2.

Leung, L. R., and Y. Qian (2009), Atmospheric rivers induced heavy precipitation and flooding in the western U.S. simulated by the WRF regional climate model, *Geophys. Res. Lett.*, *36*, L03820, doi:10.1029/2008GL036445.

Lewis, S. M., P. M. Brando, O. L. Phillips, G. M. F. van der Heijden, and D. Nepstad (2011), The 2010 Amazon drought, *Science*, *331*(6017), 554, doi:10.1126/science.1200807.

Liepert, B. G., and M. Previdi (2009), Do models and observations disagree on the rainfall response to global warming?, *J. Clim.*, *22*, 3156–3166, doi:10.1175/2008JCLI2472.1.

Liu, W. T., and W. Tang (2005), Estimating moisture transport over ocean using spacebased observations from space, *J. Geophys. Res.*, *110*, D10101, doi:10.1029/2004JD005300.

López-Moreno, J., S. Vicente-Serrano, L. Gimeno, and R. Nieto (2009), Stability of the seasonal distribution of precipitation in the Mediterranean region: Observations since 1950 and projections for the twenty-first century, *Geophys. Res. Lett.*, *36*, L10703, doi:10.1029/2009GL037956.

Lu, J., G. Vecchi, and T. Reichler (2007), Expansion of the Hadley cell under global warming, *Geophys. Res. Lett.*, *34*, L06805, doi:10.1029/2006GL028443.

Marengo, J. A., et al. (2008), The drought of Amazonia in 2005, *J. Clim.*, *21*, 495–516, doi:10.1175/2007JCLI1600.1.

Mariotti A., N. Zeng, J. Yoon, V. Artale, A. Navarra, P. Alpertand, and L. Z. W. Li (2008), Mediterranean water cycle changes: Transition to drier 21st century conditions in observations and CMIP3 simulations, *Environ. Res. Lett*, *3*, 044001, doi:10.1088/1748-9326/3/4/044001.

Massacand, A. C., H. Wernli, and H. C. Davies (1998), Heavy precipitation on the Alpine southside: An upper-level precursor, *Geophys. Res. Lett.*, *25*, 1435–1438, doi:10.1029/98GL50869.

Meehl, G. A. (1994), Influence of the land surface in the Asian Summer Monsoon: External conditions versus internal feedbacks, *J. Clim.*, *7*, 1033–1049, doi:10.1175/1520-0442(1994)007<1033:IOTLSI>2.0.CO;2.

Merlivat, L., and J. Jouzel (1979), Global climatic interpretation of the deuterium-oxygen 18 relationship for precipitation, *J. Geophys. Res.*, *84*, 5029–5033, doi:10.1029/JC084iC08p05029.

Michael, H. A., A. E. Mulligan, and C. F. Harvey (2005), Seasonal oscillations in water exchange between aquifers and the coastal ocean, *Nature*, *436*(7054), 1145–1148, doi:10.1038/nature03935.

Mo, K. C., and R. W. Higgins (1996), Large-scale atmospheric moisture transport as evaluated in the NCEP/NCAR and the NASA/DAO reanalyses, *J. Clim.*, *9*, 1531–1545, doi:10.1175/1520-0442(1996)009<1531:LSAMTA>2.0.CO;2.

Moreira, M. Z., L. D. L. Sternberg, L. A. Martinelli, R. L. Victoria, E. M. Barbosa, L. C. M. Bonates, and D. C. Nepstad (1997), Contribution of transpiration to forest ambient vapor based on isotopic measurements, *Global Change Biol.*, *3*(5), 439–450, doi:10.1046/j.1365-2486.1997.00082.x.

Mu, Q., F. A. Heinsch, M. Zhao, and S. W. Running (2007), Development of a global evapotranspiration algorithm based on MODIS and global meteorology data, *Remote Sens. Environ.*, *111*(4), 519–536, doi:10.1016/j.rse.2007.04.015.

Neiman, P. J., F. M. Ralph, A. B. White, D. E. Kingsmill, and P. O. G. Persson (2002), The statistical relationship between upslope flow and rainfall in California's coastal mountains: Observations during CALJET, *Mon. Weather Rev.*, *130*, 1468–1492, doi:10.1175/1520-0493(2002)130<1468:TSRBUF>2.0.CO;2.

Neiman, P. J., J. L. J. Schick, F. M. Ralph, M. Hughes, and G. A. Wick (2011), Flooding in western Washington: The connection to atmospheric rivers, *J. Hydrometeorol.*, *12*, 1337–1358, doi:10.1175/2011JHM1358.1.

New, M., M. Todd, M. Hulme, and P. Jones (2001), Precipitation measurements and trends in the twentieth century, *Int. J. Climatol.*, *21*(15), 1889–1922, doi:10.1002/joc.680.

Newell, R. E., Y. Zhu, and C. Scott (1992), Tropospheric rivers? A pilot study, *Geophys. Res. Lett.*, *19*(24), 2401–2404, doi:10.1029/92GL02916.

Nicholson, S. (2000), Land surface processes and Sahel climate, *Rev. Geophys.*, *38*(1), 117–139, doi:10.1029/1999RG900014.

Nieto, R., L. Gimeno, and R. M. Trigo (2006), A Lagrangian identification of major sources of Sahel moisture, *Geophys. Res. Lett.*, *33*, L18707, doi:10.1029/2006GL027232.

Nieto, R., D. Gallego, R. M. Trigo, P. Ribera, and L. Gimeno (2008), Dynamic identification of moisture sources in the Orinoco basin in equatorial South America, *Hydrol. Sci. J.*, *53*(3), 602–617, doi:10.1623/hysj.53.3.602.

Nieto, R., A. M. Durán-Quesada, and L. Gimeno (2010), Major sources of moisture over Antarctic ice-core sites identified through a Lagrangian approach, *Clim. Res.*, *41*, 45–49, doi:10.3354/cr00842.

Noone, D., and C. Sturm (2010), Comprehensive dynamical models of global and regional water isotope distributions, *Isoscapes*, *2*, 195–219, doi:10.1007/978-90-481-3354-3_10.

Numaguti, A. (1999), Origin and recycling processes of precipitating water over the Eurasian continent: Experiments using an atmospheric general circulation model, *J. Geophys. Res.*, *104*, 1957–1972, doi:10.1029/1998JD200026.

Oki, T. (2005), The hydrologic cycles and global circulation, in *Encyclopedia of Hydrological Sciences*, edited by M. G. Anderson and J. McDonnell, pp. 13–22, John Wiley, New York.

Ordóñez, P., P. Ribera, D. Gallego, and C. Peña-Ortiz (2012), Major moisture sources for western and southern India and their role on synoptic-scale rainfall events, *Hydrol. Processes*, doi:10.1002/hyp.8455, in press.

Palmer, W. C. (1965), *Meteorological Droughts*, *Weather Bur. Res. Pap.*, vol. 45, 58 pp., U. S. Dep. of Commer., Washington, D. C.

Paredes, D., R. M. Trigo, R. García-Herrera, and I. F. Trigo (2006), Understanding precipitation changes in Iberia in early Spring: Weather typing and storm-tracking approaches, *J. Hydrometeorol.*, *7*, 101–113, doi:10.1175/JHM472.1.

Payne, V. H., D. Noone, A. Dudhia, C. Piccolo, and R. G. Grainger (2007), Global satellite measurements of HDO and implications for understanding the transport of water vapor into the stratosphere, *Q. J. R. Meteorol. Soc.*, *133*(627), 1459–1471, doi:10.1002/qj.127.

Peixoto, J. P., and A. H. Oort (1982), The atmospheric branch of the hydrologic cycle and climate, in *Variations in the Global Water Budget*, edited by A. Street-Perrotte et al., pp. 5–65, D. Reidel, Dordrecht, Netherlands.

Peixoto, J. P., and A. H. Oort (1992), *Physics of Climate*, 520 pp., Am. Inst. of Phys., New York.

Peixoto, J. P., D. A. Salstein, and R. D. Rosen (1981), Intra-annual variations in large-scale moisture fields, *J. Geophys. Res.*, *86*, 1255–1264, doi:10.1029/JC086iC02p01255.

Pfahl, S., and H. Wernli (2009), Lagrangian simulations of stable isotopes in water vapor: An evaluation of nonequilibrium fractionation in the Craig-Gordon model, *J. Geophys. Res.*, *114*, D20108, doi:10.1029/2009JD012054.

Philipona, R., B. Dürr, C. Marty, A. Ohmura, and M. Wild (2004), Radiative forcing–measured at Earth's surface–corroborate the increasing greenhouse effect, *Geophys. Res. Lett.*, *31*, L03202, doi:10.1029/2003GL018765.

Philipona, R., B. Dürr, A. Ohmura, and C. Ruckstuhl (2005), Anthropogenic greenhouse forcing and strong water vapor feedback increase temperature in Europe, *Geophys. Res. Lett.*, *32*, L19809, doi:10.1029/2005GL023624.

Pierrehumbert, R. T., and R. Roca (1998), Evidence for control of Atlantic subtropical humidity, *Geophys. Res. Lett.*, *25*, 4537–4540, doi:10.1029/1998GL900203.

Poveda, G., P. R. Waylen, and R. S. Pulwarty (2006), Annual and inter-annual variability of the present climate in northern South America and southern Mesoamerica, *Palaeogeogr. Palaeoclimatol. Palaeoecol.*, *234*, 3–27, doi:10.1016/j.palaeo.2005.10.031.

Pu, B., and K. H. Cook (2011), Role of the West African westerly jet in Sahel rainfall variations, *J. Clim.*, *25*, 2880–2896, doi:10.1175/JCLI-D-11-00394.1.

Quante, M., and V. Matthias (2006), Water in the Earth's atmosphere, *J. Phys. IV*, *139*, 37–61, doi:10.1051/jp4:2006139005.

Ralph, F. M., and M. D. Dettinger (2011), Storms, floods, and the science of atmospheric rivers, *Eos Trans. AGU*, *92*(32), 265, doi:10.1029/2011EO320001.

Ralph, F. M., P. J. Neiman, and G. A. Wick (2004), Satellite and CALJET aircraft observations of atmospheric rivers over the eastern North Pacific Ocean during the winter of 1997/98, *Mon. Weather Rev.*, *132*, 1721–1745, doi:10.1175/1520-0493(2004)132<1721:SACAOO>2.0.CO;2.

Ralph, F. M., P. J. Neiman, and R. Rotunno (2005), Dropsonde observations in low-level jets over the northeastern Pacific Ocean from CALJET-1998 and PACJET-2001: Mean vertical-profile and atmospheric-river characteristics, *Mon. Weather Rev.*, *133*(4), 889–910, doi:10.1175/MWR2896.1.

Ralph, F. M., P. J. Neiman, G. A. Wick, S. I. Gutman, M. D. Dettinger, D. R. Cayan, and A. B. White (2006), Flooding on

California's Russian River: Role of atmospheric rivers, *Geophys. Res. Lett.*, *33*, L13801, doi:10.1029/2006GL026689.

Rasmusson, E. M. (1967), Atmospheric water vapor transport and the water balance of North America, *Mon. Weather Rev.*, *95*, 403–426, doi:10.1175/1520-0493(1967)095<0403:AWVTAT>2.3.CO;2.

Reale, O., L. Feudale, and B. Turato (2001), Evaporative moisture sources during a sequence of floods in the Mediterranean region, *Geophys. Res. Lett.*, *28*(10), 2085–2088, doi:10.1029/2000GL012379.

Reboita, M. S., R. Nieto, L. Gimeno, R. P. da Rocha, T. Ambrizzi, R. Garreaud, and L. F. Krüger (2010), Climatological features of cutoff low systems in the Southern Hemisphere, *J. Geophys. Res.*, *115*, D17104, doi:10.1029/2009JD013251.

Reichstein, M., et al. (2007), Reduction of ecosystem productivity and respiration during the European summer 2003 climate anomaly: A joint flux tower, remote sensing and modelling analysis, *Global Change Biol.*, *13*, 634–651, doi:10.1111/j.1365-2486.2006.01224.x.

Ren, L., and S. C. Riser (2009), Seasonal salt budget in the northeast Pacific Ocean, *J. Geophys. Res.*, *114*, C12004, doi:10.1029/2009JC005307.

Risi, C., S. Bony, F. Vimeux, L. Descroix, B. Ibrahim, E. Lebreton, I. Mamadou, and B. Sultan (2008), What controls the isotopic composition of the African Monsoon precipitation? Insights from event-based precipitation collected during the 2006 AMMA campaign, *Geophys. Res. Lett.*, *35*, L24808, doi:10.1029/2008GL035920.

Risi, C., S. Bony, F. Vimeux, C. Frankenberg, D. Noone, and J. Worden (2010a), Understanding the Sahelian water budget through the isotopic composition of water vapor and precipitation, *J. Geophys. Res.*, *115*, D24110, doi:10.1029/2010JD014690.

Risi, C., S. Bony, F. Vimeux, and J. Jouzel (2010b), Water stable isotopes in the LMDZ4 General Circulation Model: Model evaluation for present day and past climates and applications to climatic interpretation of tropical isotopic records, *J. Geophys. Res.*, *115*, D12118, doi:10.1029/2009JD013255.

Risi, C., et al. (2012), Process-evaluation of tropospheric humidity simulated by general circulation models using water vapor isotopologues: 1. Comparison between models and observations, *J. Geophys. Res.*, *117*, D05303, doi:10.1029/2011JD016621.

Roads, J., et al. (2003), GCIP water and energy budget synthesis (WEBS), *J. Geophys. Res.*, *108*(D16), 8609, doi:10.1029/2002JD002583.

Robinson, I. (2004), *Measuring the Oceans From Space: The Principles and Methods of Satellite Oceanography*, 669 pp., Springer, Berlin.

Robinson, P. J. (2000), Temporal trends in United States dew point temperatures, *Int. J. Climatol.*, *20*, 985–1002, doi:10.1002/1097-0088(200007)20:9<985::AID-JOC513>3.0.CO;2-W.

Roderick, M. L., and G. D. Farquhar (2002), The cause of decreased pan evaporation over the past 50 years, *Science*, *298*(5597), 1410–1411, doi:10.1126/science.1075390-a.

Ross, R. J., and W. P. Elliott (1996), Tropospheric water vapor climatology and trends over North America: 1973–93, *J. Clim.*, *9*, 3561–3574, doi:10.1175/1520-0442(1996)009<3561:TWVCAT>2.0.CO;2.

Ross, R. J., and W. P. Elliott (2001), Radiosonde-based Northern Hemisphere tropospheric water vapor trends, *J. Clim.*, *14*, 1602–1612, doi:10.1175/1520-0442(2001)014<1602:RBNHTW>2.0.CO;2.

Rozanski, K., C. Sonntag, and K. O. Munnich (1982), Factors controlling stable isotope composition of European precipitation, *Tellus*, *34*, 142–150, doi:10.1111/j.2153-3490.1982.tb01801.x.

Salati, E., A. D. Olio, E. Matsui, and J. R. Gat (1979), Recycling of water in the Amazon Basin: An isotopic study, *Water Resour. Res.*, *15*, 1250–1258, doi:10.1029/WR015i005p01250.

Sanchez-Gomez, E., S. Somot, S. A. Josey, C. Dubois, N. Elguindi, and M. Déqué (2011), Evaluation of Mediterranean Sea water and heat budgets simulated by an ensemble of high resolution regional climate models, *Clim. Dyn.*, *37*, 2067–2086, doi:10.1007/s00382-011-1012-6.

Santer, B. D., et al. (2007), Identification of human-induced changes in atmospheric moisture content, *Proc. Natl. Acad. Sci. U. S. A.*, *104*, 15,248–15,253, doi:10.1073/pnas.0702872104.

Sapiano, M. R. P., T. M. Smith, and P. A. Arkin (2008), A new merged analysis of precipitation utilizing satellite and reanalysis data, *J. Geophys. Res.*, *113*, D22103, doi:10.1029/2008JD010310.

Savenije, H. H. G. (1995), New definitions for moisture recycling and the relationship with land-use changes in the Sahel, *J. Hydrol.*, *167*, 57–78, doi:10.1016/0022-1694(94)02632-L.

Schanze, J. J., R. W. Schmitt, and L. L. Yu (2010), The global oceanic freshwater cycle: A state-of-the-art quantification, *J. Mar. Res.*, *68*, 569–595, doi:10.1357/002224010794657164.

Schär, C., D. Luethi, U. Beyerle, and E. Heise (1999), The soil-precipitation feedback: A process study with a regional climate model, *J. Clim.*, *12*, 722–741, doi:10.1175/1520-0442(1999)012<0722:TSPFAP>2.0.CO;2.

Schär, C., P. L. Vidale, D. Lüthi, C. Frei, C. Häberli, M. A. Liniger, and C. Appenzeller (2004), The role of increasing temperature variability in European summer heatwaves, *Nature*, *427*, 332–336, doi:10.1038/nature02300.

Schewe, J., A. Levermann, and H. Cheng (2011), A critical humidity threshold for monsoon transitions, *Clim. Past Discuss.*, *7*, 1737–1765, doi:10.5194/cpd-7-1737-2011.

Schlosser, C. A., and P. R. Houser (2007), Assessing a satellite-era perspective of the global water cycle, *J. Clim.*, *20*, 1316–1338, doi:10.1175/JCLI4057.1.

Schmitz, J. T., and S. L. Mullen (1996), Water vapor transport associated with the summertime North American Monsoon as depicted by ECMWF analyses, *J. Clim.*, *9*, 1621–1634, doi:10.1175/1520-0442(1996)009<1621:WVTAWT>2.0.CO;2.

Schneider, M., K. Yoshimura, F. Hase, and T. Blumenstock (2010), The ground-based FTIR network's potential for investigating the atmospheric water cycle, *Atmos. Chem. Phys.*, *10*, 3427–3442, doi:10.5194/acp-10-3427-2010.

Schumacher, R. S., and T. J. Galarneau (2012), Moisture transport into midlatitudes ahead of recurving tropical cyclones and its relevance in two predecessor rain events, *Mon. Weather Rev.*, *140*, 1810–1827, doi:10.1175/MWR-D-11-00307.1.

Seager, R., et al. (2007), Model projections of an imminent transition to a more arid climate in southwestern North America, *Science*, *316*, 1181–1184, doi:10.1126/science.1139601.

Seager, R., N. Naik, and G. A. Vecchi (2010), Thermodynamic and dynamic mechanisms for large-scale changes in the hydrological cycle in response to global warming, *J. Clim.*, *23*, 4651–4668, doi:10.1175/2010JCLI3655.1.

Seidel, D. J. (2002), Water vapor: Distribution and trends, in *Encyclopedia of Global Environmental Change*, pp. 750–752, Wiley, New York.

Seneviratne, C. T., et al. (2010), Investigating soil moisture-climate interactions in a changing climate: A review, *Earth Sci. Rev.*, *99*, 125–161, doi:10.1016/j.earscirev.2010.02.004.

Seneviratne, S. I., D. Luthi, M. Litschi, and C. Schär (2006), Land-atmosphere coupling and climate change in Europe, *Nature*, *443*, 205–209, doi:10.1038/nature05095.

Seo, K. W., D. E. Waliser, B. Tian, J. S. Famiglietti, and T. H. Syed (2009), Evaluation of global land-to-ocean fresh water discharge and evapotranspiration using space-based observations, *J. Hydrol.*, *373*(3–4), 508–515, doi:10.1016/j.jhydrol.2009.05.014.

Shuttleworth, W. J. (2012), *Terrestrial Hydrometeorology*, John Wiley, West Sussex, U. K., doi:10.1002/9781119951933.

Simmonds, I., D. Bi, and P. Hope (1999), Atmospheric water vapor flux and its association with rainfall in China in summer, *J. Clim.*, *12*, 1353–1367, doi:10.1175/1520-0442(1999)012<1353:AWVFAI>2.0.CO;2.

Simmons, A. J., K. M. Willett, P. D. Jones, P. W. Thorne, and D. P. Dee (2010), Low-frequency variations in surface atmospheric humidity, temperature, and precipitation: Inferences from reanalyses and monthly gridded observational data sets, *J. Geophys. Res.*, *115*, D01110, doi:10.1029/2009JD012442.

Smith, E., J. Vazquez, A. Tran, and R. Sumagaysay (1996), Satellite-derived sea surface temperature data available from the NOAA/NASA Pathfinder Program, *Eos Trans. AGU*, *77*(14), 135, doi:10.1029/96EO00091.

Sodemann, H., and A. Stohl (2009), Asymmetries in the moisture origin of Antarctic precipitation, *Geophys. Res. Lett.*, *36*, L22803, doi:10.1029/2009GL040242.

Sodemann, H., C. Schwierz, and H. Wernli (2008), Interannual variability of Greenland winter precipitation sources: Lagrangian moisturediagnostic and North Atlantic Oscillation influence, *J. Geophys. Res.*, *113*, D03107, doi:10.1029/2007JD008503.

Sousa, P., R. M. Trigo, P. Aizpurua, R. Nieto, L. Gimeno, and R. Garcia-Herrera (2011), Trends and extremes of drought indices throughout the 20th century in the Mediterranean, *Nat. Hazards Earth Syst. Sci.*, *11*, 33–51, doi:10.5194/nhess-11-33-2011.

Starr, V. P., and J. P. Peixoto (1958), On the global balance of water vapor and the hydrology of deserts, *Tellus*, *10*(2), 189–194.

Sterl, A. (2004), On the (in)homogeneity of reanalysis products, *J. Clim.*, *17*, 3866–3873, doi:10.1175/1520-0442(2004)017<3866:OTIORP>2.0.CO;2.

Stewart, M. K. (1975), Stable isotope fractionation due to evaporation and isotopic exchange of falling waterdrops: Applications to atmospheric processes and evaporation of lakes, *J. Geophys. Res.*, *80*, 1133–1146, doi:10.1029/JC080i009p01133.

Stohl, A., and P. James (2004), A Lagrangian analysis of the atmospheric branch of the global water cycle. Part I: Method description, validation, and demonstration for the August 2002 flooding in central Europe, *J. Hydrometeorol.*, *5*, 656–678, doi:10.1175/1525-7541(2004)005<0656:ALAOTA>2.0.CO;2.

Stohl, A., and P. James (2005), A Lagrangian analysis of the atmospheric branch of the global water cycle. Part II: Earth's river catchments, ocean basins, and moisture transports between them, *J. Hydrometeorol.*, *6*, 961–984, doi:10.1175/JHM470.1.

Stohl, A., M. Hittenberger, and G. Wotawa (1998), Validation of the Lagrangian particle dispersion model FLEXPART against large scale tracer experiment data, *Atmos. Environ.*, *32*, 4245–4264, doi:10.1016/S1352-2310(98)00184-8.

Stohl, A., C. Forster, A. Frank, P. Seibert, and G. Wotawa (2005), Technical Note: The Lagrangian particle dispersion model FLEXPART version 6.2, *Atmos. Chem. Phys.*, *5*, 2461–2474.

Stohl, A., C. Forster, and H. Sodemann (2008), Remote sources of water vapor forming precipitation on the Norwegian west coast at 60°N–a tale of hurricanes and an atmospheric river, *J. Geophys. Res.*, *113*, D05102, doi:10.1029/2007JD009006.

Sturaro, G. (2003), A closer look at the climatological discontinuities present in the NCEP/NCAR reanalysis temperature due to the introduction of satellite data, *Clim. Dyn.*, *21*, 309–316, doi:10.1007/s00382-003-0334-4.

Sudradjat, A., K. L. Brubaker, and P. A. Dirmeyer (2003), Interannual variability of surface evaporative moisture sources of warm-season precipitation in the Mississippi River Basin, *J. Geophys. Res.*, *108*(D16), 8612, doi:10.1029/2002JD003061.

Syed, T. H., J. S. Famigliettia, D. P. Chamber, J. K. Willis, and K. Hilburn (2010), Satellite-based global-ocean mass balance estimates of interannual variability and emerging trends in continental freshwater discharge, *Proc. Natl. Acad. Sci. U. S. A.*, *107*(42), 17,916–17,921, doi:10.1073/pnas.1003292107.

Tapley, B. D., S. Bettadpur, M. Watkins, and C. Reigber (2004a), The gravity recovery and climate experiment: Mission overview and early results, *Geophys. Res. Lett.*, *31*, L09607, doi:10.1029/2004GL019920.

Tapley, B. D., S. Bettadpur, J. C. Ries, P. F. Thompson, and M. M. Watkins (2004b), GRACE measurements of mass variability in the Earth system, *Science*, *305*(5683), 503–505, doi:10.1126/science.1099192.

Trenberth, K. E., and C. J. Guillemot (1995), Evaluation of the global atmospheric moisture budget as seen from analyses, *J. Clim.*, *8*, 2255–2272, doi:10.1175/1520-0442(1995)008<2255:EOTGAM>2.0.CO;2.

Trenberth, K. E., and C. J. Guillemot (1996), Physical processes involved in the 1988 drought and 1993 floods in North America, *J. Clim.*, *9*, 1288–1298, doi:10.1175/1520-0442(1996)009<1288:PPIITD>2.0.CO;2.

Trenberth, K. E., A. Dai, R. M. Rasmussen, and D. B. Parsons (2003), The changing character of precipitation, *Bull. Am. Meteorol. Soc.*, *84*, 1205–1217, doi:10.1175/BAMS-84-9-1205.

Trenberth, K. E., J. Fasullo, and L. Smith (2005), Trends and variability in column integrated atmospheric water vapor, *Clim. Dyn.*, *24*, 741–758, doi:10.1007/s00382-005-0017-4.

Trenberth, K. E., L. Smith, T. Qian, A. Dai, and J. Fasullo (2007a), Estimates of the global water budget and its annual cycle using observational and model data, *J. Hydrometeorol.*, *8*, 758–769, doi:10.1175/JHM600.1.

Trenberth, K. E., et al. (2007b), Observations: Surface and atmospheric climate change, in *Climate Change 2007: The Physical Science Basis: Working Group I Contribution to the Fourth Assessment Report of the IPCC*, edited by S. Solomon et al., pp. 235–336, Cambridge Univ. Press, New York.

Trenberth, K. E., J. T. Fasullo, and J. Mackaro (2011), Atmospheric moisture transports from ocean to land and global energy flows in reanalyses, *J. Clim.*, *24*, 4907–4924, doi:10.1175/2011JCLI4171.1.

Trigo, I. F., T. D. Davies, and G. R. Bigg (1999), Objective climatology of cyclones in the Mediterranean region, *J. Clim.*, *12*, 1685–1696, doi:10.1175/1520-0442(1999)012<1685:OCOCIT>2.0.CO;2.

Trigo, R. M., C. Gouveia, and D. Barriopedro (2010), The intense 2007–2009 drought in the Fertile Crescent: Impacts and associated atmospheric circulation, *Agric. For. Meteorol.*, *150*, 1245–1257, doi:10.1016/j.agrformet.2010.05.006.

Tuinenburg, O. A., R. W. A. Hutjes, C. M. J. Jacobs, and P. Kabat (2011), Diagnosis of local land-atmosphere feedbacks in India, *J. Clim.*, *24*, 251–266, doi:10.1175/2010JCLI3779.1.

Tuinenburg, O. A., R. W. A. Hutjes, and P. Kabat (2012), The fate of evaporated water from the Ganges basin, *J. Geophys. Res.*, *117*, D01107, doi:10.1029/2011JD016221.

Ummenhofer, C. C., M. H. England, P. C. McIntosh, G. A. Meyers, M. J. Pook, J. S. Risbey, A. S. Gupta, and A. S. Taschetto (2009), What causes southeast Australia's worst droughts?, *Geophys. Res. Lett.*, *36*, L04706, doi:10.1029/2008GL036801.

United Nations (UN) (2008), *Trends in Sustainable Development, Agriculture, Rural Development, Land, Desertification and Drought*, Dep. of Econ. and Social Affairs, New York.

Uppala, S. M., et al. (2005), The ERA-40 re-analysis, *Q. J. R. Meteorol. Soc.*, *131*, 2961–3012, doi:10.1256/qj.04.176.

Vachon, R. W., J. M. Welker, J. W. C. White, and B. H. Vaughn (2010), Monthly precipitation isoscapes (δ^{18}O) of the United States: Connections with surface temperatures, moisture source conditions, and air mass trajectories, *J. Geophys. Res.*, *115*, D21126, doi:10.1029/2010JD014105.

Valsala, K. V., and M. Ikeda (2005), An extreme drought event in the 2002 summer monsoon rainfall and its mechanisms proved with a moisture flux analysis, *Sci. Online Lett. Atmos.*, *1*, 173–176.

van der Ent, R. J., H. H. G. Savenije, B. Schaefli, and S. C. Steele-Dunne (2010), Origin and fate of atmospheric moisture over continents, *Water Resour. Res.*, *46*, W09525, doi:10.1029/2010WR009127.

Vautard, R., P. Yiou, F. D'Andrea, N. de Noblet, N. Viovy, C. Cassou, J. Polcher, P. Ciais, M. Kageyama, and Y. Fan (2007), Summertime European heat and drought waves induced by wintertime Mediterranean rainfall déficit, *Geophys. Res. Lett.*, *34*, L07711, doi:10.1029/2006GL028001.

Vicente-Serrano, S. M., S. Beguería, and J. I. López-Moreno (2010), A multiscalar drought index sensitive to global warming: The standardized precipitation evapotranspiration index, *J. Clim.*, *23*, 1696–1718, doi:10.1175/2009JCLI2909.1.

Vinukollu, R. K., R. Meynadier, J. Sheffield, and E. F. Wood (2011), Multi-model, multi-sensor estimates of global evapotranspiration: Climatology, uncertainties and trends, *Hydrol. Processes*, *25*, 3993–4010, doi:10.1002/hyp.8393.

Wagner, T., S. Beirle, M. Grzegorski, S. Sanghavi, and U. Platt (2005), El Niño induced anomalies in global data sets of total column precipitable water and cloud cover derived from GOME on ERS-2, *J. Geophys. Res.*, *110*, D15104, doi:10.1029/2005JD005972.

Wang, C. (2007), Variability of the Caribbean low-level jet and its relations to climate, *Clim. Dyn.*, *29*, 411–422, doi:10.1007/s00382-007-0243-z.

Wang, J. X. L., and D. J. Gaffen (2001), Trends in extremes of surface humidity, temperatures and summertime heat stress in China, *Adv. Atmos. Sci.*, *18*, 742–751.

Wang, K., and R. E. Dickinson (2012), A review of global terrestrial evapotranspiration: Observation, modeling, climatology, and climatic variability, *Rev. Geophys.*, *50*, RG2005, doi:10.1029/2011RG000373.

Wang, X. F., and D. Yakir (2000), Using stable isotopes of water in evapotranspiration studies, *Hydrol. Processes*, *14*, 1407–1421, doi:10.1002/1099-1085(20000615)14:8<1407::AID-HYP992>3.0.CO;2-K.

Wei, J., P. A. Dirmeyer, M. J. Bosilovich, and R. Wu (2012), Water vapor sources for Yangtze River Valley rainfall: Climatology, variability, and implications for rainfall forecasting, *J. Geophys. Res.*, *117*, D05126, doi:10.1029/2011JD016902.

Welp, L. R., X. Lee, K. Kim, T. J. Griffis, K. A. Billmark, and J. M. Baker (2008), δ18O of water vapour, evapotranspiration and the sites of leaf water evaporation in a soybean canopy, *Plant Cell Environ.*, *31*(9), 1214–1228, doi:10.1111/j.1365-3040.2008.01826.x.

Wentz, F. J., and M. Schabel (2000), Precise climate monitoring using complementary satellite data sets, *Nature*, *403*, 414–416, doi:10.1038/35000184.

Wentz, F. J., L. Ricciardulli, K. Hilburn, and C. Mears (2007), How much more rain will global warming bring?, *Science*, *317*(5835), 233–235, doi:10.1126/science.1140746.

Wernli, H. (1997), A Lagrangian-based analysis of extratropical cyclones, II, A detailed case study, *Q. J. R. Meteorol. Soc.*, *123*, 1677–1706, doi:10.1002/qj.49712354211.

Werth, S., and A. Güntner (2010), Calibration analysis for water storage variability of the global hydrological model WGHM, *Hydrol. Earth Syst. Sci.*, *14*(1), 59–78, doi:10.5194/hess-14-59-2010.

Williams, D. G., et al. (2004), Evapotranspiration components determined by stable isotope, sap flow and eddy covariance techniques, *Agric. For. Meteorol.*, *125*, 241–258, doi:10.1016/j.agrformet.2004.04.008.

Wolfe, D. E., and S. I. Gutman (2000), Developing an operational, surface-based, GPS, water vapor observing system for NOAA: Network design and results, *J. Atmos. Oceanic Technol.*, *17*, 426–440, doi:10.1175/1520-0426(2000)017<0426:DAOSBG>2.0.CO;2.

Worden, J., et al. (2006), Tropospheric emission spectrometer observations of the tropospheric HDO/H_2O ratio: Estimation approach and characterization, *J. Geophys. Res.*, *111*, D16309, doi:10.1029/2005JD006606.

Wunsch, C., and P. Heimbach (2007), Practical global oceanic state estimation, *Physica D*, *230*, 197–208, doi:10.1016/j.physd.2006.09.040.

Xie, P., and P. Arkin (1997), Global precipitation: A 17-year monthly analysis based on gauge observations, satellite estimates, and numerical model outputs, *Bull. Am. Meteorol. Soc.*, *78*, 2539–2558, doi:10.1175/1520-0477(1997)078<2539:GPAYMA>2.0.CO;2.

Xie, X., W. T. Liu, and B. Tang (2008), Spacebased estimation of moisture transport in marine atmosphere using support vector regression, *Remote Sens. Environ.*, *112*(4), 1846–1855, doi:10.1016/j.rse.2007.09.003.

Yakir, D., and L. D. L. Sternberg (2000), The use of stable isotopes to study ecosystem gas exchange, *Oecologia*, *123*(3), 297–311, doi:10.1007/s004420051016.

Yakir, D., and X.-F. Wang (1996), Fluxes of CO_2 and water between terrestrial vegetation and the atmosphere estimated from isotope measurements, *Nature*, *380*, 515–517, doi:10.1038/380515a0.

Yepez, E., D. Williams, R. Scott, and G. Lin (2003), Partitioning overstory and understory evapotranspiration in a semi-arid savanna ecosystem from the isotopic composition of water vapor, *Agric. For. Meteorol.*, *119*, 53–68, doi:10.1016/S0168-1923(03)00116-3.

Yepez, E., R. Scott, W. Cable, D. Williams, and G. Lin (2007), Intraseasonal variation in water and carbon dioxide flux components in a semiarid riparian woodland, *Ecosystems N. Y.*, *10*(7), 1100–1115, doi:10.1007/s10021-007-9079-y.

Yoon, J. H., and N. Zeng (2010), An Atlantic influence on Amazon rainfall, *Clim. Dyn.*, *34*, 249–264, doi:10.1007/s00382-009-0551-6.

Yoshimura, K., T. Oki, and K. Ichiyanagi (2004), Evaluation of two-dimensional atmospheric water circulation fields in reanalyses by using precipitation isotopes databases, *J. Geophys. Res.*, *109*, D20109, doi:10.1029/2004JD004764.

Yoshimura, K., M. Kanamitsu, D. Noone, and T. Oki (2008), Historical isotope simulation using reanalysis atmospheric data, *J. Geophys. Res.*, *113*, D19108, doi:10.1029/2008JD010074.

Yoshimura, K., C. Frankenberg, J. Lee, M. Kanamitsu, J. Worden, and T. Röckmann (2011), Comparison of an isotopic atmospheric general circulation model with new quasi-global satellite measurements of water vapor isotopologues, *J. Geophys. Res.*, *116*, D19118, doi:10.1029/2011JD016035.

Yu, L. (2007), Global variations in oceanic evaporation (1958–2005), The role of the changing wind speed, *J. Clim.*, *20*(21), 5376–5390, doi:10.1175/2007JCLI1714.1.

Yu, L. (2009), Sea surface exchanges of momentum, heat, and freshwater determined by satellite remote sensing, in *Encyclopedia of Ocean Sciences 2e*, edited by J. Steele, S. Thorpe, and K. Turekian, pp. 202–211, Academic, London, doi:10.1016/B978-012374473-9.00800-6.

Yu, L. (2011), A global relationship between the ocean water cycle and near-surface salinity, *J. Geophys. Res.*, *116*, C10025, doi:10.1029/2010JC006937.

Yu, L., and R. A. Weller (2007), Objectively analyzed air-sea heat fluxes for the global ice-free oceans (1981–2005), *Bull. Am. Meteorol. Soc.*, *88*, 527–539, doi:10.1175/BAMS-88-4-527.

Yu, L., X. Jin, and R. A. Weller (2008), Multidecade global flux datasets from the Objectively Analyzed Air-sea Fluxes (OAFlux) project: Latent and sensible heat fluxes, ocean evaporation, and related surface meteorological variables, *OAFlux Proj. Tech. Rep. OA-2008-01*, 64 pp., Woods Hole Oceanogr. Inst., Woods Hole, Mass.

Zakharov, V. I., R. Imasu, K. G. Gribanov, G. Hoffmann, and J. Jouzel (2004), Latitudinal distribution of the deuterium to hydrogen ratio in the atmospheric water vapor retrieved from IMG/ADEOS data, *Geophys. Res. Lett.*, *31*, L12104, doi:10.1029/2004GL019433.

Zangvil, A., D. H. Portis, and P. Lamb (2004), Investigation of the large-scale atmospheric moisture field over the Midwestern United States in relation to summer precipitation. Part II: Recycling of local evapotranspiration and association with soil moisture and crop yields, *J. Clim.*, *17*, 3283–3301, doi:10.1175/1520-0442(2004)017<3283:IOTLAM>2.0.CO;2.

Zhu, Y., and R. E. Newell (1998), A proposed algorithm for moisture fluxes from atmospheric rivers, *Mon. Weather Rev.*, *126*, 725–735, doi:10.1175/1520-0493(1998)126<0725:APAFMF>2.0.CO;2.